3D FINITE ELEMENT ANALYSIS OF INTEGRAL ABUTMENT BRIDGES SUBJECTED TO THERMAL LOADING

by

BHAVIK RAMESHCHANDRA SHAH

B.Engg.(Civil), L.D. College of Engineering, India, 2004

A THESIS

submitted in partial fulfillment of the requirements for the degree

MASTER OF SCIENCE

Department of Civil Engineering
College of Engineering

KANSAS STATE UNIVERSITY
Manhattan, Kansas

2007

Approved by:

Major Professor
Dr. Dunja Perić

Copyright

Abstract

Integral Abutment Bridges (IABs) are Jointless Bridges whereby the deck is continuous and monolithic with abutment walls. IABs are outperforming their non-integral counterparts in economy and safety. Their principal advantages are derived from the absence of expansion joints and sliding bearings in the deck, making them the most cost-effective system in terms of construction, maintenance, and longevity. The main purpose of constructing IABs is to prevent the corrosion of structure due to water seepage through joints. The simple and rapid construction provides smooth, uninterrupted deck that is aesthetically pleasing and safer for riding. The single structural unit increases the degree of redundancy enabling higher resistance to extreme events.

However, the design of IABs not being an exact science poses certain critical issues. The continuity achieved by this construction results in thermally induced deformations. These in turn introduce a significantly complex and nonlinear soil-structure interaction into the response of abutment walls and piles of the IAB. The unknown soil response and its effect on the stresses in the bridge, creates uncertainties in the design.

To gain a better understanding of the mechanism of load transfer due to thermal expansion, which is also dependent on the type of the soil adjacent to the abutment walls and piles, a 3D finite element analysis is carried out on a representative IAB using state-of-the-art finite element code ABAQUS/Standard 6.5-1. A literature review focusing on past numerical models of IABs is presented followed by details of the numerical model developed in this study using the interactive environment ABAQUS/CAE 6.5-1 along with the analysis details. A discussion of results for the analysis of the IAB with three different soil conditions and each experiencing three different temperature change scenarios is presented. Conclusions of the study and recommendations for future research wrap up the thesis. The advancement of knowledge enabled by this research will provide a basis for introduction of new guidelines in Kansas Bridge Design Manual.

Table of Contents

List of Figures

List of Tables

Acknowledgements

Throughout this study, numerous people have provided me support, motivation and encouragement. I would like to thank my major advisor Dr. Dunja Perić for her intense efforts, deep insight, guidance and support during the course of my study at Kansas State University.

I would also like to thank my co-advisor Dr. Asadollah Esmaeily for his highly valuable and critical inputs towards making this project a success.

I extend my sincere appreciation to Dr. Hayder Rasheed for his valuable time by serving as my supervisory committee member.

Kansas Department of Transportation (KDOT) provided funding for this project. Department of Civil Engineering at Kansas State University and Dr. Dunja Perić provided me financial support during the course of my masters' study. These contributions are greatly acknowledged.

I would also thank my family and friends for their mental and motivational support through all times.

Dedication

I would dedicate this work to my mother Chetna R. Shah, my father Rameshchandra B. Shah and my brother Pratik R. Shah. It is their love, support, efforts and most importantly sacrifice that have brought me to this level of success that I have achieved in my life till now and whatever I will achieve in future as well.

CHAPTER 1 Introduction

1.1 Background

Highway bridges traditionally have a system of expansion joints, roller supports, abutment bearings and other structural releases to account for cyclic thermal expansion and contraction, creep and shrinkage (Arockiasamy *et al.*, 2004). Failure of proper functioning of the expansion joints and abutment bearings due to various reasons leads to highly critical and serious problems. Leakage of water laden with salt, deicing chemicals and contaminants through the joints results in the corrosion of the reinforced concrete, girder ends, bearings and pier caps underneath (Ng *et al.*, 1998). Failure to move properly due to unanticipated movements results in overstress and subsequent structural damage to the bridge elements viz. split and rupture of abutment bearings, abutment-rotation and abutment-overturning (Arockiasamy *et al.*, 2004; Wasserman, 2001). Expansion joints are very expensive to design, manufacture and install. The continuous maintenance and replacements costs are not meager either (Arockiasamy *et al.*, 2004). Integral Abutment Bridges (IABs) came to the fore as a result of a need for a definite change in the design of highway bridges.

1.2 Integral Abutment Bridge Concept

1.2.1 What are Integral Abutment Bridges?

IABs are defined as bridges without expansion joints or sliding bearings, thus eliminating all the issues associated with them. They are alternatively referred to as *integral bridges, jointless bridges, integral bent bridges* and *rigid frame bridges* (Lock, 2002). IABs are constructed continuous and monolithic with the abutment walls (Faraji *et al.*, 2001, Jayaram *et al.*, 2001), thus enabling the superstructure and the abutment to act as a single structural unit and assuring a full moment transfer (Khodair *et al.*, 2005) through a moment-resisting connection between them. (Faraji *et al.*, 2001; Jayaram *et al.*, 2001). Figure 1-1 shows a simplified geometry of an IAB (Arsoy, 2000).

Figure 1-1 Simplified Geometry of an Integral Abutment Bridge (Arsoy, 2000)

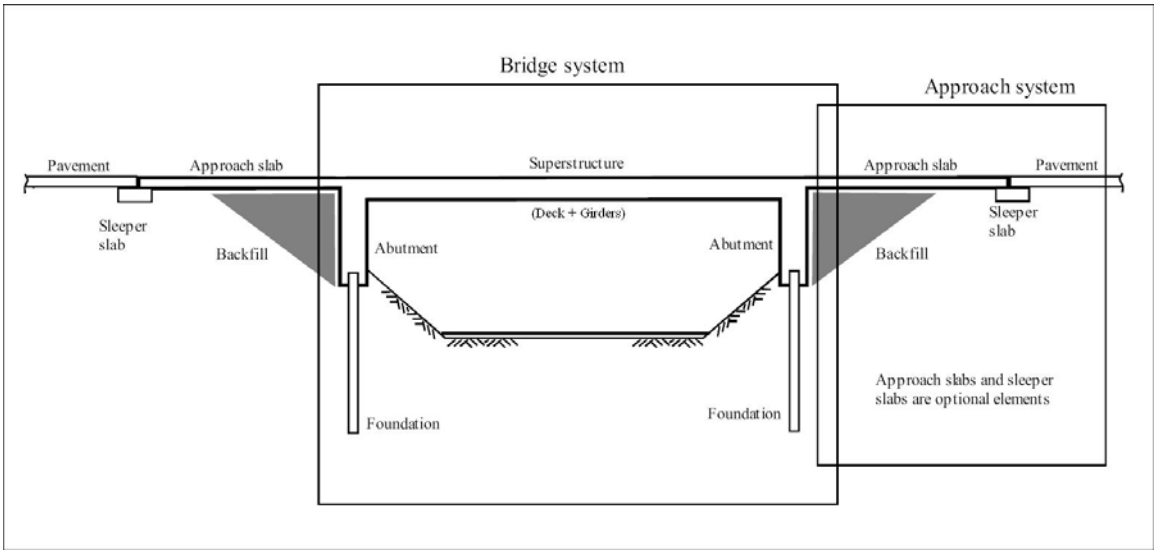

Single or multiple span IABs are generally supported by a single row of flexible H-piles driven into pre-augered holes beneath the abutment wall, and aligned such that the weaker axis of bending is along the transversal direction, thus allowing a higher flexibility. According to Arockiasamy *et al.* (2004), the substructure should be flexible enough to absorb the movements induced in the superstructure due to secondary loads like thermal variations, concrete creep and shrinkage. While the flexibility can be attained by a stub abutment supported by single row of piles (Arockiasamy *et al.*, 2004), in order to maximize the flexibility, rotational as well as translational, loose sand is usually placed around each pile in the pre-augered holes to a depth of about 10 ft (Ting & Faraji, 1998). The connections between abutment and piles are constructed as rigid connections, thus allowing full moment transfer from the abutment wall to the piles.

1.2.2 History of Integral Abutment Bridges

The earliest examples of IABs are masonry arch bridges. According to Bakeer *et al.* (2004), the first IAB in the USA was constructed in the state of Massachusetts in 1930, while Kansas was the second state to do so in 1935. Today there are more than 1000 IABs in the state of Kansas alone (Bakeer *et al.*, 2004). The longest IAB constructed till date is 1175 ft long bridge carrying Route 50 over the Happy Hollow Creek constructed in the state of Tennessee (Bakeer *et al.*, 2004). The construction of

IABs has been pursued in other countries including Canada, U.K., Sweden, Poland, Germany and Japan (Ng *et al.*, 1998)

1.2.3 Advantages of Integral Abutment Bridges

IABs are rapidly gaining popularity among bridge owners due to their durability, safety and cost effectiveness. Principal advantages of integral bridges, which are derived from the absence of expansion joints, are:

1. Simpler, rapid and more affordable construction
2. Reduced material and construction costs due to the absence of expansion joints (Yang *et al.*, 1985; Greimann *et al.*, 1987; Soltani & Kukreti, 1992)
3. Prevention of corrosion resulting in longevity and reduced maintenance costs (Yang *et al.*, 1985; Soltani & Kukreti, 1992, Hoppe & Gomez, 1996)
4. Smooth, uninterrupted aesthetically pleasing deck giving improved vehicular riding quality (Loveall, 1996; Soltani & Kukreti, 1996) and significantly reducing hazards and hence liability
5. Inherently increased degree of redundancy, hence an enhanced load capacity and distribution, resulting in a higher resistance to overloads, catastrophic or extreme events and earthquakes (Hoppe & Gomez, 1996; Wasserman, 2001)
6. Ease in future widening or replacement of bridge – simpler design lends itself to simpler structural modifications (Roman, *et al.* 2002)

1.2.4 Critical Design Issue – Soil-Structure Interaction

IAB is a classical example of soil-structure interaction (Ting & Faraji, 1998; Wood, 2004). The continuity achieved by this type of construction results in the transfer of thermally induced deformations in the bridge deck to the abutment walls, piles and surrounding soil. A significant and complex non-linear soil-structure interaction that takes place behind the abutment walls and piles has remained largely unknown. Secondary stresses due to thermal and moisture changes of the whole structure and settlements of substructure add to the intricacies of the entire problem. The magnitude and mode of deformation, the overall soil response and the overall structural response are decidedly dominated by the level of compaction in the granular fill behind the abutment walls and adjacent to the piles along with the relative flexural stiffness of the bridge deck,

abutment wall, foundation piles, lateral pressure of soil behind the wall and confining stress level in the soil (Jayaram *et al.*, 2001).

These unresolved issues create grave uncertainties in the design of IABs. Consequently, the current design guidelines are experientially based rather than scientifically based (Bakeer *et al.*, 2004). Arockiasamy *et al.* (2004) state that the limited design and construction guidelines by AASHTO and a lack of a unified procedure has led to wide variations in analysis, design and construction procedures from one state to another. According to Bakeer *et al.* (2004) the length limits vary from 150 ft in Maine to 1000 ft in Louisiana while Tennessee specifies a maximum movement of 2 inches as the criteria instead of maximum length. The length limit for the state of Kansas is 450ft (Bakeer *et al.*, 2004). Also, Bakeer *et al.* (2004) list the variations in skew angle limits from 0° (zero) in Louisiana and Oklahoma to 45° in California and no limit in Tennessee. Bakeer *et al.* (2004) have reported the experiences with the performances of IABs in different states. While Kansas and Tennessee rate having very good experience; expensive repairs of the approaches have led to withdrawal of use of IABs in Arizona (Bakeer *et al.*, 2004).

Lack of design specifications to account for the secondary stresses and the non-linear soil behavior (Shoukry *et al.*, 2006) has called for extensive research comprising:

1. collection of field data from instrumented bridges
2. geotechnical centrifuge experiments, and
3. numerical modeling efforts

It is not a surprise that sixteen states throughout the U.S. have indicated a definite need for future research on IABs (Bakeer *et al.*, 2004).

1.3 Objectives and Scope of Research

The diurnal and seasonal temperature changes induce critical secondary thermal stresses in the IABs, whose behavior is also dependent on the type of soil behind the abutment and piles. It is highly important to explore and examine the details of the complex soil-structure interaction in order to formulate recommendations for improvements in design and construction procedures. Thus, the primary objectives of this research are:

1. Conduct a literature review to establish the current state of knowledge in the area of response of IABs to thermal loads
2. Conduct numerical simulations of the response of a typical IAB to thermal loads by using the finite element software ABAQUS/CAE 6.5-1
3. Include the non-linear soil behavior behind the abutments and piles into the numerical model
4. Investigate the soil-structure interaction due to different temperature changes on IABs with different types of soil behind the abutments and piles

1.4 Contents of Thesis

A literature review focusing mainly on the past numerical models of IABs is presented in Chapter 2. Chapter 3 discusses the details of the numerical model of the IAB-soil system used in this study. Chapter 4 presents and discusses the results of the series of finite element analyses that were performed to investigate the soil-structure interaction of IABs subjected to different thermal loads and various soil conditions. Chapter 5 comprises the conclusions drawn from this research and recommendations for future studies.

CHAPTER 2 Literature Review

2.1 Introduction

Over the years behavior of IABs has been studied by various transportation agencies and researchers to advance the knowledge base and improve upon the prevalent design procedures and guidelines. Observations of field performance of IABs and related issues reported by different researches are summarized in this literature review along with the detailed discussion of the previous finite element studies on IABs.

Mourad *et al.* (1999) compared deck slab stresses in IABs with those in simply-supported jointed bridges by applying loading of HS20-44 trucks. A finite element analysis using computer program ALGOR (1995) was carried out for this purpose. The results indicated a more uniform distribution of loads and 25-50 % lower maximum stresses in the transverse direction in IABs as compared to the corresponding simply supported bridges.

According to Roman *et al.* (2002) the secondary stresses in the bridge deck due to temperature changes and substructure settlement of the substructure can be significantly higher than those permitted by current design specifications, thus highlighting the lack of sufficient knowledge base with reference to IABs.

After inspecting and rating 30 steel IABs Alampalli *et al.* (1998) concluded that the higher the skew of the bridge deck, the lower the condition and performance ratings were for the deck, approach slab and abutment stem.

Arockiasamy, M. *et al.*, 2004, conducted a parametric study for the response of laterally loaded piles supporting integral bridges with an emphasis on predrilled holes, elevation of the water table, soil types and pile orientation by using finite-difference program LPILE and finite-element program FB-Pier. The study concluded that horizontal displacement at the pile top, maximum shear, axial force and moments in the pile significantly depend on the type of the soil around the pile, its degree of compaction and the orientation of pile axis; while the water table elevation has very little significance.

Ng *et al.* (1998) studied the behavior of abutments of IABs and how it differed from that of simply supported bridges subjected to cyclic loading conditions. Effects of temperature variations on the soil-structure interaction were investigated by using the centrifuge modeling technique. Displacement-controlled loading was employed in the centrifuge model tests, which were conducted on a spread-base integral bridge abutment. This was done by imposing controlled cyclic displacements at the top of the abutment wall thereby simulating the thermal expansion and contraction of the bridge. According to Ng *et al.* (1998), "The three temperature ranges considered included one extreme for 120-year design period, seasonal cycles between summer and winter temperatures, and daily cycles between day and night temperatures". Based on these temperature ranges, controlled displacements at the deck level for a 100 m long concrete bridge deck were measured. Results showed rigid body motions, both translational as well as rotational. Three factors affected the abutment movement: magnitude of displacements imposed at the abutment top, the number of strain cycles for which the experiments were carried out, and the density of the fill materials. A strain ratcheting effect was observed due to the densification and settlement of the fill, progressively increasing the outward movement of the abutment wall with the number of strain cycles; the effect being more significant in dense than in loose fill calling for a careful consideration of sliding resistance of spread-base abutments during design.

2.2 Past Finite Element Studies on IABs

Very few detailed finite element studies with focus on thermal loading have been carried out on IABs. This section of the literature review discusses those in details.

2.2.1 "Nonlinear Analysis of Integral Bridges: Finite-Element Model" by Faraji et al. (2001)

One of the most complete finite element studies of IABs was performed by Faraji *et al.* (2001) with the aim to design and construct longer span bridges and to evaluate their performance during seismic loads. A 3D finite element model of "Bemis Road Bridge: F-4-20" in Fitchburg, Massachusetts was analyzed using the finite element code GT-STRUDL. Non-linear soil behavior, modeled using non-linear springs, was incorporated in the model. The nonlinear force-deflection relations for the soil adjacent to

the abutment walls were based on the recommendations by the National Cooperative Highways Research Program (NCHRP, 1991) design manual. The "*p-y*" design curves recommended by American Petroleum Institute (API) (1993) were used for nonlinear force-deflection relations for the soil adjacent to the piles. Figure 2-1 shows the GT-STRUDL finite element model of the bridge.

Figure 2-1 GT-STRUDL Finite Element Model of the Bridge (Faraji *et al.*, 2001)

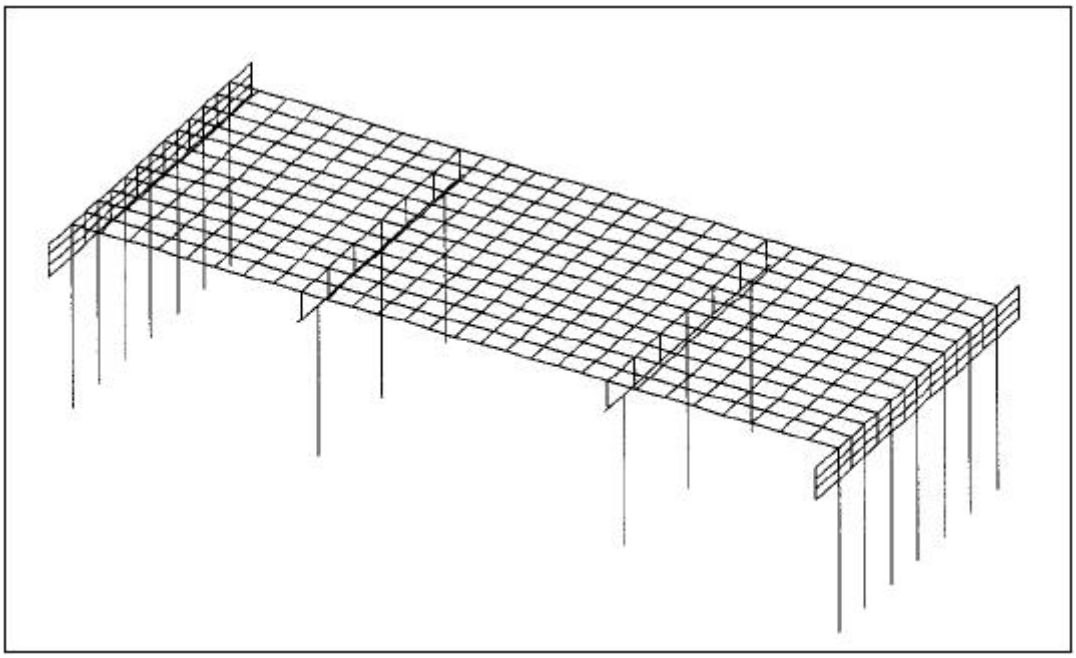

Bending and stretching plate elements were used to model the deck of 150 ft long 3-span IAB with two 45 ft long end spans. The deck is 54 ft wide and 8.5 in thick concrete slab. On the other hand, beam elements were employed to model the W36x135 steel stringers and diaphragms. Beam elements modeled the 3 ft high, 3.5 ft wide and 56.5 ft long pier caps, and 3 ft diameter concrete piers as well. Rigid links were used to model the connection between deck slab and girders ensuring "strain compatibility and shear transfer between the deck slab and girder elements. The 8 ft high, 2.5 ft wide and 69 ft long abutment wall was modeled by using plate elements with an overall effective height of 6 ft, connected to the girder ends by a fixed connection. Uncoupled nonlinear Winkler springs were used to model the soil response behind the abutment. Each of the seven HP12x74 piles was modeled using beam elements, which were fixed into the

abutment wall. The fixity allows a full moment transfer from the superstructure to the piles. The *p-y* curves modeled the soil response by using a series of nonlinear springs. Figure 2-1 shows the GT-STRUDL finite element model of the bridge.

In all, more than 1000 beam, beam-column, and slab members and elements for the deck, wall, pier, and pile systems; and over 350 nonlinear soil substituting springs were used in the finite element model. Figure 2-2 shows finite element details of north abutment wall and HP piles.

Figure 2-2 Finite Element Model Details for North Abutment Wall and HP Piles (Faraji et al., 2001)

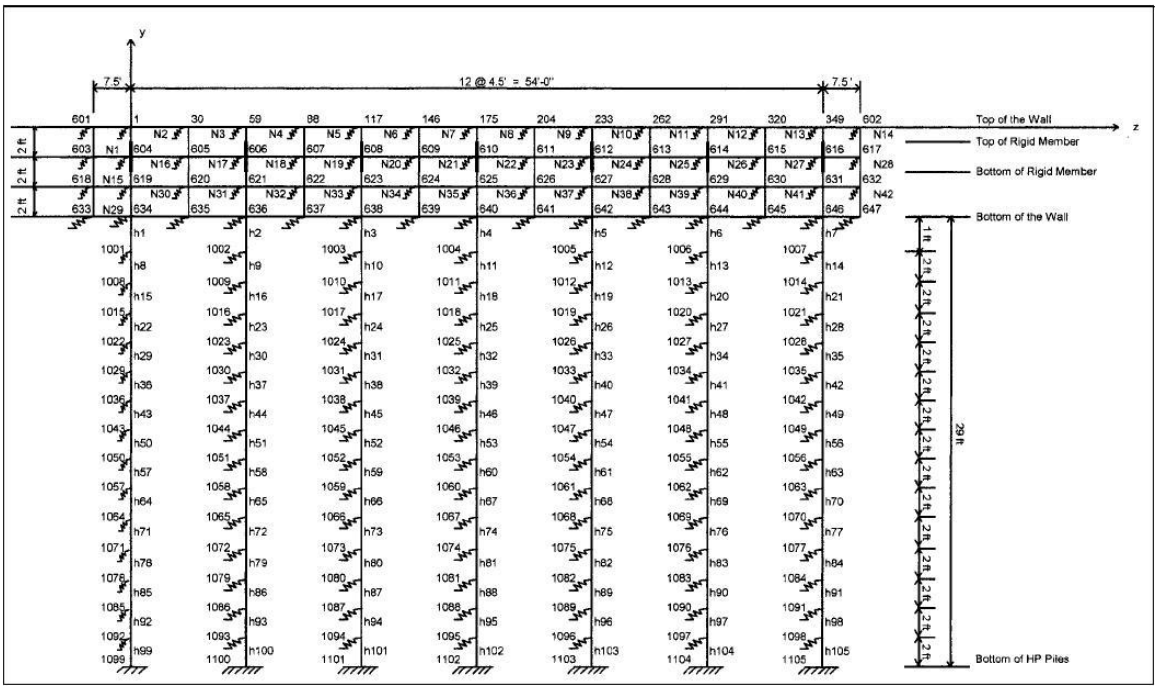

The bridge was subjected to a temperature increase of 80˚ F for different combinations of soil properties behind the abutment and adjacent to the piles based on the compaction levels. The results of the analysis called for proper care to be taken while modeling the composite action of the superstructure. The level of soil compaction behind the abutment wall played a vital role in affecting the overall bridge behavior in terms of axial forces and moments in the deck increasing both by more than twice in peak value when varied from loose to dense compaction range. Though the level of soil compaction

adjacent to the HP piles had an impact on the moments in the piles, it was not significant in affecting the behavior of the abutment wall and the superstructure. The results also indicated that soil pressures behind the abutment wall could reach the full passive state and be considerably nonlinear for longer bridges. Faraji *et al.* (2001) recommended a more refined and full 3D modeling of the sample bridge as well as modeling of longer bridges for a more advanced understanding of the behavior of IABs.

The research carried out at Kansas State University is aligned with the direction of this recommendation by Faraji *et al.* (2001) by using a full, detailed and refined 3D model of the same bridge along with different temperature ranges, thus modeling the response of longer bridges.

2.2.2 "Analysis of Soil-Pile Interaction in Integral Abutment" by Khodair & Hassiotis, (2005)

Khodair & Hassiotis (2005) studied the soil-structure interaction of the soil-pile system of the Scotch Road IAB in Trenton, New Jersey built over I-95. Khodair & Hassiotis (2005) listed two objectives of the research. First, determine the thermal stresses in the piles due to temperature changes; and second, determine "lateral load transfer from the piles to the MSE (Mechanically Stabilized Earth) wall supporting the bridge foundation" (Khodair & Hassiotis, 2005). To go about achieving the objectives, they performed three tasks. First, instrumentation of abutment and piles; second, development of a 3D FE model of the substructure; and third, updating the FE model using the data obtained from monitoring the instrumented bridge.

Scotch Road, I-95 IAB, located in Ewing/ Hopewell Township, is a composite concrete slab IAB with 10 non-standard steel girders, of depth 5.51 ft, connected by shear studs. Nineteen HP 360x152 piles supported the 2.95 ft wide and 9.45 ft deep reinforced concrete abutment through an embedded connection ensuring the full moment transfer (Figure 2-5). A sleeper slab supported the approach slab at the far end, which was rigidly connected to the abutment on the near end. "The soil behind the abutment and under the approach slab consisted of a well-compacted porous fill" (Khodair & Hassiotis, 2005).

Figure 2-3 Elevation View of the Scotch Road, I-95 IAB (Khodair & Hassiotis, 2005)

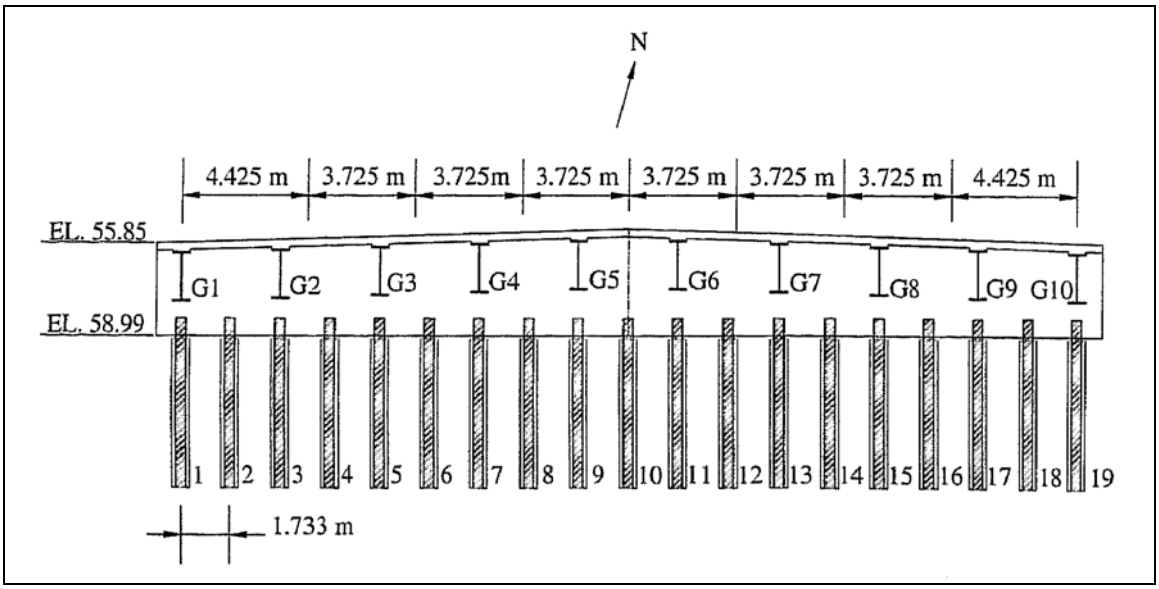

Instrumentation included four types of measuring devices: strain gages, soil pressure cells, inclinometers having temperature sensors and tiltmeters. Figure 2-6 shows the instrumentation details. Data was collected for a period of one year at the interval of every 2 hours.

Figure 2-4 Instrumentation of Experimental Devices on the Substructure of the Scotch Road, I-95 IAB (Khodair & Hassiotis, 2005)

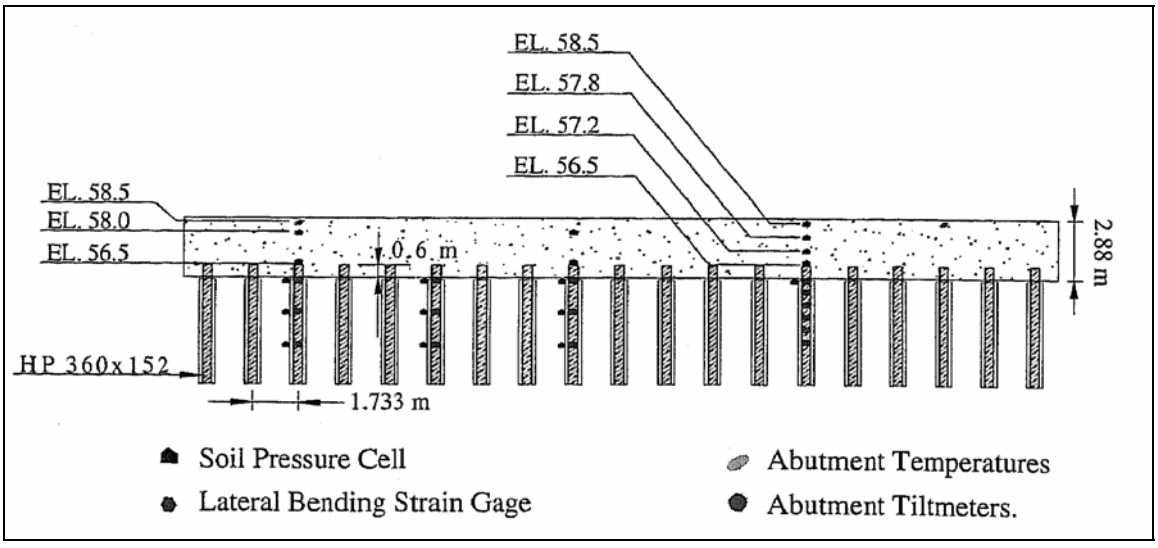

According to Khodair & Hassiotis (2005) ABAQUS/Standard 6.3.1 was used to develop a 3D FE model of the HP piles embedded into a 1.97 ft diameter sand filled galvanized steel sleeve. Both, pile and soil were modeled using eight-node solid continuum elements with a non-linear response. While an elastic-plastic response was adopted for the pile elements, Mohr-Coulomb model with strain hardening idealized the non-linear soil response. Surface-to-surface contact algorithm was employed to model the sand-pile interaction. To model the tangential contact, friction coefficient for the interaction between pile and soil materials was calculated.

Two load cases were analyzed by the FE model. In the first load case, a displacement and rotation boundary condition was imposed by applying a displacement of 0.0755 ft. In words of Khodair & Hassiotis (2005) "the displacement was applied at a location corresponding to the neutral axis of the attached girder in a pattern that simulates rigid body motion". This displacement corresponds to a temperature increase on 107.6°F calculated according to the following equation:

$$d = \alpha \delta T_{EB} L \qquad (2.1)$$

where,

d = maximum horizontal displacement

L = span of the bridge

α = coefficient of thermal expansion

δT_{EB} = change in EBT (Effective Bridge Temperature)

The concept of EBT, defined as the assumed uniform temperature state for the observed thermal expansion, was introduced in UK in compliance with the material of the bridge deck and the geographical location of the bridge. A parametric study for the first load case was also carried out by incrementally increasing the steel sleeve diameter from 1.97 ft to 6.56 ft.

In the second load case, the displacements and rotations measured from the field experiment were applied to the abutment in the FE model.

In order to verify the FE model, the results of the first load case of the FE model were compared with the results obtained from the Finite Difference (FD) analysis software LPILE. The results were not similar and had discrepancy which was attributed to the difference in the size of the diameter of the sand surrounding the piles in FE

analysis and FD analysis. It was also observed from the parametric study that there was a substantial decrease in the discrepancy when the size of the diameter was increased up to a value defined by LPILE as an extended single layer of sand.

The axial strains calculated from the analyses in the second loading case when compared to the measured values from the strain gages matched very favorably for piles #3 and #9, although they did not match for pile #6. This discrepancy is due to the fact that "the loading considered in the FE model was formulated to account for the effect of the girders #2 and #5" which were placed directly above piles #3 and #9 and the axes of the piles coincided with the girders. On the other hand, pile #6 was not affected directly by any of the 10 girders in the superstructure.

One interesting observation that Khodair & Hassiotis (2005) made was that irrespective of the change in the diameter of the galvanized steel sleeves, the calculated values of the crushed stone pressure at the perimeter of the galvanized steel sleeves remained approximately zero. The experimentally measured values by the soil pressure cells substantiated these calculations.

Khodair & Hassiotis (2005) made two conclusions from this research:

1. The diameter of 1.97 ft of the galvanized steel sleeve filled with sand is sufficient to accommodate the pressure developing due to the thermal loads, equivalent to 0.0755 ft displacement corresponding to 107.6°F temperature increase.
2. Increase in the size of the diameter of the steel sleeve results in higher lateral load capacity of piles.

2.2.3 "Field Monitoring and 3D FE Modeling of an Integral Abutment Bridge in West Virginia" by Shoukry et al. (2006)

Shoukry *et al.* (2006) studied the axial effect of the backfill pressure against expansion of IABs in the steel girders of a three-span IAB located in Evansville, West Virginia. Stating that the effect of backfill forces is being taken into account to a certain extent in the design of piles and abutment but not that of the girders, where secondary thermal axial stresses get generated, Shoukry *et al.* (2006) evaluated the response of the IAB, which had been instrumented and monitored for a period of twenty months. A better

understanding of the bridge behavior was attempted by a 3-D finite element model of the three girder section of the bridge, whose construction had been completed during the first phase, using finite element software ADINA (2000).

Evansville Bridge, which carries WV Route 92 over Little Sandy Creek located in Preston County, West Virginia, is a three-span 147 ft long steel girder continuous bridge with a skew angle of 55°. The 44 ft wide Evansville Bridge had two end spans of 48.5 ft and a central span of 50 ft in length. A single row comprising eight HP 12x53 piles with an embedded length of 0.98 ft support the 5.97 ft high, 2.95 ft wide and 53.15 ft long abutment wall. The 0.66 ft minimum thickness of the deck reaches to 0.74 ft over the haunches as shown in Figure 2-3 (Shoukry *et al.*, 2006).

Figure 2-5 Evansville Bridge (a) Elevation (b) Side View (c) Plan (Shoukry *et al.*, 2006)

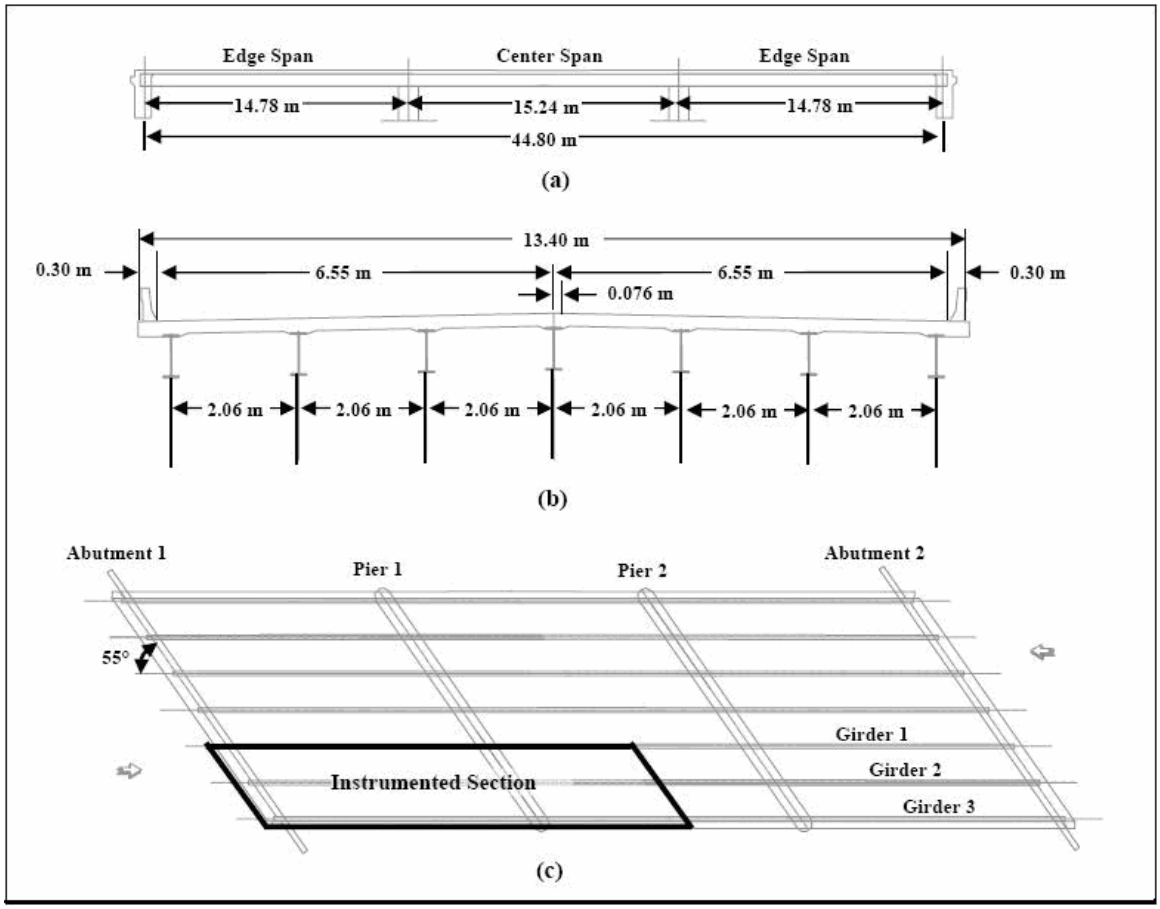

While the bridge deck, abutment walls, girders and cross members at the piers were idealized using 4-node shell elements, hermitian beam elements modeled the piles and remaining cross members. Modeling of piers was taken care of by corresponding boundary conditions at the respective locations on the girders. The soil backfill and the piles, fixed at their base, supported the abutments. To allow the stiffness of the deck-girder connection to be varied, spring tied elements were employed at their interface. Nonlinear spring elements modeled the soil backfill as well as the soil around the piles.

Using the design curves by National Cooperative Highway Research Program (NCHRP, 1991), passive and active earth pressure effects behind the abutment were modeled for the soil found to have 18 kN/m^3 as the unit weight and Φ=36° as the angle of internal friction. On the other hand, the guidelines by the American Petroleum Institute (API) (1993) were utilized to develop the "*p-y*" curves, which represented the stiffness for the nonlinear springs substituting the soil around the piles. The "*p-y*" relationship is a hyperbolic tangent curve defined as follows:

$$p = Ap_u \tanh\left[\frac{kz}{Ap_u} y\right] \tag{2.2}$$

where,

p_u = ultimate bearing capacity,

k = parameter defined by Φ,

z = depth in soil,

$y = y$ = lateral displacement of pile,

A = parameter that varies with soil depth in case of static loading according to the equation 2.2

$$A = 3.0 - 0.8\frac{X}{D} \geq 0.9 \tag{2.3}$$

where,

X = soil depth,

D = average pile length.

For the FE analysis, self-weight of the structure followed by a uniform temperature change of ±20°C with ±5°C intervals was applied to the model. Figure 2-4 shows the finite element model of the three girder section of the bridge.

Figure 2-6 Finite Element Model of Evansville Bridge (a) Full Model (b) Non-Linear Springs Modeling the Soil-Abutment Interaction (c) Non-Linear Springs Modeling the Soil-Pile Interaction (Shoukry *et al.*, 2006)

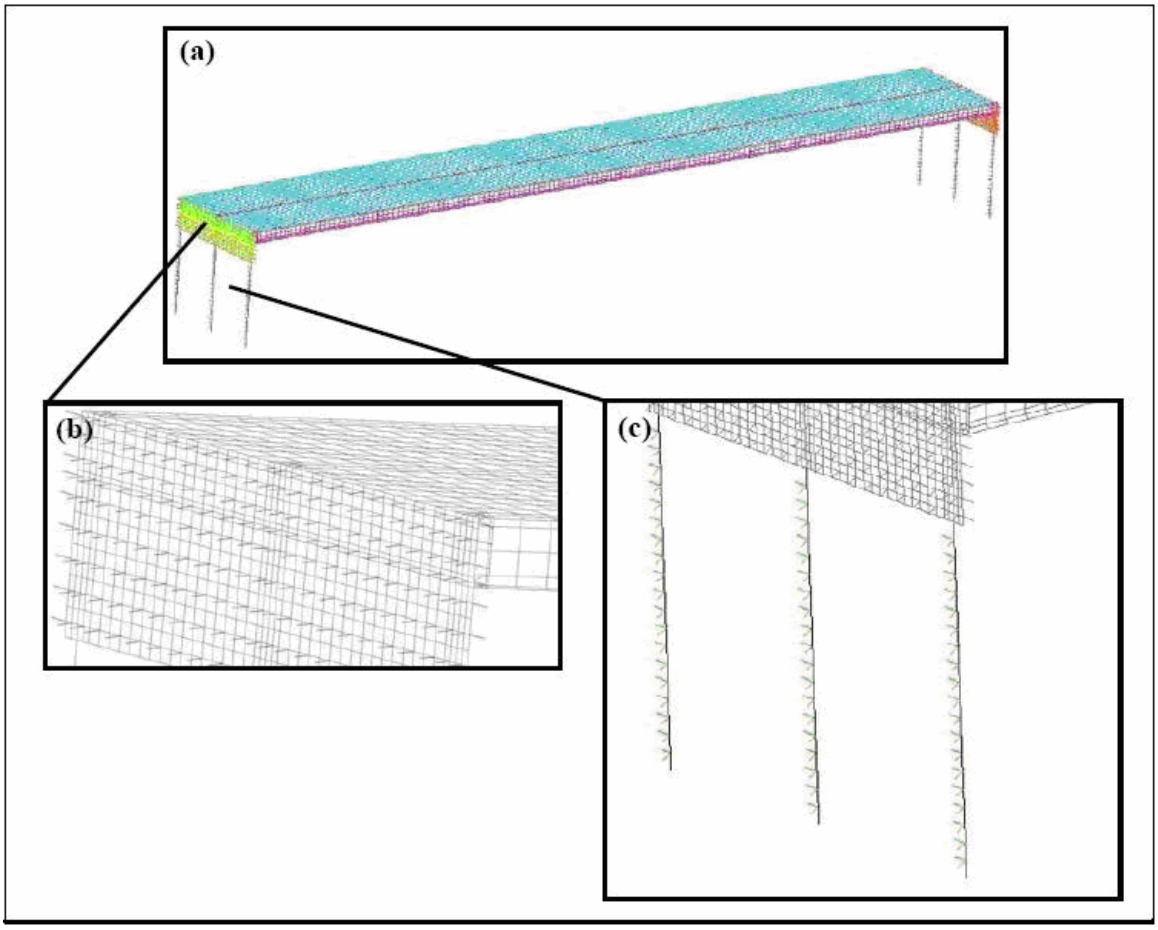

The validation of the accuracy of the finite element analysis required a comparison with the field data, whereby the field data was interpreted for self-weight and thermal loads only so as to have the consistency in the response comparison. The measured values of displacements, strains and subsequently calculated stresses matched well with the finite element results. Also, both, measurements and analysis, indicated that secondary axial thermal stresses were induced in the girders along with the piles. According to Shoukry *et al.* (2006) the secondary effects, which are taken into consideration in the design provisions for piles, have not been explicitly addressed in the design of the superstructure. Since location of the bracing cross-members can be affected by these stresses and their ignorance may lead to the failure to meet the AASHTO

Standard Specifications (2002) for stability and yield, Shoukry *et al.,* 2006, concluded that there is a definite need to address their effects while designing the components of a bridge superstructure.

CHAPTER 3 Numerical Modeling

3.1 The Bridge Model

A refined and detailed 3D finite element model of the "Bemis Road Bridge: F-4-20" over the Nashua River in Fitchburg, Massachusetts (Ting and Faraji, 1998), which was subsequently modified slightly according to the requirements of KDOT, is developed using the interactive environment of finite element software ABAQUS/CAE 6.5-1.

The selection of this is bridge was based on two reasons as follows:

1. It is a typical IAB within the length limit of 450ft for the state of Kansas (Bakeer *et al.*, 2004).
2. The availability of variety of results as per the report by Ting & Faraji (1998) enabled better validation and verification of the FE model.

Due to the symmetry of the bridge geometry and loading, only half of the 150 ft long 3-span steel IAB is modeled. The length of central span is 60 ft while the two end spans are 45 ft each, with the width of the bridge being 54 ft. Figure 3-1 shows the elevation view schematic of the bridge.

Figure 3-1 Schematics of the Bridge (Faraji *et al.*, 2001)

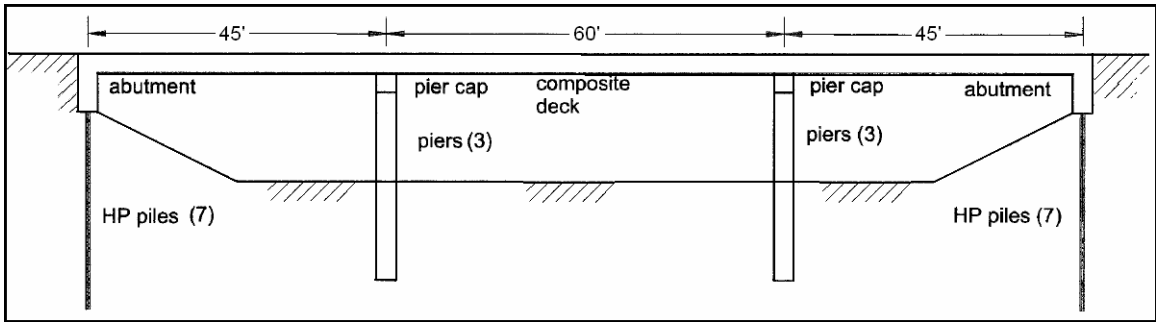

The superstructure comprises the following parts:

1. 8.5 in thick, 150 ft long and 54 ft wide concrete slab,
2. Seven W36x135 steel girders spaced 9 ft apart, and

3. Seven transverse W36x135 steel beams, 54 ft long, one at the center and one at the end of each span.

Figure 3-2 shows the schematics of the FE model of bridge along with the coordinate system employed for presenting the results.

Figure 3-2 Schematics of FE Model of the Bridge

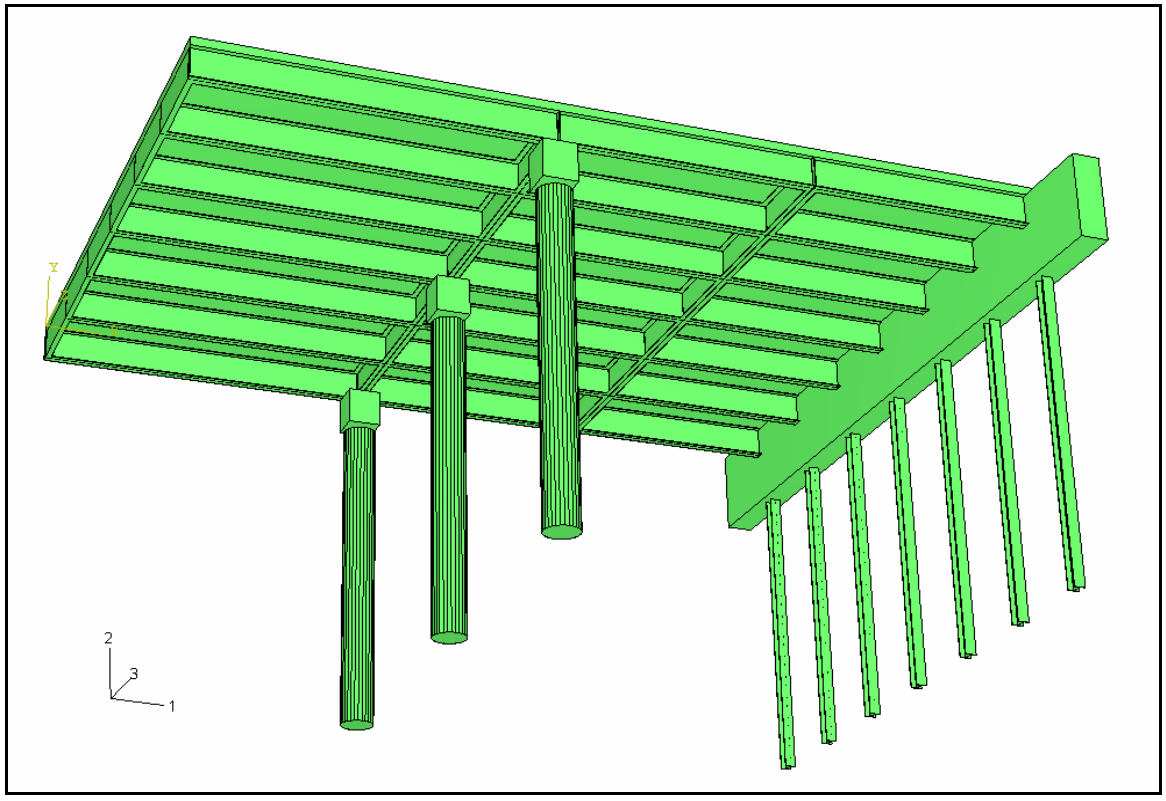

The superstructure rests on substructure comprising the following:

1. Two sets of 3 concrete piers, one set on each end of the central span, which are connected by hinge connections to the superstructure.
2. The piers are 3 ft in diameter and 30.2 ft long. Each is capped by a 3 ft x 3 ft x 3.5 ft pier cap.
3. Concrete abutments are 8 ft high, 2.5 ft wide and 69 ft long.
4. Each abutment is supported by seven HP12x74 piles, 29 ft long, spaced 9 ft apart allowing a full moment transfer.

5. The nonlinear force-lateral displacement relationship for the soil is modeled by linear springs and iterative equivalent linear approach. The springs are attached to the nodes located on the abutment and piles.

Finite element code ABAQUS/Standard, release 6.5-1 is used for the analyses. The FE model of the bridge-soil system consists of total 191894 eight-node coupled temperature-displacement elements (C3D8T), 277530 nodes, 12 connector elements (CONN3D2) modeling hinges, and 546 linear spring elements. Figure 3-3 shows the finite element model of the bridge.

Figure 3-3 Finite Element Model of the Bridge (Including the Soil Substituting Springs)

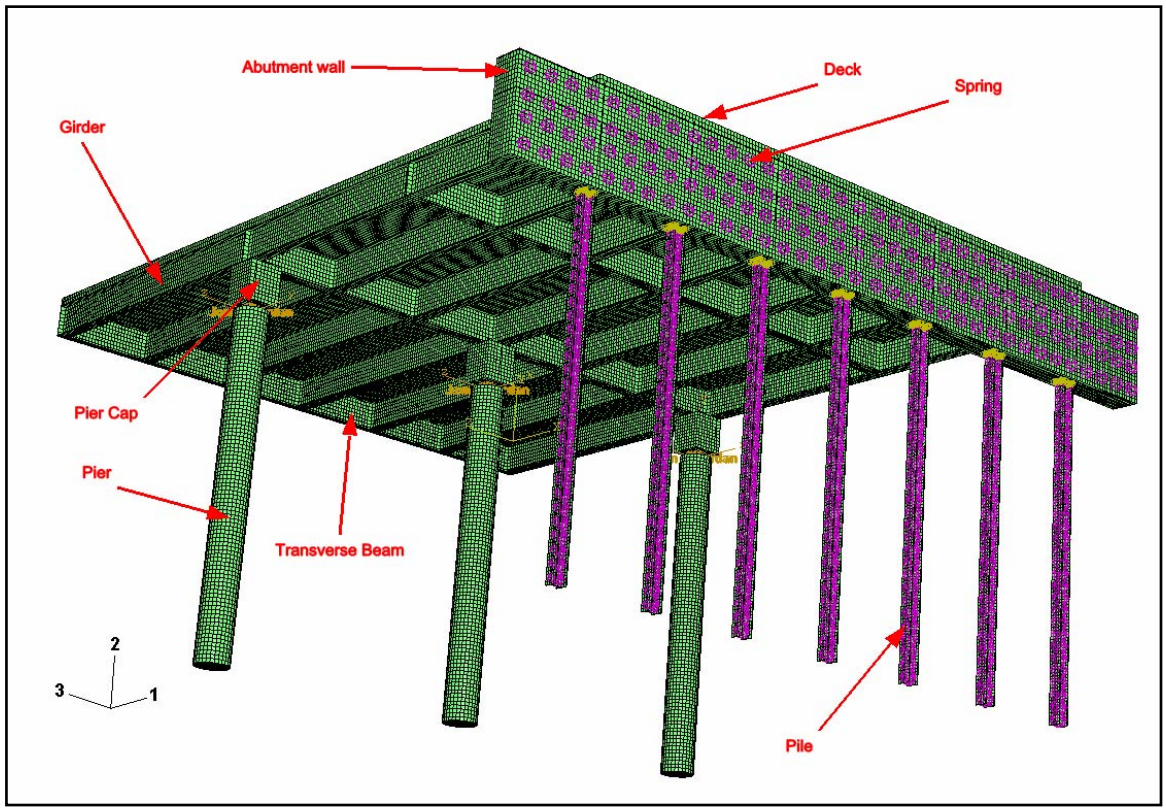

3.2 Loads

Thermal stresses are induced in the structure due to its continuity and presence of the soil behind the abutment and piles, which prevents a free expansion. For the finite element analyses, the temperatures of the superstructure and a partial region of the

substructure exposed to the atmosphere were increased by an amount ΔT, while the temperature of the partial region of the substructure under the ground was held constant at 50˚F. Three different values for ΔT were used herein corresponding to 60˚F, 80˚F and 100˚F. Figure 3-4 depicts nodal temperatures for the scenario when $\Delta T = 80$˚F.

Figure 3-4 Nodal Temperatures for ΔT = 80˚F

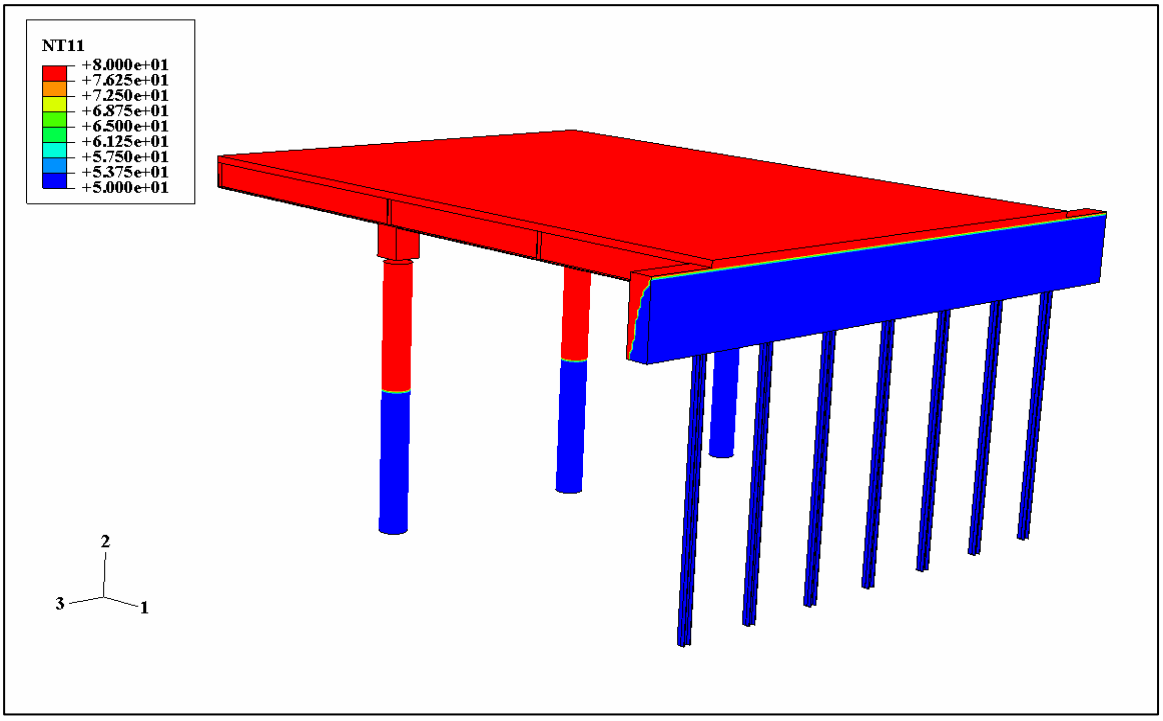

The analysis is performed in two steps. In the first step, to account for the self-weight before any temperature changes take place, a gravity acceleration of 32.2 ft/s^2 is applied to the bridge model. In the second step, a temperature increase of amount ΔT is prescribed at each node in accordance to the Figure 3-4, while the self-weight effect from the previous step is carried forward. The analysis procedure is "coupled temperature-displacement analysis" as explained in the ABAQUS user manual.

3.3 Concrete and Steel properties

The stress-strain behaviors of concrete and steel are assumed to be linear elastic. The corresponding material properties are listed in Table 3.1. They include Young's

modulus E, Poisson's ratio υ, coefficient of thermal expansion α, mass density ρ and, thermal conductivity κ.

Table 3.1 Material Properties

Property	**Concrete**	**Steel**
Young's Modulus E (psi)	4.35×10^6	3×10^7
Poisson's ratio υ	0.3	0.3
Coefficient of thermal expansion α(per ˚F)	6×10^{-6}	6.5×10^{-6}
Mass Density ρ (slugs/ft^3)	4.66	15.23
Mass Density ρ (slugs/in^3)	0.0027	0.0088
Thermal conductivity κ (Btu/in*hr*˚F)	0.15	2.5

3.4 Soil Model and its Properties

The soil structure interaction is modeled by attaching linear springs at the selected nodes of the abutment and piles. The springs simulate the effect of the abutment fill on the bridge. The non-linear force-displacement relationship of the soil is simulated by an iterative equivalent linear approach described in the sections 3.4.1 and 3.4.2.

3.4.1 Springs Behind Abutment

Four rows of springs are attached behind the abutment such that each spring has a tributary area of

$$\Delta A = \Delta h \times \Delta b \qquad (3.1)$$

where,

$\Delta h = 24$ in and

$\Delta b = 23.66$ in.

Thus there are a 35 springs in each row summing up to a total of 140 springs representing the soil behind the abutment. The stiffnesses of these springs depend on the types of soils adjacent to the abutment and piles. They are determined by an iterative equivalent linear approach that comprises multiple iterations. The corresponding steps are described below:

1. In the first iteration, lateral displacements of the abutment top (δ_0) are obtained based on the bridge model without springs thus disregarding the presence of the soil.
2. Next, the initial stiffnesses of lateral springs to be attached to the abutment are determined, based on the displacements determined in step-1 and in accordance with the following equation

$$k_{1,j}(\delta_0) = \frac{F(\delta_0)}{\delta_{0,j}} = \frac{K(\delta_0)\gamma_d z \Delta A}{\delta_{0,j}} \qquad j = 1 \text{ to } 4 \qquad (3.2)$$

where,

$K(\delta_0)$ = the coefficient of lateral earth pressure, whose magnitude depends on the magnitude of the corresponding horizontal displacement δ_0 of the abutment top. The relationships between the coefficient of lateral earth pressure (K) and lateral displacement of the top of the wall (δ) used herein are discussed later.

$\delta_{0,j}$ = lateral displacement at the location of the selected spring, obtained from the step above

γ_d = dry unit weight of soil behind the abutment

z = depth of the spring, from the top of the abutment

This stiffness is entered into the subsequent FE run and corresponding displacement at the top of the abutment δ_1 is obtained from the output.

3. Next, step 2 is repeated by using the displacements obtained from the updated output from the most recent iteration. The stiffnesses in each subsequent iteration are calculated according to the following equation

$$k_{i+1,j}(\delta_i) = \frac{F(\delta_i)}{\delta_{i,j}} = \frac{K(\delta_i)\gamma_d z \Delta A}{\delta_{i,j}} \qquad (3.3)$$

where,

$\delta_{i,j}$ = output from the current iteration

$k_{i+1,j}$ = input into the subsequent iteration.

For the purpose of determining the spring stiffnesses the motion of the abutment is approximated by a rigid body motion as shown in Figure 3-5.

Figure 3-5 Abutment Motion

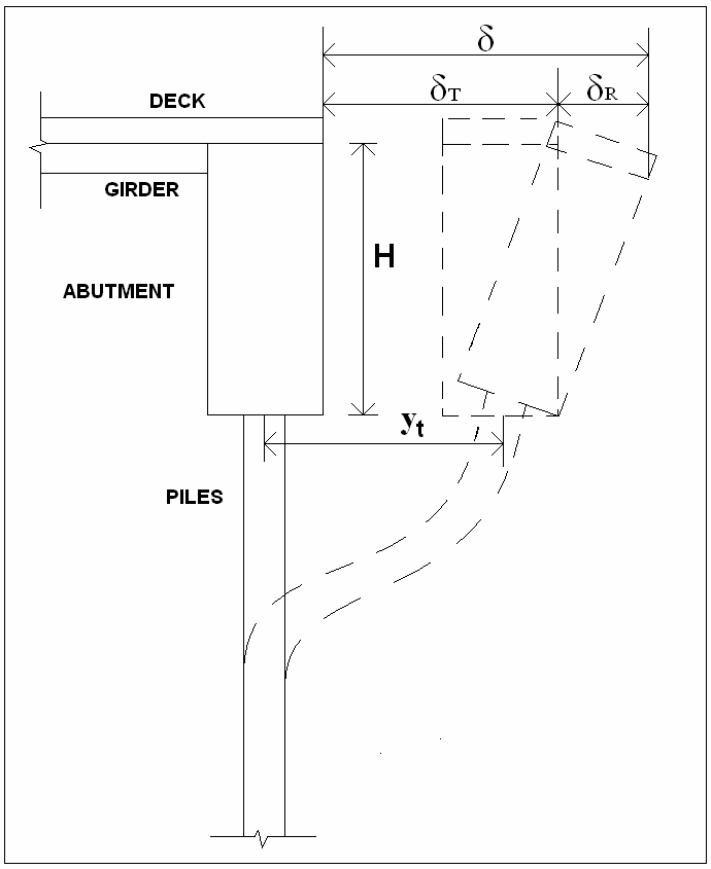

Thus,

$$\delta = \delta_T + \delta_R \qquad (3.4)$$

where,

δ_T = abutment translation and

δ_R = displacement due to the rotation of the abutment

The relationships between the lateral displacement of the abutment top δ, and coefficient of lateral earth pressure in soil recommended by two different design agencies viz. National Cooperative Highways Research Program (NCHRP, 1991) design manual and Canadian Foundation Engineering Manual by Canadian Geotechnical Society (CGS, 1992) are used herein. The corresponding response curves shown in Figures 3-6 and 3-7

are used to determine the coefficient of lateral earth pressure $K(\delta)$. Table 3.2 lists the type of soils for which these design response curves have been recommended.

Figure 3-6 Design Curves Recommended by NCHRP (1991)

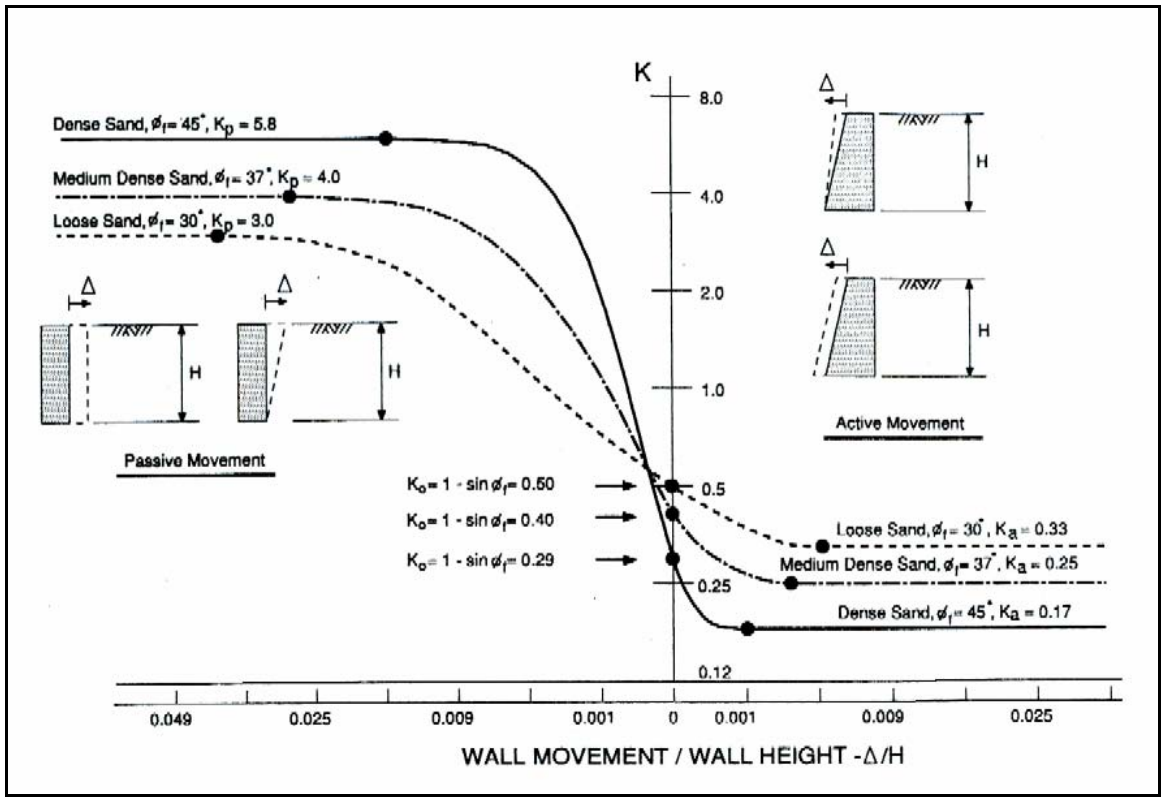

Table 3.2 Soil Properties

Type of sand	**Angle of internal friction Φ(°)**
Dense sand (NCHRP, 1991)	45°
Dense sand (CGS, 1992)	N/A
Loose sand (NCHRP, 1991)	30°

It is assumed that maximum dry density $\gamma_{d,\max} = 125$ lb/ft^3, and the relative densities D_R of dense and loose sands are 80% and 50% respectively. It is also noted that a sand of relative density of 50% falls between a loose and medium dense sand. Herein, it is referred to as loose sand.

Lee & Singh (1971) proposed the following relationship based on observations of 47 granular soil samples:

$$R = 80 + 0.2D_R \tag{3.5}$$

where,

R = relative compaction defined as follows (Das,1999):

$$R = \frac{\gamma_{d,field}}{\gamma_{d,\max}} \tag{3.6}$$

Actual dry unit weights ($\gamma_{d,field}$) are calculated by using equations (3.5) and (3.6). The corresponding values used in the analyses are reported in Table 3.3.

Figure 3-7 Design Curves Recommended by CGS (1992)

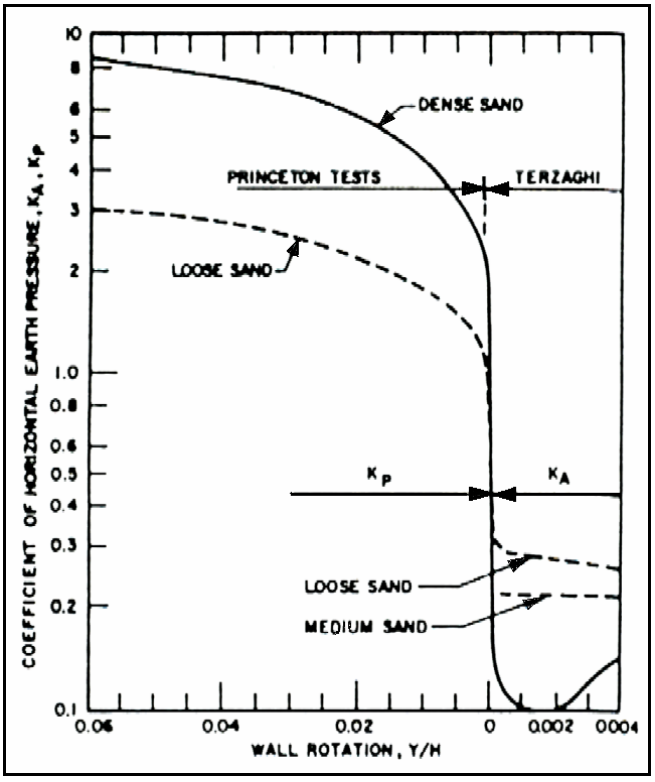

Table 3.3 Dry Unit Weights of Soils

Type of sand	$\gamma_{d\max}$ **(lb/ ft^3)**	D_R **(%)**	R **(%)**	γ_d **(lb/ ft^3)**
Dense sand	125 lb/ft^3	80%	96%	120 lb/ft^3
Loose sand	125 lb/ft^3	50%	90%	112.5 lb/ft^3

For the purpose of determining δ in 3D analysis, the abutment was divided into 9 vertical zones, and longitudinal displacement at the center of each zone was used for all springs located in that zone. The abutment top central points (nodes) whose displacements were used are highlighted in Figure 3-8 along with the corresponding zones.

Figure 3-8 Vertical Zones of the Abutment and the Corresponding Nodes

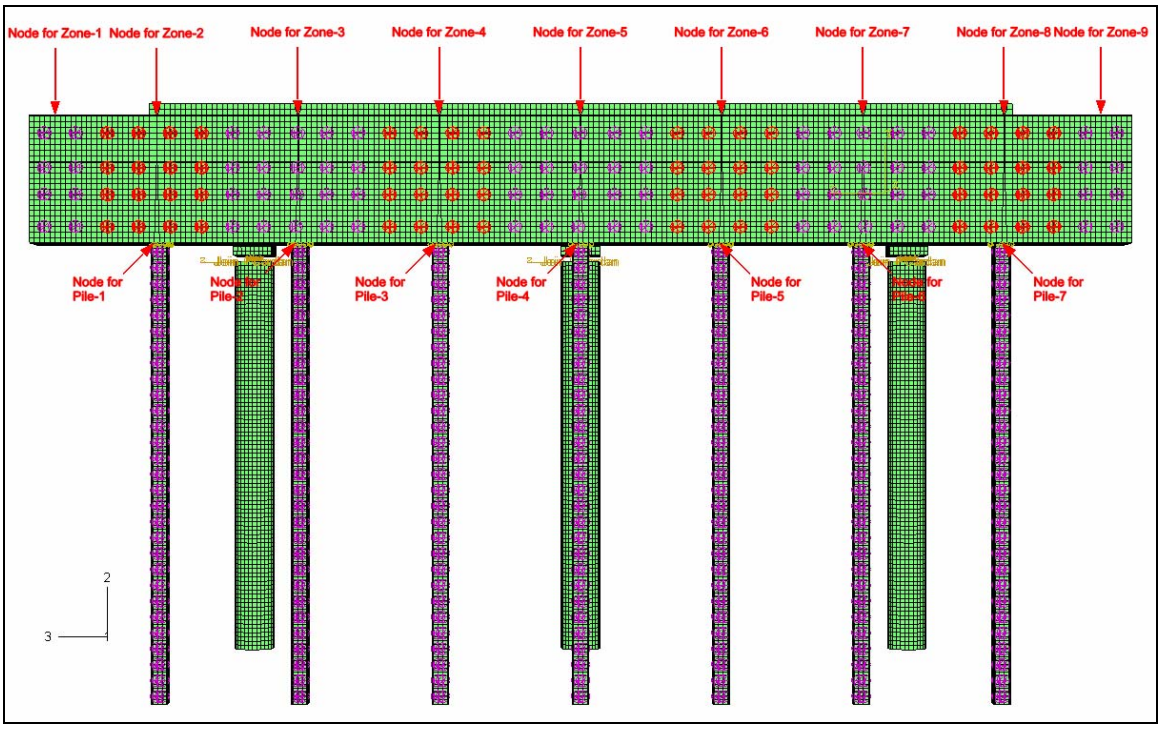

The procedure of determination of the spring stiffness based on one set of displacement results obtained after one iteration of the finite element analysis is as follows:

1. A normalized displacement of the abutment top $\left(\frac{\delta}{H}\right)$, where H = the abutment height, is determined based on the FE analysis output from the current iteration.

2. The coefficient of lateral earth pressure $K\left(\frac{\delta}{H}\right)$ generated due to the abutment motion, is then determined from the recommended response curves for the type of soil considered.
3. A vertical effective stress $\sigma_Z^{'}$ is calculated at each depth where the spring is attached as per the following equation.

   $$\sigma_z^{'} = \gamma z \qquad (3.7)$$

   where,

   $z =$ depth from abutment top. The effective weight of soil is equal to dry weight due to a deep ground water level.
4. The horizontal effective stress $\sigma_Y^{'}$ and the horizontal force F_Y at each spring depth are then calculated as per equations (3.8) and (3.9) respectively.

   $$\sigma_Y^{'} = K\left(\frac{\delta}{H}\right)\sigma_Z^{'} \qquad (3.8)$$

   $$F_Y = \sigma_Y^{'}\Delta A \qquad (3.9)$$
5. The stiffness of a spring $k_{i+1,k}$ is then calculated as described previously by equation (3.3) and used as input into the subsequent iteration.

3.4.2 Springs Behind Piles

Twenty-nine sets of two springs each, are attached behind each pile such that each spring has a tributary area of ΔA_P given by the following equation

$$\Delta A_P = \Delta L(\frac{B}{2}) \qquad (3.10)$$

where

$\Delta L = 12$ in and

$B =$ depth of the pile section = 12.2 in.

Thus, a total of 406 springs represent the soil behind the seven piles. Figure 3-9 shows the arrangement of springs behind a pile.

Prakash & Kumar (1996) proposed a method alternative to "*p-y*" curves, which describes a load-displacement relationship for a single laterally loaded pile by

considering the non-linear behavior of soil. The method is based on experimental observations collected from 14 full-scale lateral pile load tests reported by Mwindo (1992). This method describes a degradation of the spring stiffness at one meter depth below the pile head as a function of strain, according to the following equation.

$$k_h = a\gamma^{-b} k_{h\max} \tag{3.11}$$

where,

k_h = modulus of horizontal subgrade reaction [FL^{-2}];

$k_{h\max}$ = value of k_h at shear strain of 0.002 or 0.2% in sand;

γ = shear strain in sand;

a, b = empirical coefficients established by Mwindo (1992)

Prakash & Kumar (1996) expressed the average shear strain γ in terms of lateral displacement by the following equation:

$$\gamma = \frac{1+\upsilon}{2.5B} y_t \tag{3.12}$$

where,

υ = Poisson's ratio of sand;

B = width of the pile;

y_t = lateral displacement of the pile head for each individual pile as shown in Figure 3-9.

Figure 3-9 Arrangement of Springs Behind a Pile

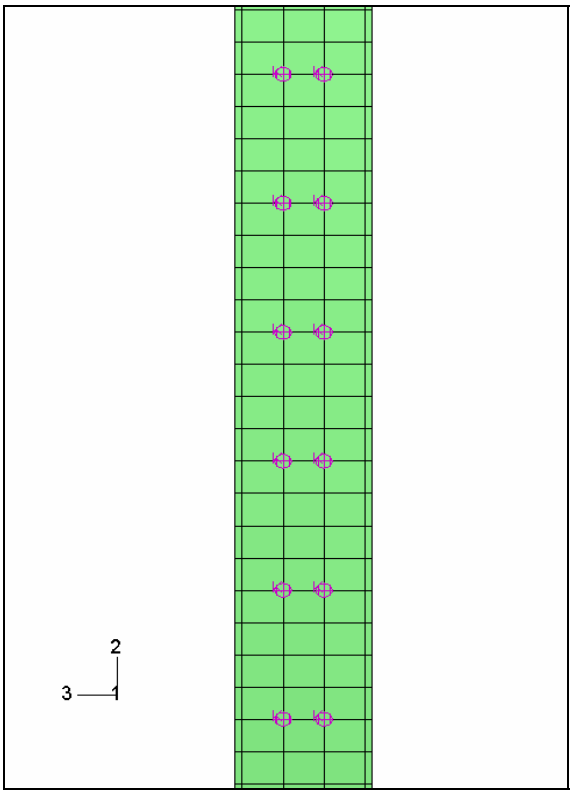

It was also assumed that the variation of the lateral spring stiffness with depth z is linear according to the following equation.

$$k_h = n_h z \tag{3.13}$$

where,

n_h = constant of horizontal subgrade reaction [FL^{-3}]

Thus, equations (3.12) and (3.13) provide the basis for the calculation of lateral spring stiffnesses for the springs adjacent to piles. $k_{h\,\max}$ is the input material parameter whose value is taken as 10.15 ksi for dense sand behind the piles and 10 ft to 15 ft deep ground water table, based on the recommendations given by Prakash & Kumar (1996).

The remaining input parameters for calculating the stiffnesses included the coefficients a and b in equation (3.10) whose values were selected to be equal to 0.05 and 0.5, respectively, as suggested by Mwindo (1992) for H steel piles.

3.4.3 Convergence of Iterations

At the end of each iteration errors e in δ_T, δ_R and y_t are calculated according to equations (3.14) and (3.15) respectively,

$$e(\delta_T) = \left| \frac{(\delta_T)_{i+1} - (\delta_T)_i}{(\delta_T)_{i+1}} \right| \tag{3.14}$$

$$e(\delta_R) = \left| \frac{(\delta_R)_{i+1} - (\delta_R)_i}{(\delta_R)_{i+1}} \right| \tag{3.15}$$

$$e(y_t) = \left| \frac{(y_t)_{i+1} - (y_t)_i}{(y_t)_{i+1}} \right| \tag{3.16}$$

The convergence criterion used herein requires that the errors given by equations (3.14), (3.15) and (3.16) must be less than or equal to 0.01 or 1%. Upon meeting these criteria, iterations are completed and final solution is obtained.

CHAPTER 4 Results And Discussion

The refined and detailed 3D finite element model of the "Bemis Road Bridge: F-4-20" over the Nashua River in Fitchburg, Massachusetts is analyzed using the finite element code ABAQUS/Standard 6.5-1. This chapter presents the results along with their verification and validation. An additional discussion is also included.

4.1 Nomenclature

Since the main objective of the numerical modeling was to assess the influence of temperature changes and the soil conditions on the response of the bridge, the conditions that covered a full range of soil densities and/or relative compactions for the soil adjacent to abutment were studied. The nomenclature of the cases studied is based on the soil densities recommended by the different design agencies. Table 4.1 lists the three soil combinations studied:

Table 4.1 Soil Combination Nomenclature

Case	Details
LD	Loose sand adjacent to abutment (using NCHRP,1991 design curve) and dense sand adjacent to piles
DD	Dense sand adjacent to abutment (using NCHRP, 1991 design curve) and dense sand adjacent to piles
DcD	Dense sand adjacent to abutment (using CGS, 1992 design curve) and dense sand adjacent to piles

In addition, three different values of temperatures change ranges were investigated in this research, thereby also replicating the response of longer bridges. Table 4.2 lists the nomenclature of the 9 cases thus analyzed herein.

Table 4.2 Nomenclature for the Cases Studied

ΔT(˚F) / Soil combination	60	80	100
LD	LD 60˚F	LD 80˚F	LD 100˚F
DD	DD 60˚F	DD 80˚F	DD 100˚F
DcD	DcD 60˚F	DcD 80˚F	DcD 100˚F

4.2 Results

Displacements and stresses obtained for DD 100˚F are presented in this section.

4.2.1 Displacements

Figures 4-1, 4-2 and 4-3 show the longitudinal displacements U1, the vertical displacements U2 and the lateral displacements U3 of the bridge, respectively. The corresponding coordinate system are shown in the figures.

Figure 4-1 DD 100˚F - Longitudinal Displacement U1 (in) of the Bridge (Deformation Scale Factor=130)

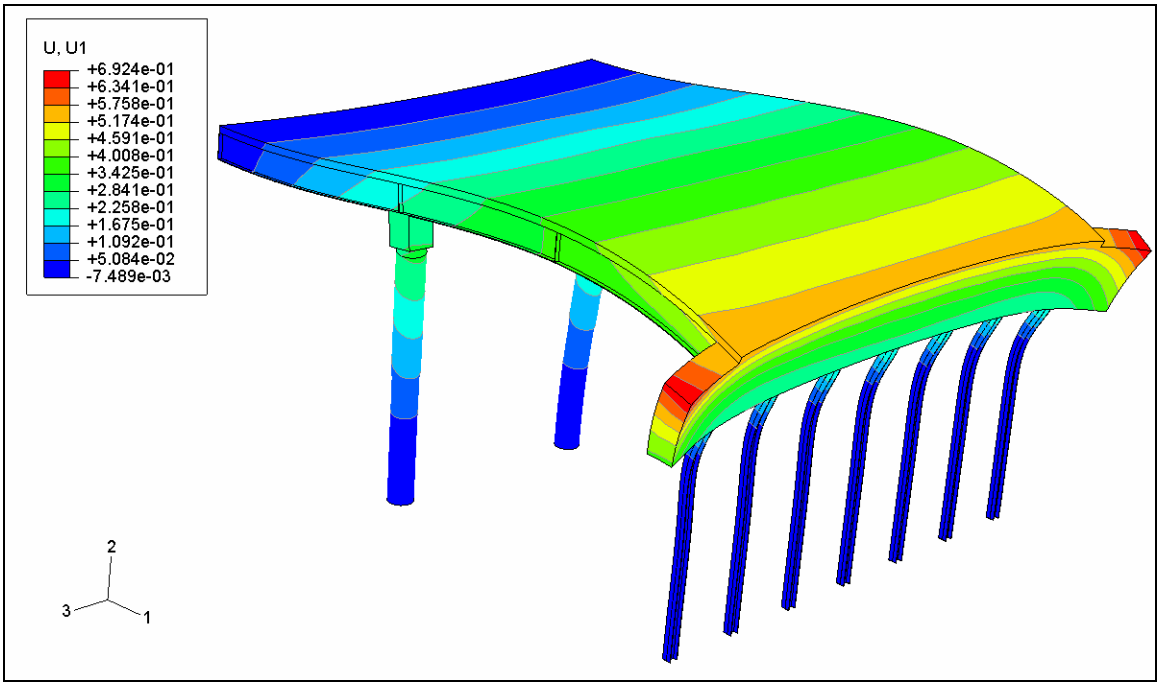

Figure 4-2 DD 100˚F - Vertical Displacement U2 (in) of the Bridge (Deformation Scale Factor=130)

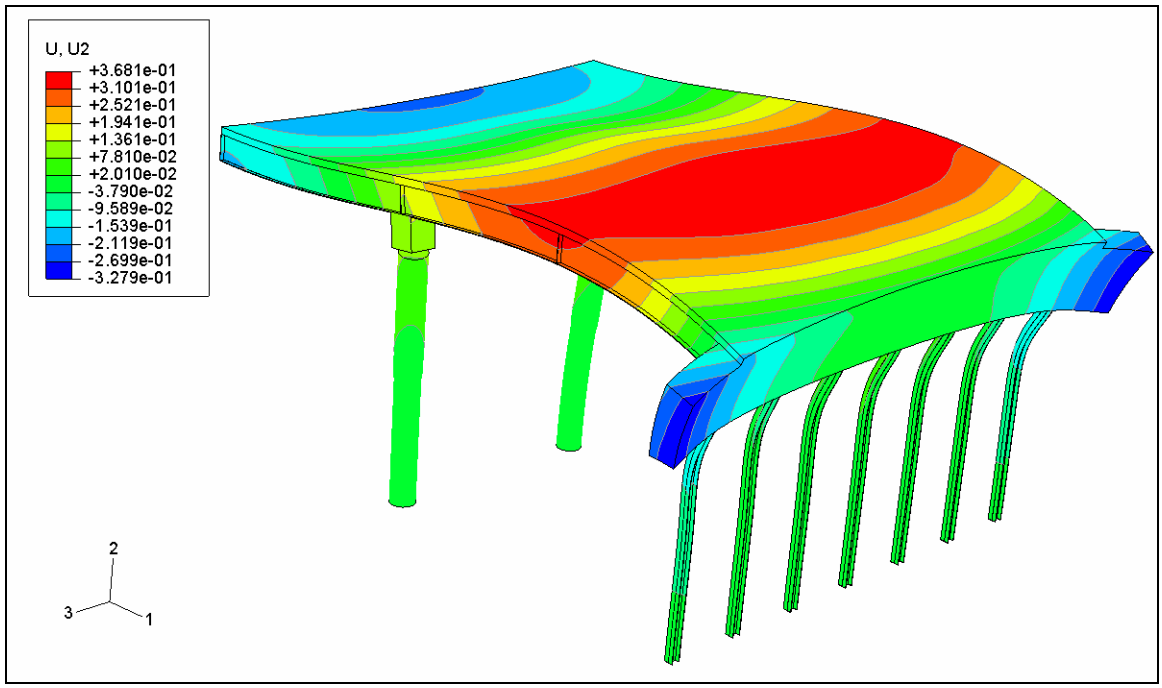

Figure 4-3 DD 100˚F - Lateral Displacement U3 (in) of the Bridge (Deformation Scale Factor=130)

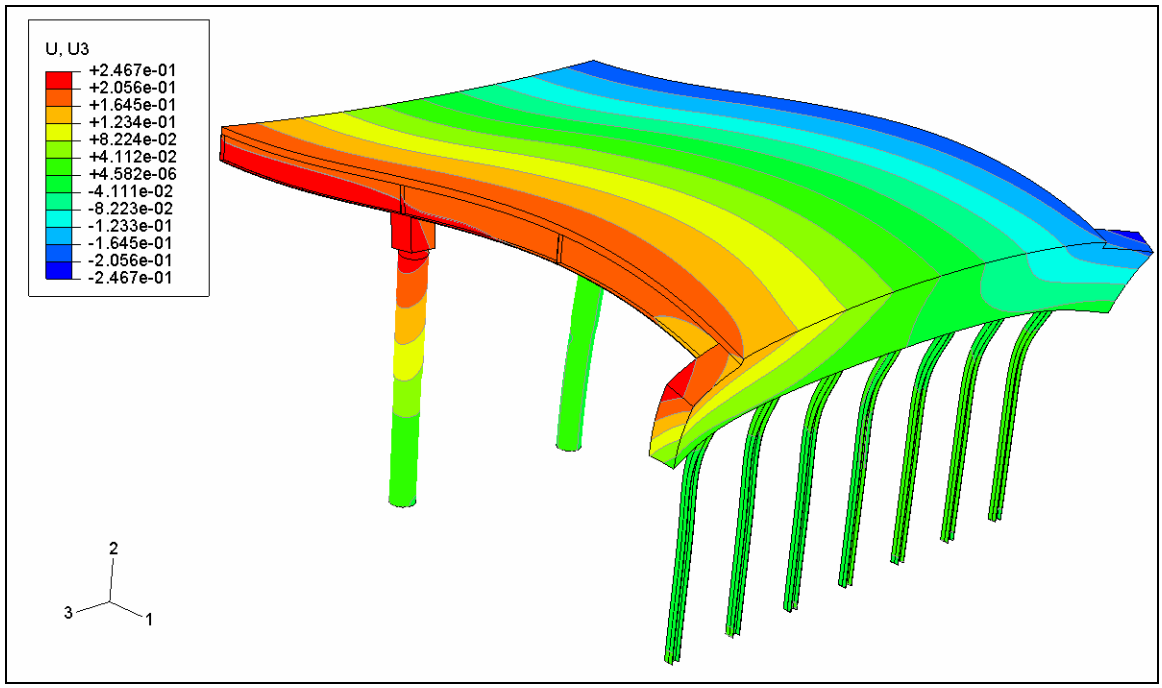

4.2.2 Stresses

Figure 4-4 shows the axial stress S22 in the central pile.

Figure 4-4 DD 100˚F - Axial Stress S22 in the Piles (Deformation Scale Factor=130)

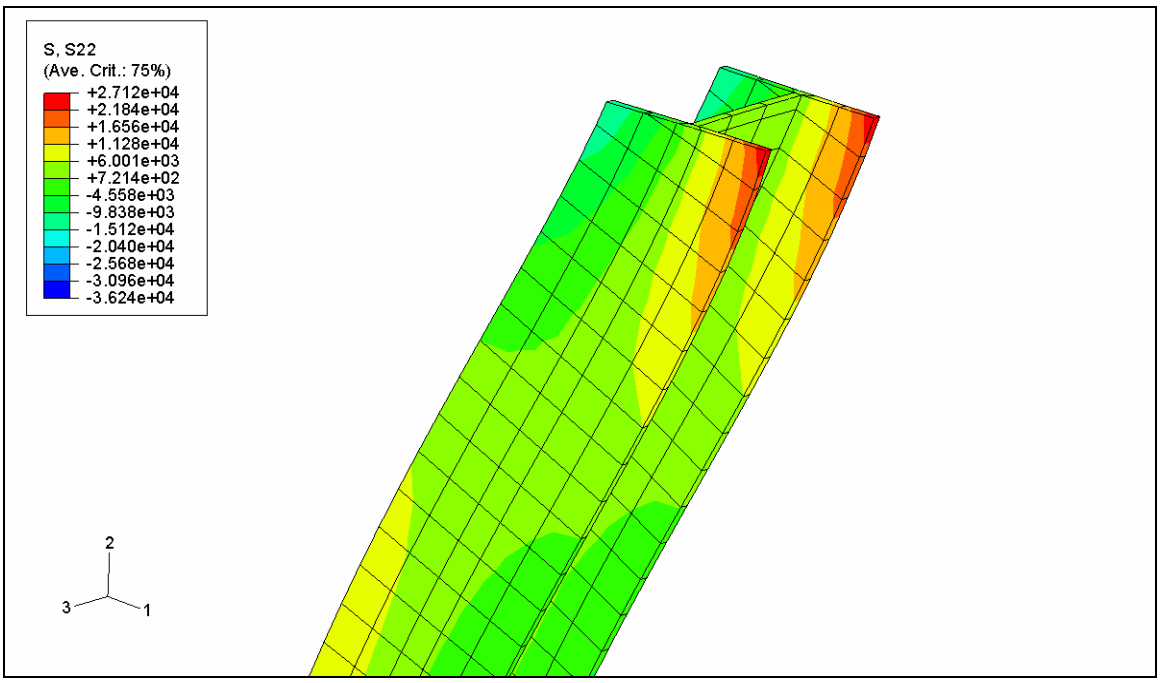

Figure 4-5 shows the axial stress S11 in the girders.

4.3 Comparison of the Two FE Models

In this research, the model used by Ting & Faraji (1998) has been refined. Certain modeling changes have also been incorporated as per the requirements by the KDOT. The differences are listed below:

4.3.1 Differences in the Bridge Model

Complete 3D model of the selected IAB: The model developed in this research does not include any simplifications. All parts of the bridge have been modeled using eight-node coupled temperature-displacement elements – C3D8T. On the other hand, Ting & Faraji (1998) had used 1D beam elements for girders, transverse beams and piles; and bending plate and shell elements for the deck and abutment walls. While rigid links were used to model the connection between deck slab and girders ensuring “strain

compatibility and shear transfer between the deck slab and girder elements" by Ting & Faraji (1998); the composite action at the connection of the deck and girders, for the model used in this research, is produced by no-slip connection using the "merge and tie" feature offered by ABAQUS/CAE 6.5-1.

Figure 4-5 DD 100˚F - Axial Stress S11 in the Girders (Deformation Scale Factor=130)

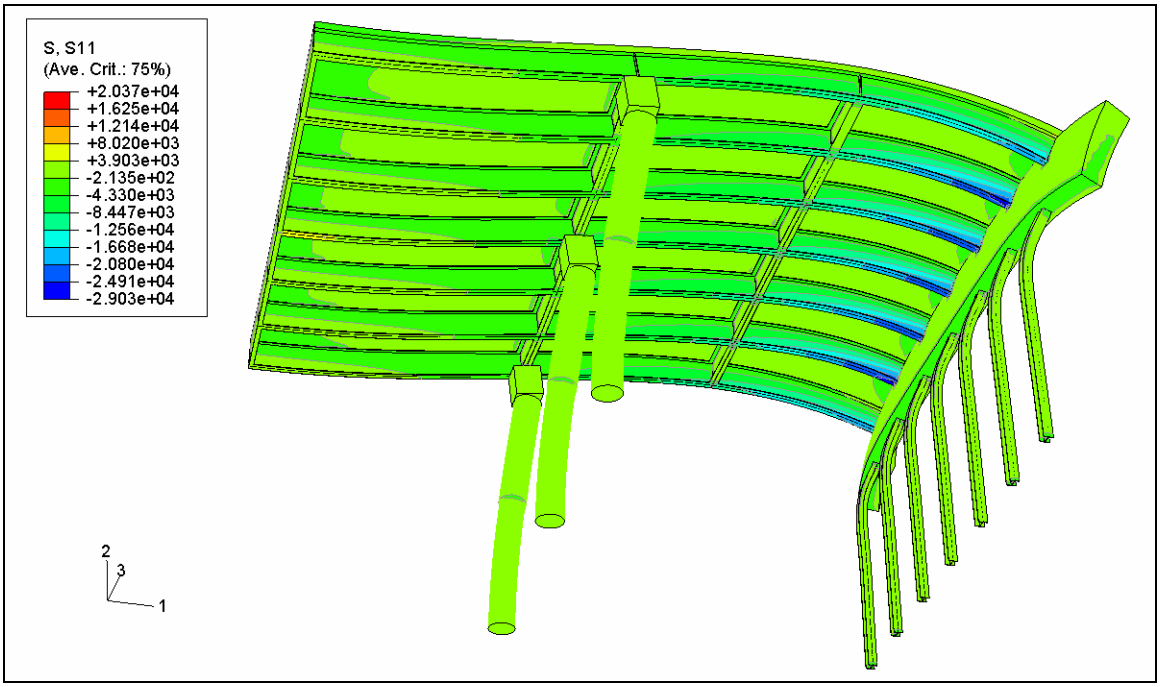

Hinges: To prevent any moment transfer to the piers, as required by KDOT, the connection between the bridge superstructure and the piers is modeled by a hinge using CONN3D2 connector elements. On the contrary, Ting & Faraji (1998) modeled a fixed connection between the bridge superstructure and piers.

Pier caps: A single pier cap of dimensions 3.5 ft x 3 ft x 56.5 ft, supported by three columns, was used by Ting & Faraji (1998). In this research, each pier was capped by an individual pier cap of dimension 3 ft x 3 ft x 3.5 ft.

Transverse beams: Eight lines of transverse beams were used by Ting & Faraji (1998), each consisting of channels and angles. In this research, seven lines of transverse steel beams of section W36x135 were used.

4.3.2 Differences in Material Properties

Coefficient of thermal expansion: While Ting & Faraji (1998) used a coefficient of thermal expansion α of 6.5 x 10^{-6} per ˚F for the composite deck, this research uses two different values of coefficient of thermal expansion α, one for concrete and one for steel as listed in Table 3.1, according to the recommendations of KDOT Bridge Design Manual (2007).

4.3.3 Differences in Soil Model

Soil adjacent to abutment: The $K - \delta$ relationships used for dense and loose soils as recommended by NCHRP (1991) were also used by Ting & Faraji (1998). In addition, the recommendations by CGS (1992) have also been used in this research. However, an iterative equivalent linear approach was been adopted in this research, while Ting & Faraji (1998) used nonlinear springs. The unit weights of the soils used for this research are listed in Table 3.3. Ting & Faraji (1998) used the unit weight of 120 lb/ft^3 regardless of the soil density and they did not quantify the soil density either in terms of relative density or relative compaction.

Soil adjacent to piles: Ting & Faraji (1998) adopted the "*p*-*y*" design curves recommended by American Petroleum Institute (1993) for nonlinear force-deflection relations for the soil adjacent to the piles. On the other hand, a method proposed by Prakash & Kumar (1996) as alternative to "*p*-*y*" curves was used herein. The method describes a load-displacement relationship for a single laterally loaded pile by considering the non-linear behavior of soil.

4.3.4 Differences in Loads

Self-weight: The analysis for this research includes load application in two steps as discussed in section 3.2. Ting & Faraji (1998) applied only the thermal loading without the self-weight.

Thermal gradient within the abutment: Ting & Faraji (1998) applied the thermal loading only to the composite deck. Abutment was not subjected to any temperature changes. Herein, a thermal gradient was applied within the abutment wall (Figure 4-6) in order to better model the transition of temperatures within the bridge structure as experienced in the field. Figure 4-6 shows the thermal gradient in the abutment

simulating the field conditions whereby the part of the abutment exposed to atmosphere gets heated up while the part that is not exposed remains at a lower temperature.

Figure 4-6 Thermal Gradient in the Abutment (ΔT = 80˚ F)

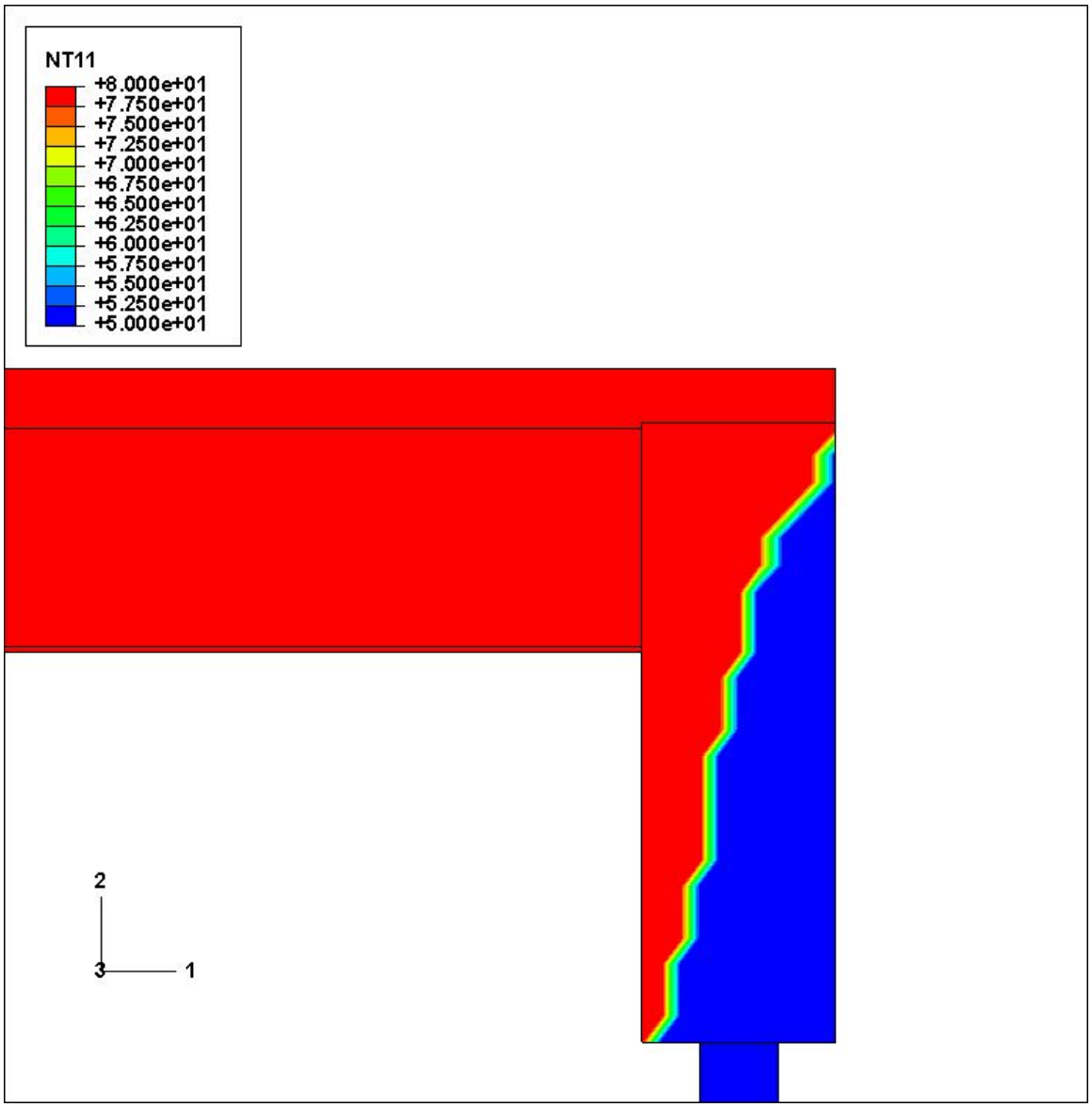

4.4 Validation and Verification of the Model

The method of analysis described in Chapter 3 was first validated and verified against the results reported by Ting & Faraji (1998). For that purpose, the same coefficient of thermal expansion α of 6.5 x 10^{-6} (per ˚F) was used for both steel and concrete as done by Ting & Faraji, 1998 and FE analysis was conducted for the loading

case DD 80˚F. The unit weight on the soil was also changed to 120 lb/ft^3, disregarding the relative density D_r and relative compaction R . In addition, gravity load was removed and hinge connection was replaced by a fixed connection in accordance to the model of Ting & Faraji (1998). Also, in this case there was no internal temperature gradient within the abutment. All other modeling differences as explained in section 4.2 remained as they were.

The results so obtained during the validation process were close to those reported by Ting & Faraji (1998) as depicted in Figure 4-7. Small differences are attributed to the differences in the FE models as explained in section 4.3.

Figure 4-7 Comparison of Longitudinal Displacements, U11 (in)

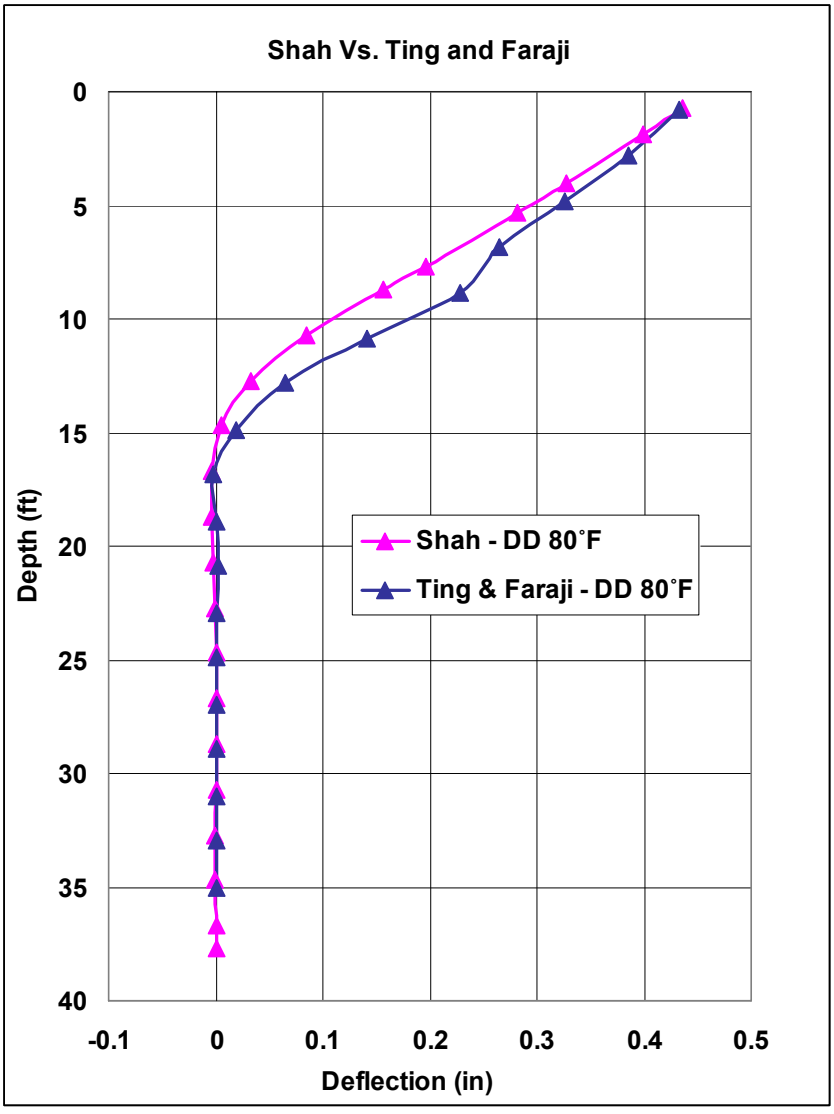

Based on the comparison presented in Figure 4-7 between the results obtained herein and those obtained by Ting & Faraji, 1998, it was concluded that the model used for this research is sufficiently verified and validated.

4.5 Results and Discussion

Each set of results is presented in two formats. The first format shows the trends observed due to different temperature changes for the selected soil properties. The second format shows the trends observed due to different soil properties for a selected thermal load.

Table 4.3 lists the converged values of the coefficients of lateral earth pressure *K* for the soil behind the abutment for the nine cases analyzed.

Table 4.3 Converged values of the coefficient of lateral earth pressure *K*

Soil combination / Temperatures	LD	DD	DcD
60˚F	1.029	4.235	2.853
80˚F	1.2179	4.698	3.127
100˚F	1.293	5.362	3.3709

As per the design curves by NCHRP, 1991 the fully passive state for loose sand is reached when the value of coefficient of lateral earth pressure *K* is 3.0, while for dense sand, the value is 5.8. The design curves by CGS, 1992 indicate a value of 8.3 for coefficient of lateral earth pressure *K* at fully passive state. Thus none of the analyses conducted herein resulted in reaching the failure stage. Though DD 100˚ F comes close to failure state, DcD 100˚ F still remains far from failure. The converged values of *K* for 100˚F are depicted in Figures 4-8 and 4-9.

Figure 4-8 Converged Value of K for 100˚F – DcD case

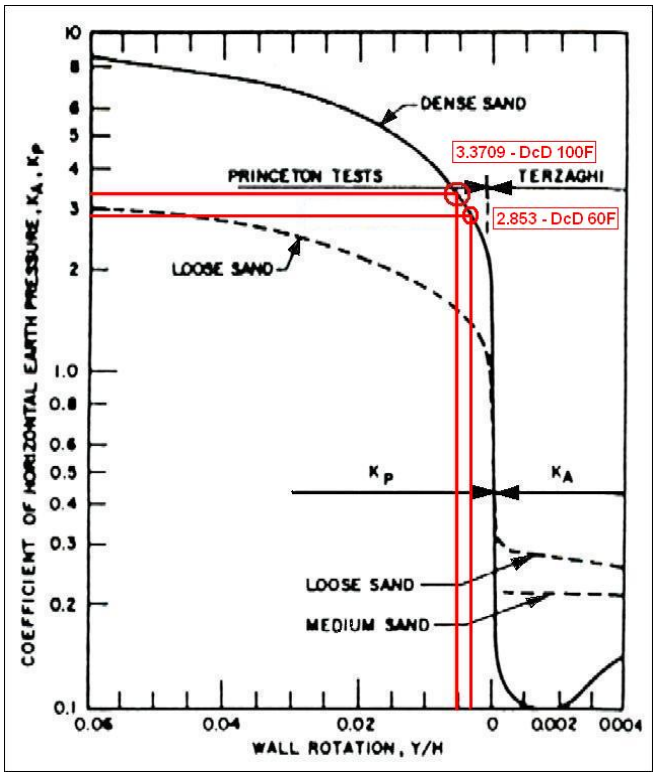

Figure 4-9 Converged Value of K for 100˚F – DD and LD cases

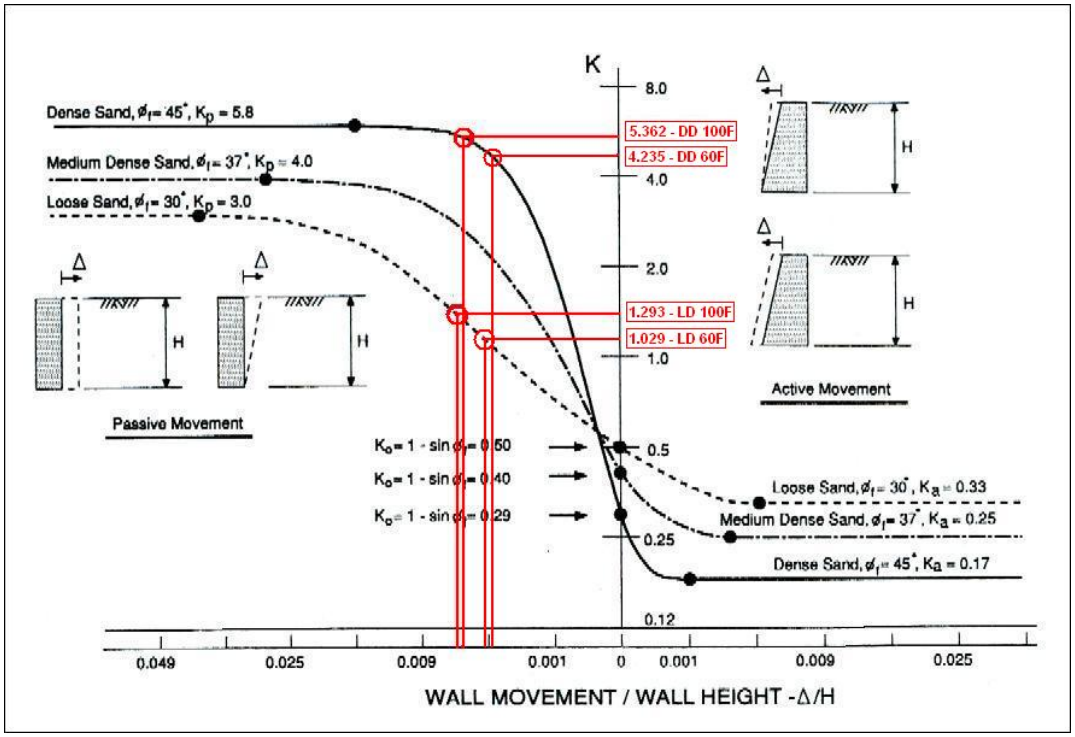

4.5.1 Longitudinal Displacement at Centerline of the Bridge

4.5.1.1 Trends Due to Change in the Thermal Load for the Particular Soil Properties

Figure 4-10 Trends in Longitudinal Displacement Due to Changes in Thermal Load

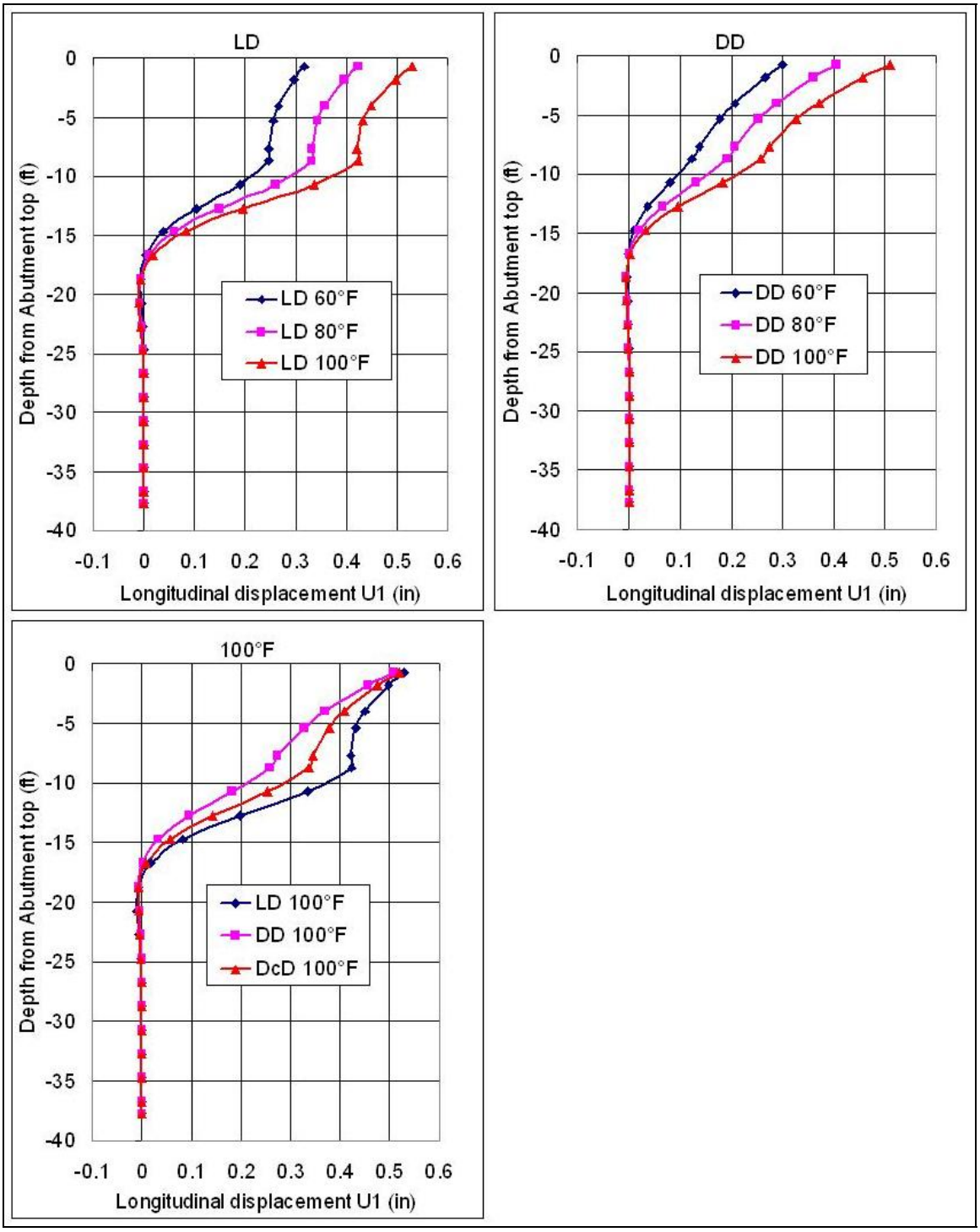

4.5.1.2 Trends Due to Change in Soil Properties for the Particular Thermal Load

Figure 4-11 Trends in Longitudinal Displacement Due to Changes in Soil Properties

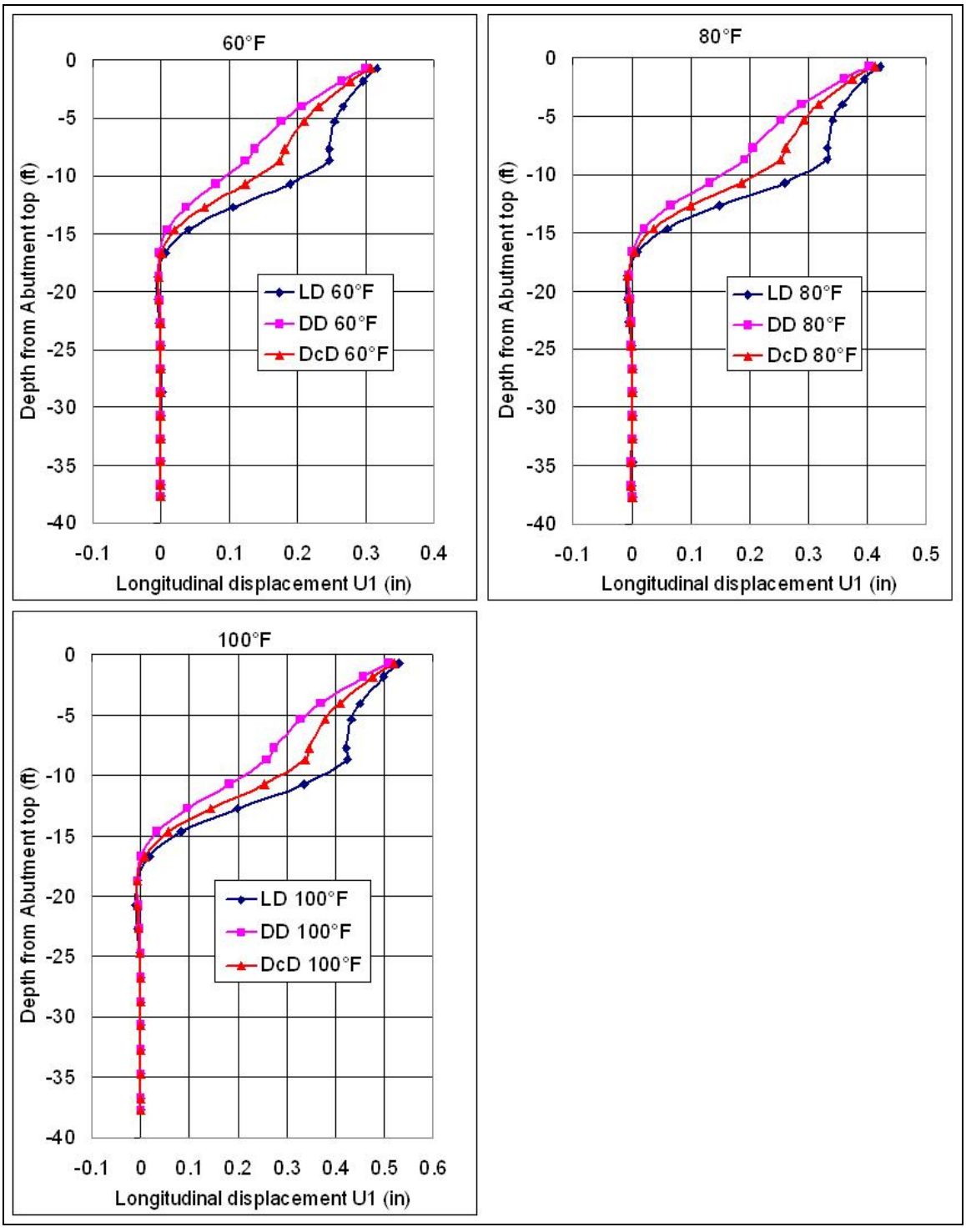

4.5.1.3 Discussion

Based on the plots in Figure 4-10, it can be stated that the behavior of the bridge is qualitatively independent of the temperature change range for the selected soil properties. On the contrary, plots in Figure 4-11 clearly indicate that the behavior of the bridge is qualitatively and quantitatively dependent on the soil properties. Figure 4-11 indicated that properties if the soil behind abutment have a significant influence on the pile head displacement. Specifically, for any given range of temperature change, the pile head displacement is reduced by 39% or more when relative compaction of the soil is increased from 90% to 96%. It is also observed from the plots in Figure 4-10 that the displacements are varying in a linear fashion with the change in temperature, for the particular soil properties. The displacements at the abutment top are extracted from these results and plotted versus temperature changes in (Figure 4-12) which confirms the linearity of the results. It is also observed from this plot that soil properties have negligible influence on the displacement of the deck.

Figure 4-12 Displacement at the Abutment Top vs. ΔT

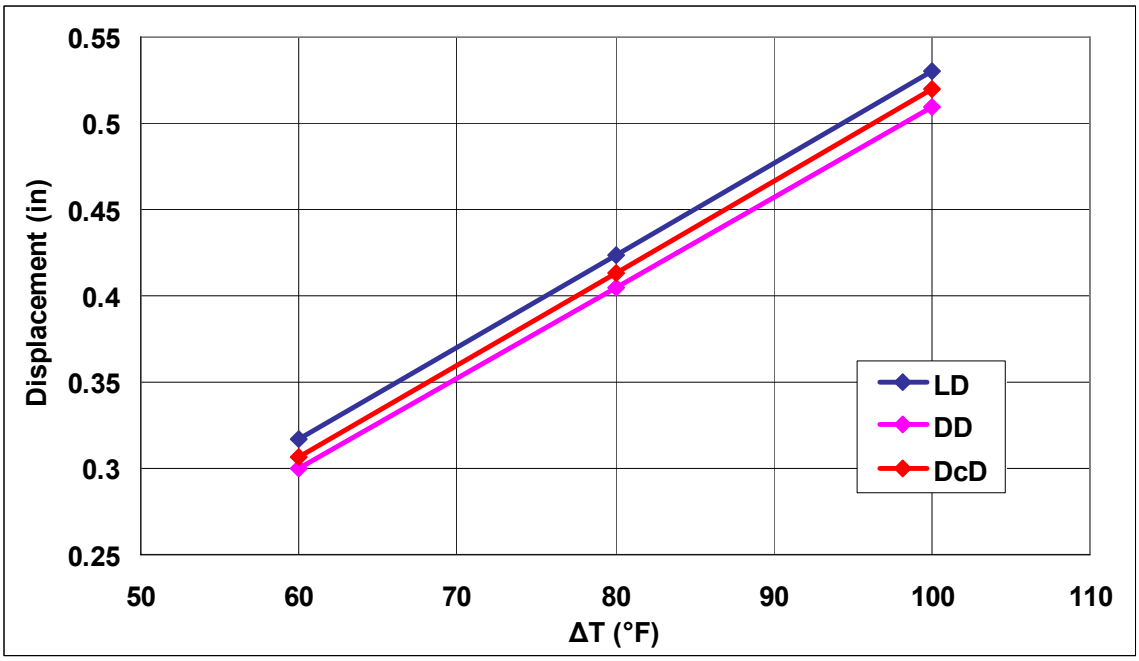

Another behavior observed is the bending of the abutment, which becomes less significant when the soil adjacent to the abutment gets denser. While this bending of the

abutment originates from the thermal gradient of the temperatures applied to the abutment, the density of the soil adjacent to the abutment controls the extent of bending taking place. The bending behavior is prominent in the LD case, the effect gets reduced for DcD case and even more so for DD case (Figure 4-11). This is due to the fact that the soil stiffness increases at a faster rate with depth when the soils are denser. So while the translation of the abutment (δ_T) is significantly higher than the rotation (δ_R) of the abutment in LD case, the difference gets reduced as the soil behind the abutment becomes denser as demonstrated by DcD case depicted in Figure 4-13. Moreover, in DD case rotation is larger than translation, but the difference gets reduced with increase in the temperature range resulting in the rotation being equal to translation for temperature change of 100 ° F (Figure 4-13).

Figure 4-13 δ_T and δ_R Vs. ΔT

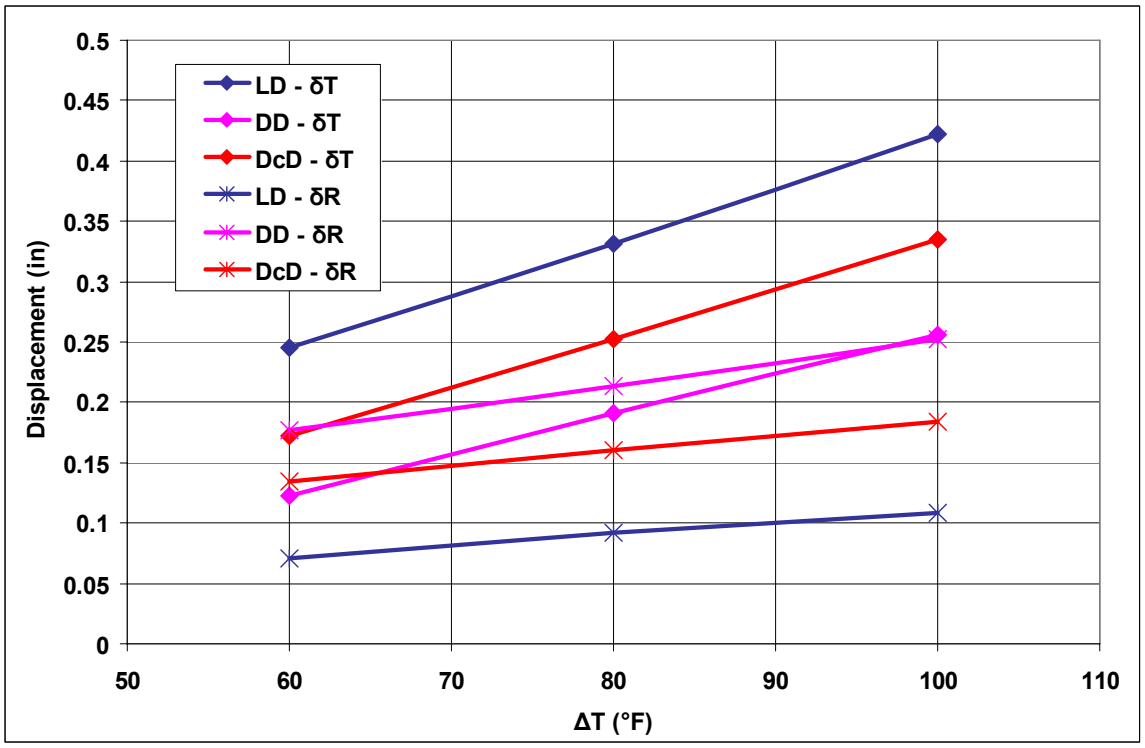

Figures 4-11 and 4-12 clearly show that while the displacement at the abutment top is very similar for a given temperature change and for all soil properties, it starts to vary with depth (Figure 4-11), depending on the type of soil adjacent to the abutment.

It is noteworthy to mention that the displacement at the pile top is dictated mainly by the type of soil behind the abutment. The deflected shape of the pile remains the same for different soils behind the abutment. Also the depth at which the lateral pile deflection becomes negligible is slightly affected by the soil type behind the abutment; i.e. the depth is larger for LD case than for DD and DcD cases (Figure 4-11). These trends can be explained by the presence of same soil behind the piles in all cases, showing that the influence of the type of soil adjacent to the abutment on the pile behavior diminishes as one goes deeper along the pile length.

Plots in Figure 4-14 show the comparison of displacements at various locations along the depth from the deck to the pile top and compare it with the deck displacement calculated analytically by using the following equation:

$$\Delta l = \alpha_{comp} \Delta T \frac{L}{2} \tag{4.1}$$

where,

$\Delta l =$ expansion of the deck for half of the bridge

$\Delta T =$ temperature change

$\frac{L}{2} =$ Half-length of the bridge = 75ft

$\alpha_{comp} =$ composite coefficient of thermal expansion of the concrete deck and steel girders calculated using the following equation:

$$\alpha_{comp} = \frac{\alpha_s A_s + \alpha_c A_c}{A_s + A_c} \tag{4.2}$$

where,

$\alpha_c, \alpha_s =$ coefficients of thermal expansion of concrete and steel, respectively, as listed in Table 3.1

$A_c, A_s =$ total area of cross-section of the concrete deck and steel girders, respectively.

Figure 4-14 Comparison of Deck Displacement

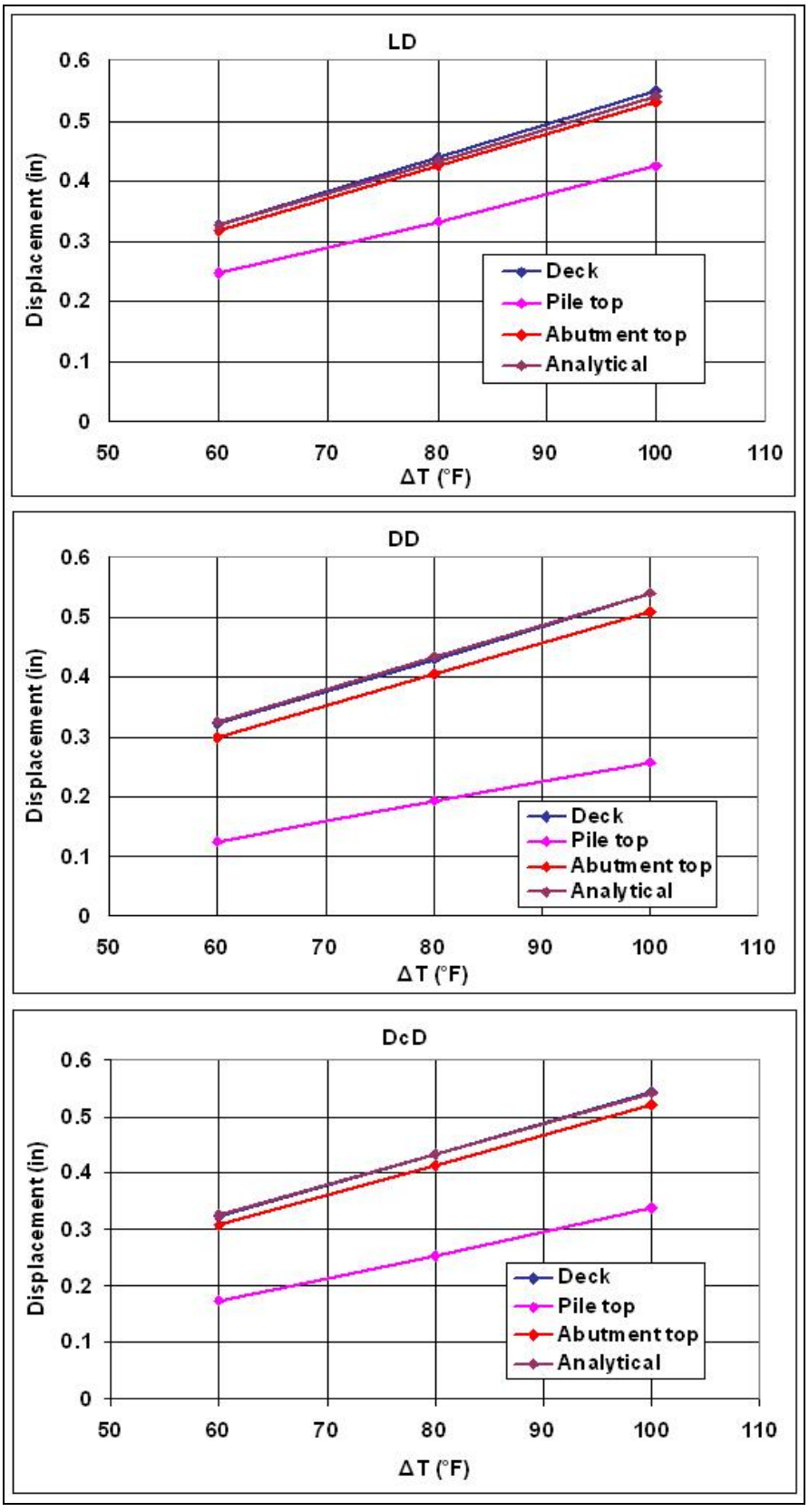

Figure 4-14 shows that presence of soil has virtually no influence on the deck displacement. This is confirmed by the fact that the deck displacement obtained from FE simulation matches very closely to the one calculated from Equation (4.1). The longitudinal displacement of the abutment top is affected by the presence of soil, more significantly in the DD case than in the DcD case. In LD case influence of soil on the abutment top displacement is negligible. However, the longitudinal displacement of the pile top is significantly affected by the presence of soil behind abutment in all cases studied. The largest difference between long displacements of the abutment top and bottom displacement is observed in DD case which is followed by DcD case. The difference is the smallest in the LD case.

4.5.2 Central Pile Bending Moment

4.5.2.1 Trends Due to Change in Thermal Load for the Particular Soil Properties

Figure 4-15 Trends in Central Pile Bending Moment Due to Changes in Thermal Load

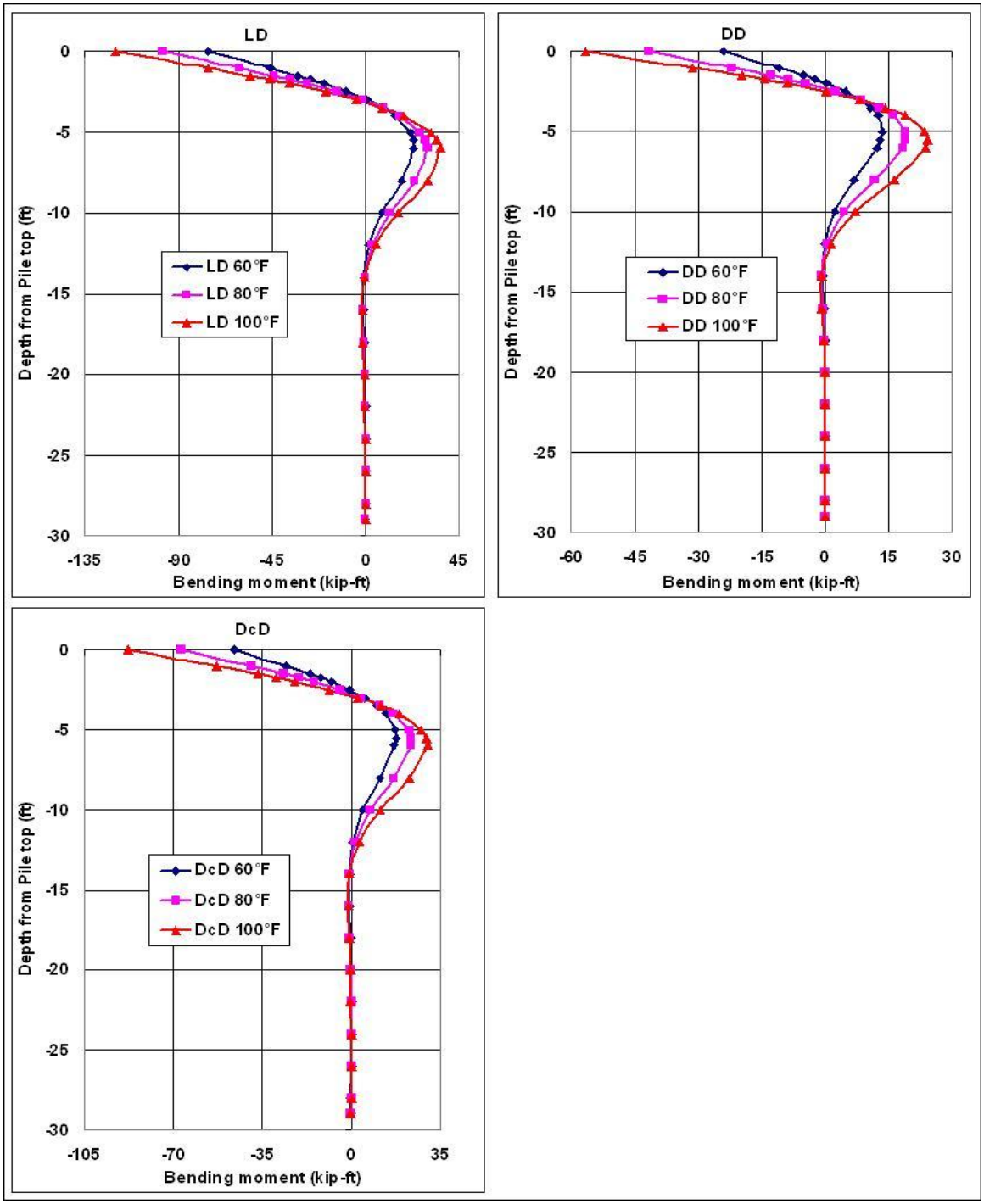

4.5.2.2 Trends Due to Change in Soil Properties for the Particular Thermal Load

Figure 4-16 Trends in Central Pile Bending Moment Due to Changes in Soil Properties

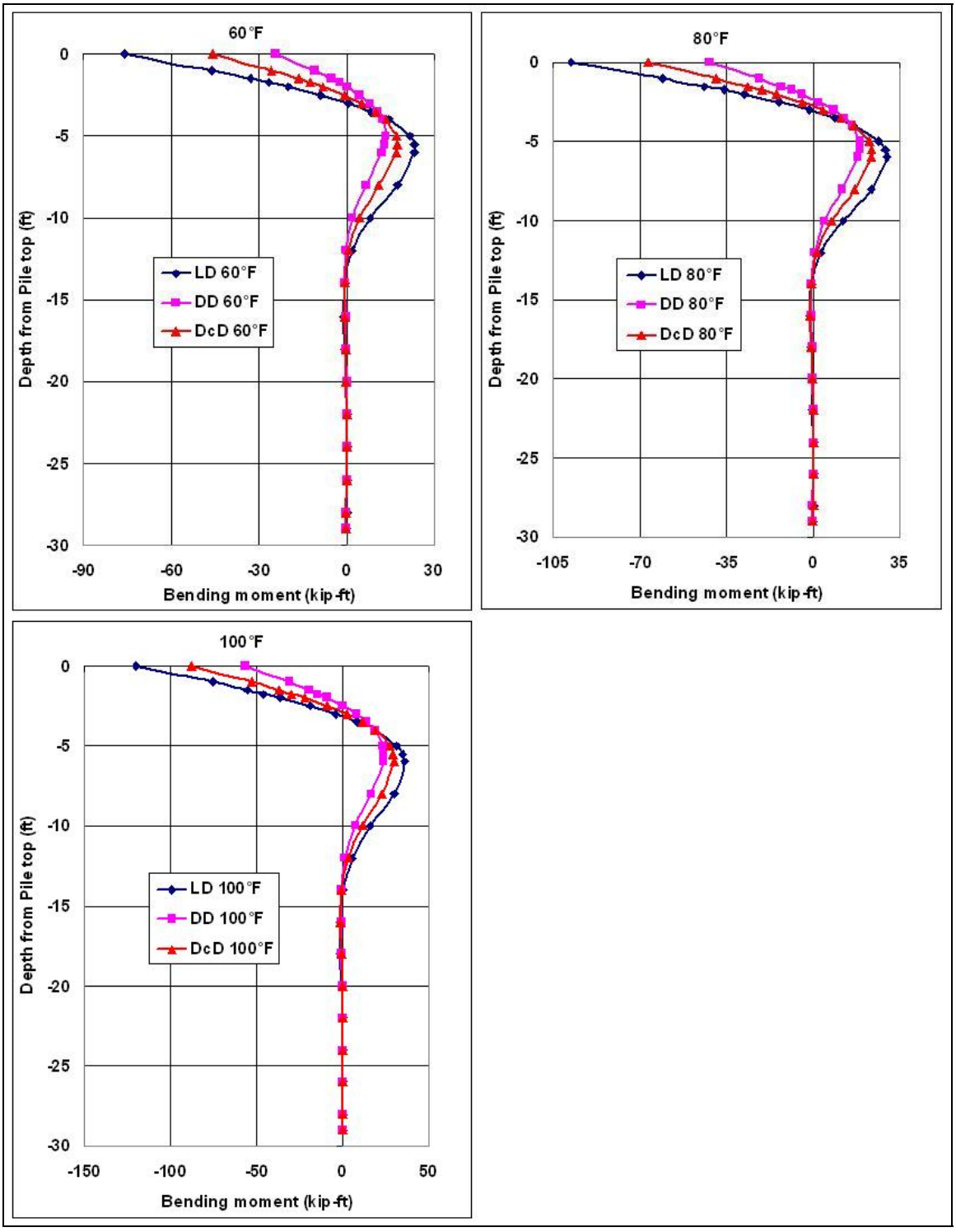

4.5.2.3 Discussion

The displacements at the pile top are extracted from these results and plotted versus temperature changes in (Figure 4-17) which confirms the linearity of the results. It is also observed from this plot that soil properties have major influence on the displacement of the pile top.

Figure 4-17 Displacement at the Pile Top in Central Pile vs. ΔT

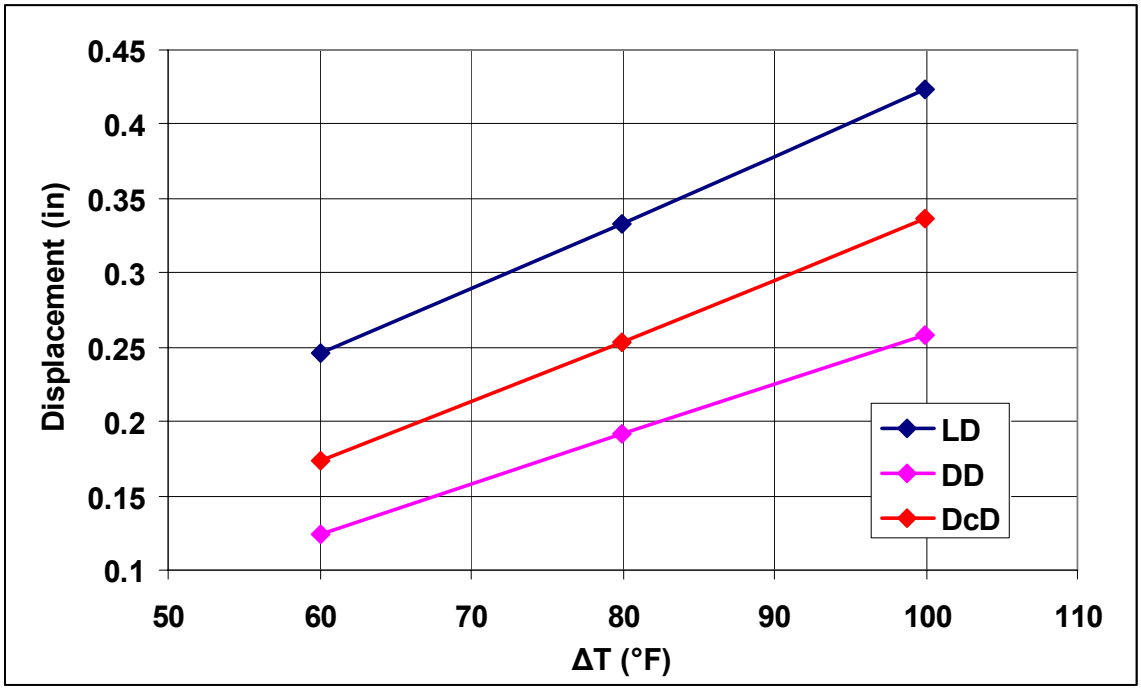

The bending moment in a pile depends mainly on the pile top displacement y_t. y_t is in turn dependent on the temperature change range, the stiffness of the soil adjacent to the abutment and piles, and stiffness of the pile itself. The larger the value of y_t, the larger is the maximum bending moment, which is located at the pile top. Thus, for the particular soil properties, higher temperature change produces, larger y_t resulting in larger maximum bending moments (Figure 4-15). The difference between maximum bending moments at $\Delta T = 60^{\circ}$ F and $\Delta T = 100^{\circ}$ F is the largest for LD case and equal to 44.4604 kip-ft.

Figure 4-18 Maximum Bending Moment in Central Pile Vs. ΔT

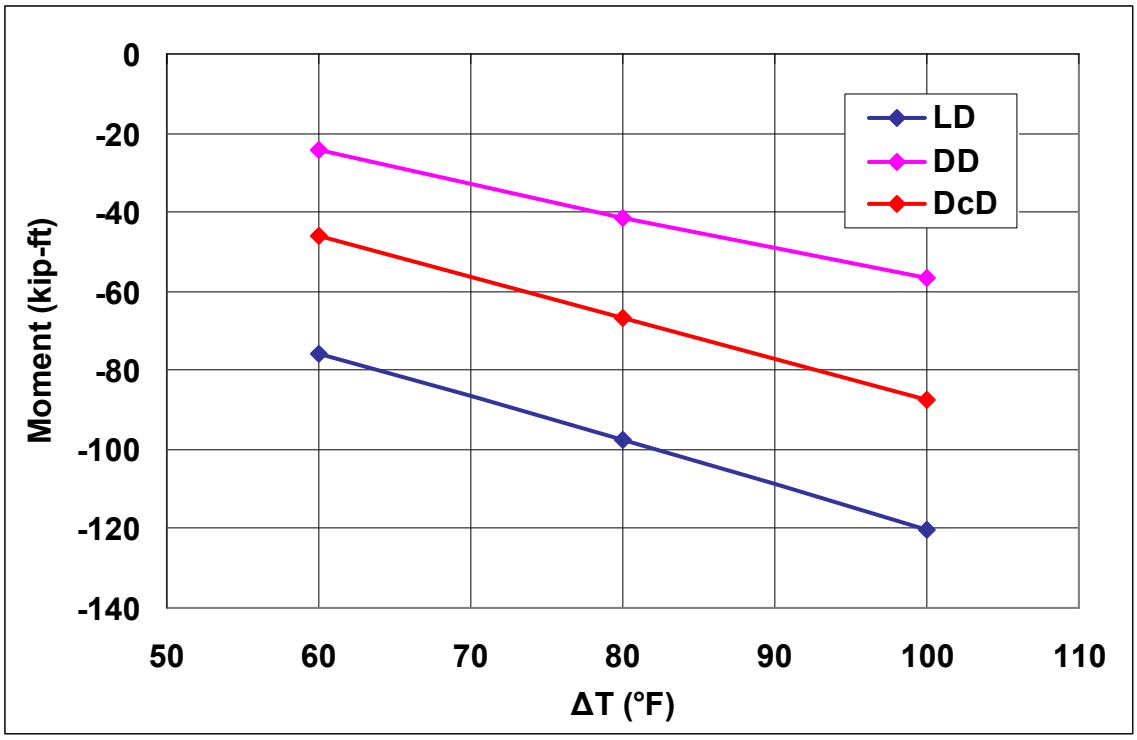

For a particular temperature change, looser soil behind abutments results in larger y_t and subsequently larger maximum bending moment. As the soil gets denser, y_t decreases thereby reducing the value of the maximum bending moment. Difference between maximum bending moments for any given temperature change range, due to different soils are significant. Maximum bending moment for DD case is about 47% of the maximum bending moment for LD case. Thus, maximum bending moments which occur at the pile head are significantly influenced by the change in the stiffness of the soil behind the abutment. Change in relative density from 50% to 80%, which corresponds to change in relative compaction from 90% to 96% reduces maximum bending moment by about 53% or more for any temperature change ranges considered herein. The reduction in bending moments is more significant for lower temperature change range (Figure 4-18)

4.5.3 Central Pile Bending Stress

4.5.3.1 Trends Due to Change in Thermal Load for the Particular Soil Properties

Figure 4-19 Trends in Central Pile Bending Stress Due to Changes in Thermal Load

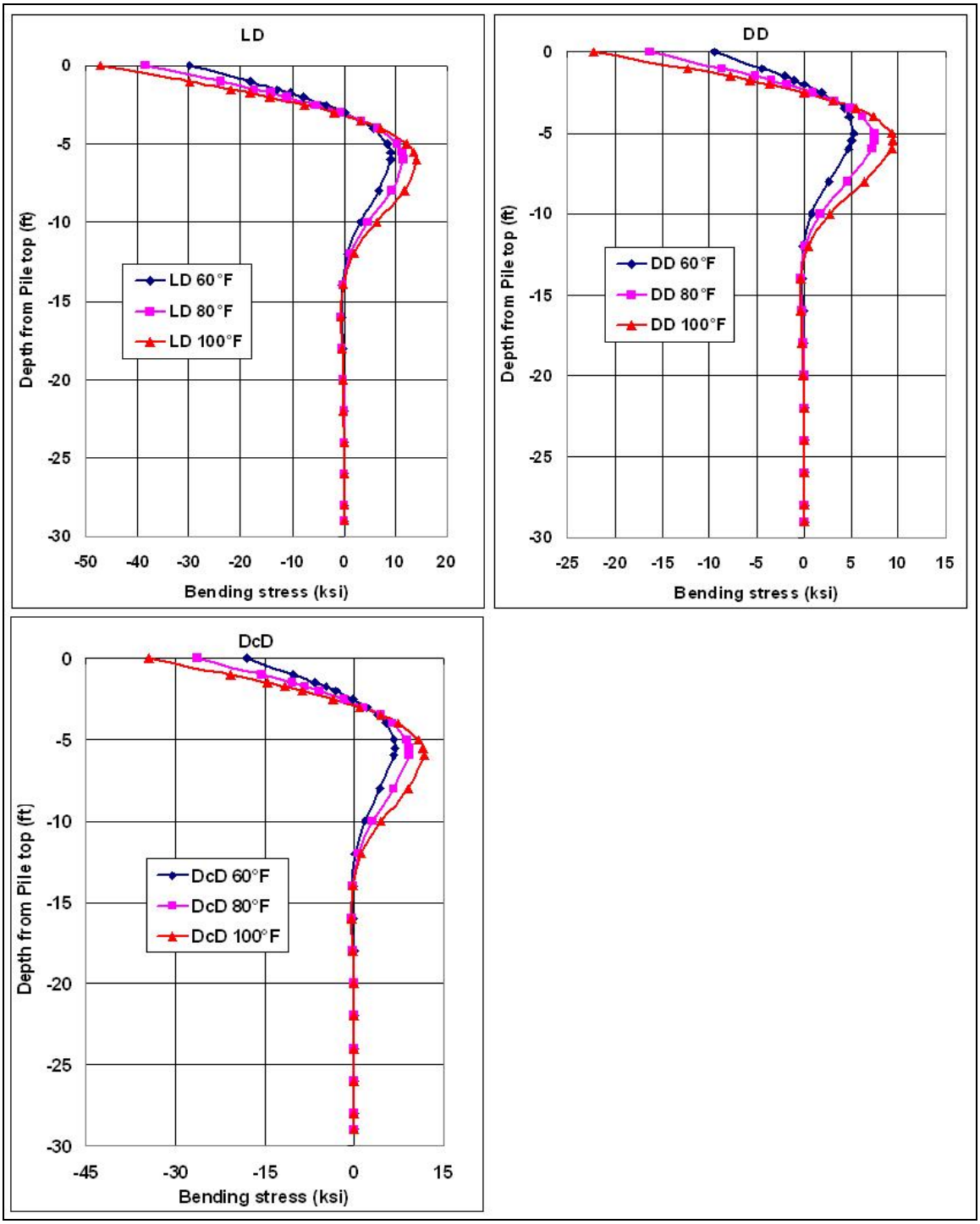

4.5.3.2 Trends Due to Change in Soil Properties for the Particular Thermal Load

Figure 4-20 Trends in Central Pile Bending Stress Due to Changes in Soil Properties

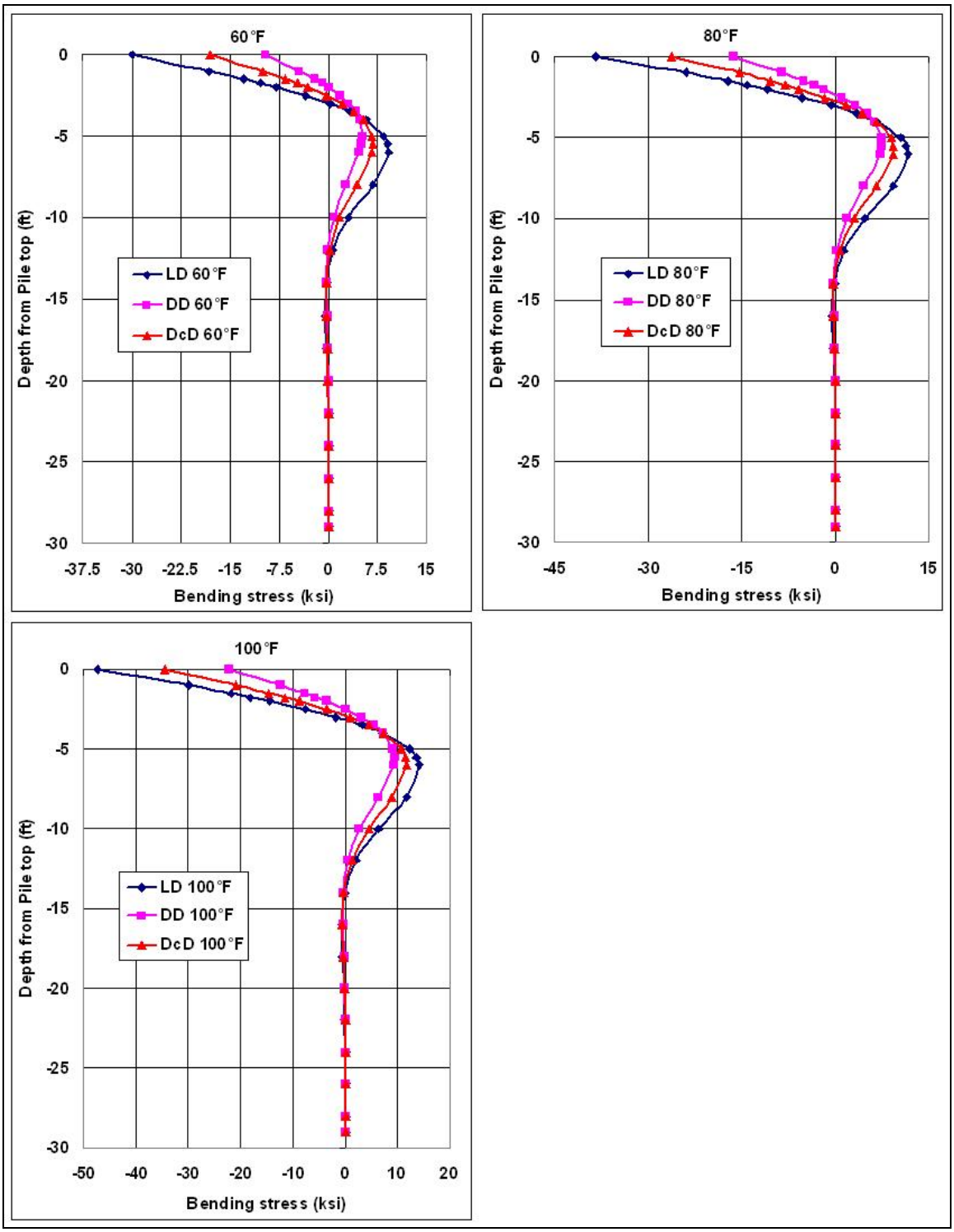

4.5.3.3 Discussion

The bending stresses in piles are directly dependent on the bending moment. Thus a higher bending moment results in a higher bending stress on the pile cross-section. Figures 4-19 and 4-20 clearly indicate this trend. The behavior observed in these two figures corresponds to trends in Figures 4-15 and 4-16, respectively.

Figure 4-21 confirms the observation of linearity of the results with temperature change range for the particular soil properties. It is important to note the sign convention employed for presenting the results for normal stresses: tension is positive and compression is negative.

Figure 4-21 Maximum Bending Stress in Central Pile vs. ΔT

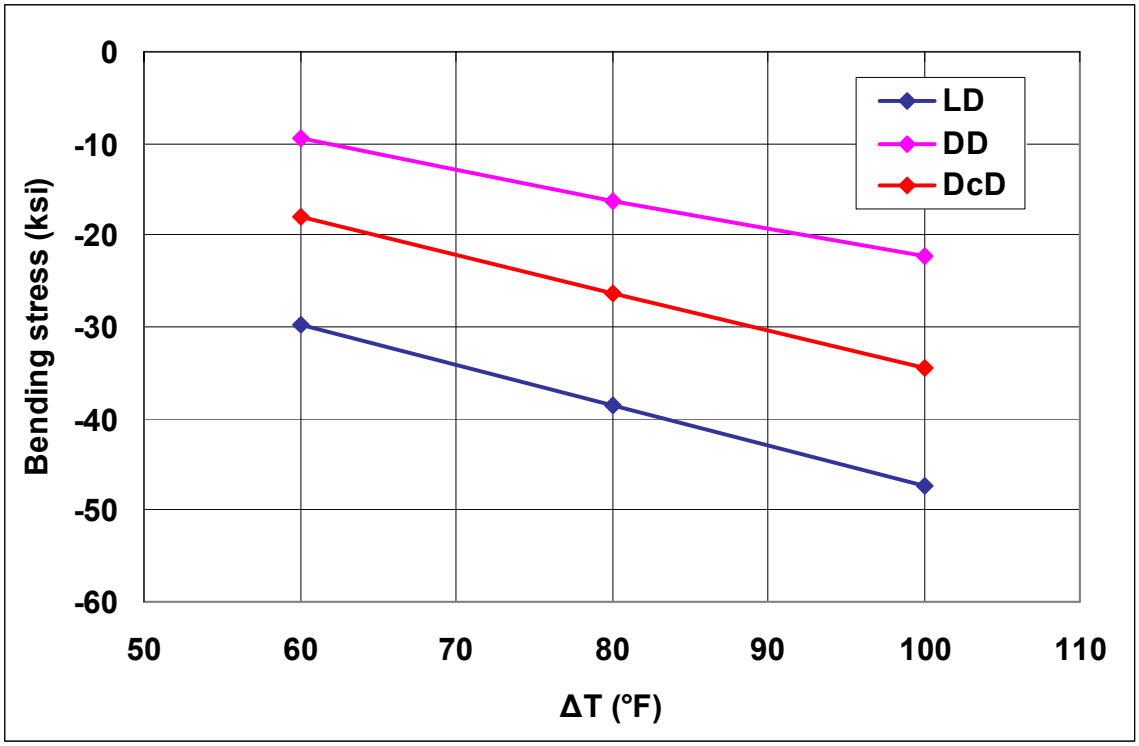

4.5.4 Soil pressure on abutment

4.5.4.1 Trends Due to Change in Thermal Load for the Particular Soil Properties

Figure 4-22 Trends in Soil Pressure on Abutment Due to Changes in Thermal Load

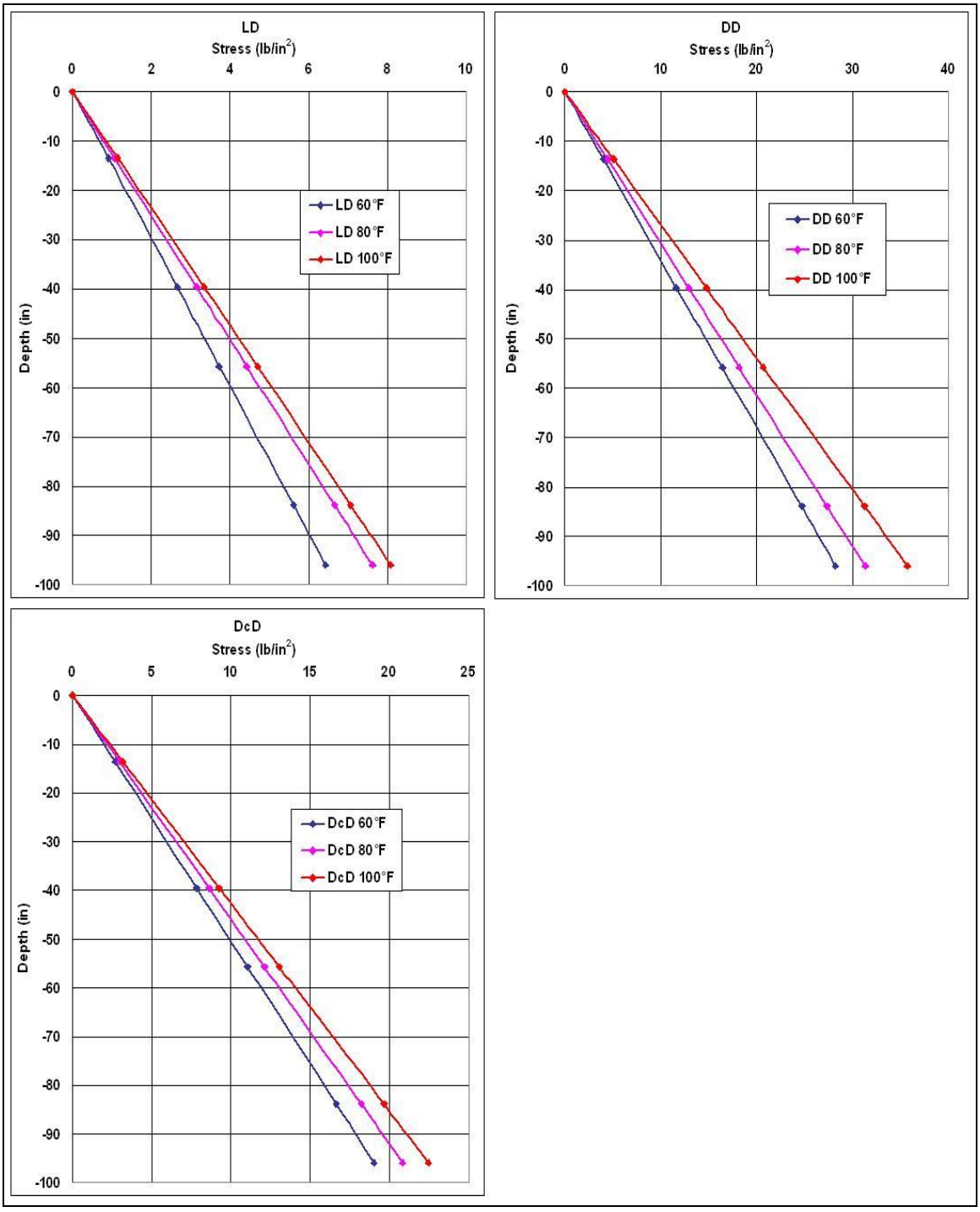

4.5.4.1 Trends Due To Change in Soil Properties for the Particular Thermal Load

Figure 4-23 Trends in Soil Pressure on Abutment Due to Changes in Soil Properties

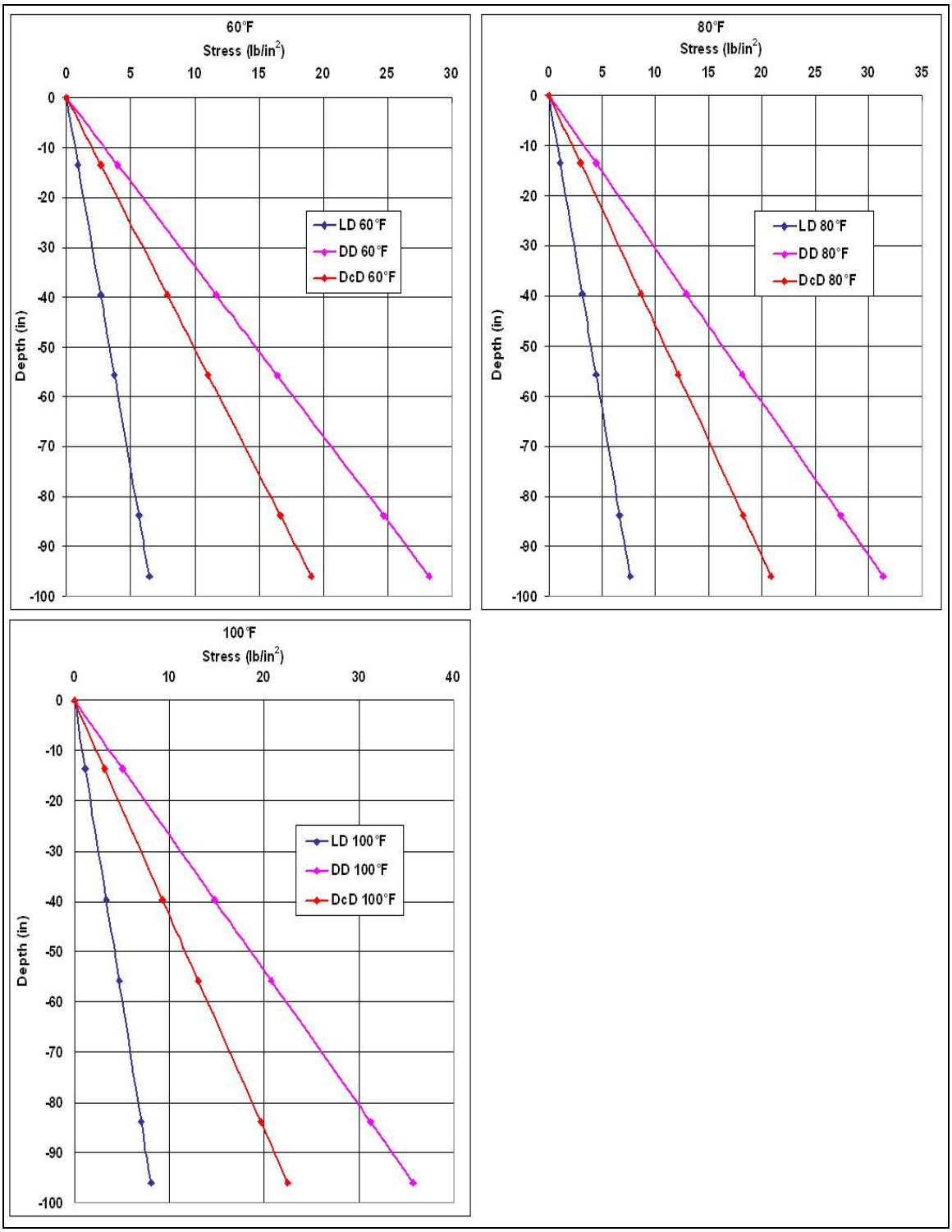

4.5.4.2 Discussion

A soil pressure acting on the abutment on the coefficient of lateral earth pressure $K(\delta)$, the vertical effective stress in soil and the unit weight of the soil. The coefficient of lateral earth pressure $K(\delta)$ is a function of the abutment top displacement, as discussed in section 3.4.1, and horizontal effective stress in soil is a linear function of depth. As expected, the stress exerted by the soil on the abutment increases linearly with depth (Figures 4-22 and 4-23). In addition, the larger the temperature change range, the larger the stress. For the selected soil properties, the soil pressure exerted on abutment increases between 4 to 4.5 times as relative compaction increases from 90% to 96%.

4.5.5 Comparisons between the Central Pile and End Pile

4.5.5.1 Longitudinal displacement

Figure 4-24 Longitudinal Displacement Comparison of Central Pile Vs. End Pile

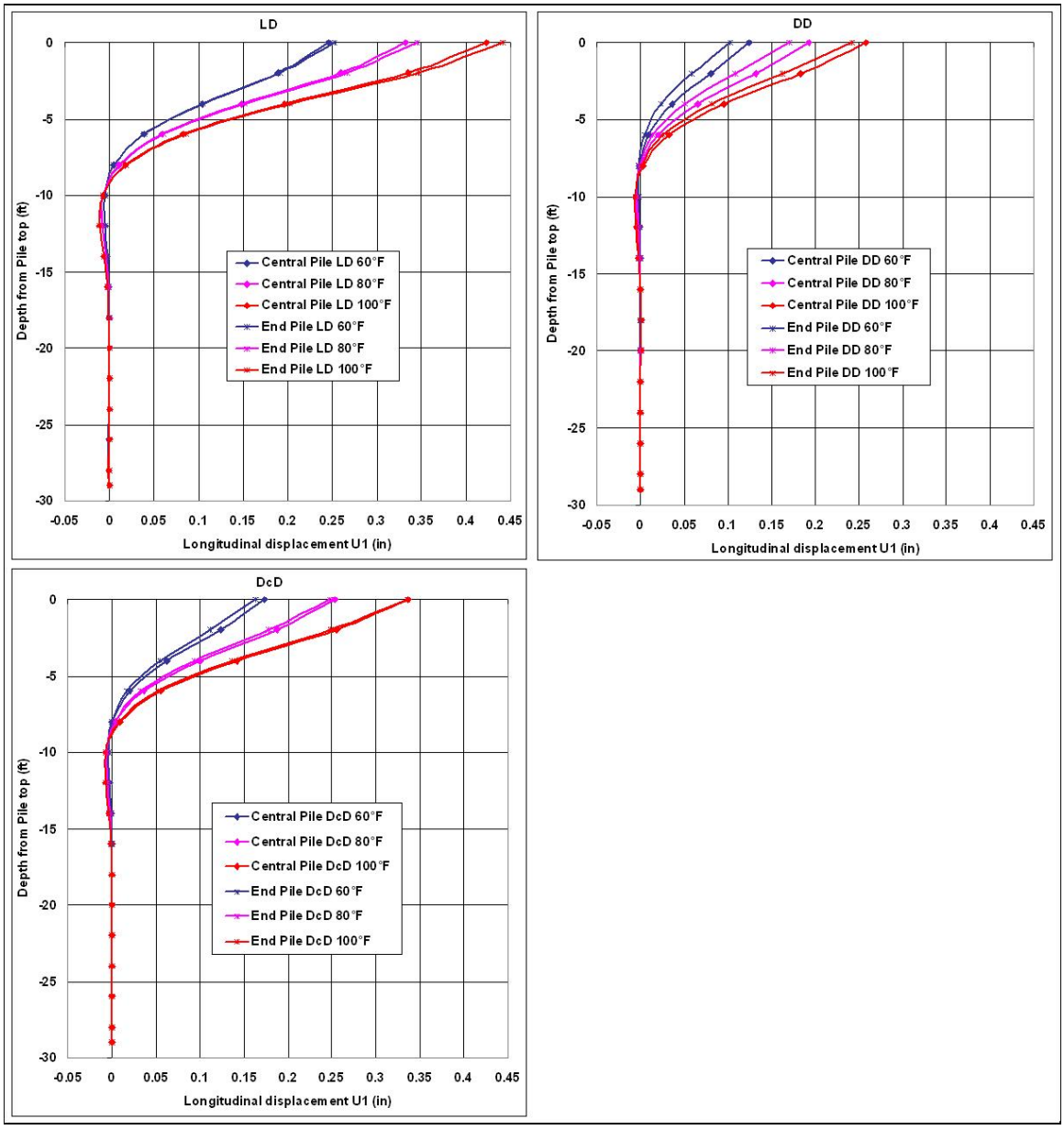

4.5.5.2 Pile Bending Moment

Figure 4-25 Bending Moment Comparison of Central Pile Vs. End Pile

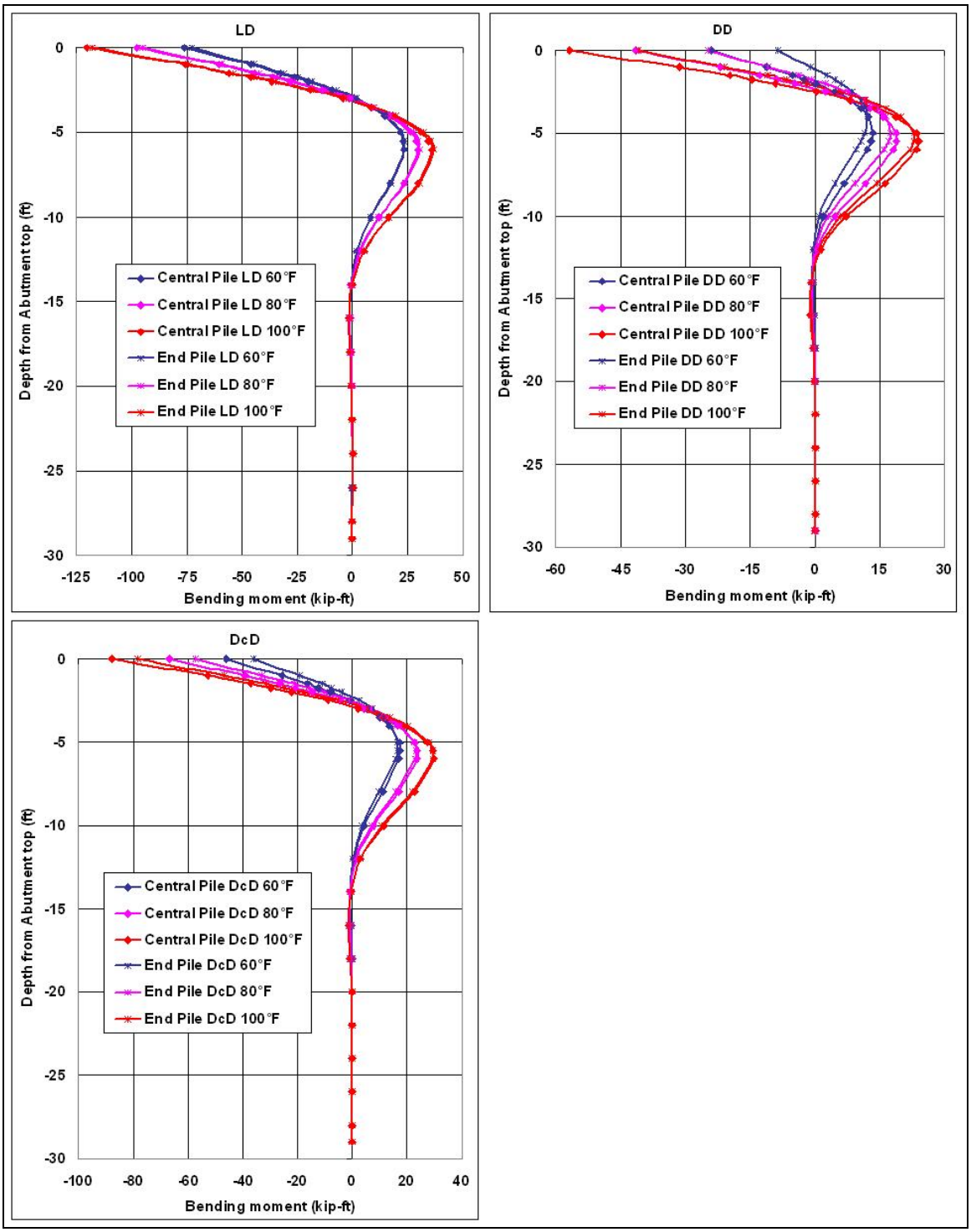

4.5.5.3 Pile Bending Stress

Figure 4-26 Bending Stress Comparison of Central Pile Vs. End Pile

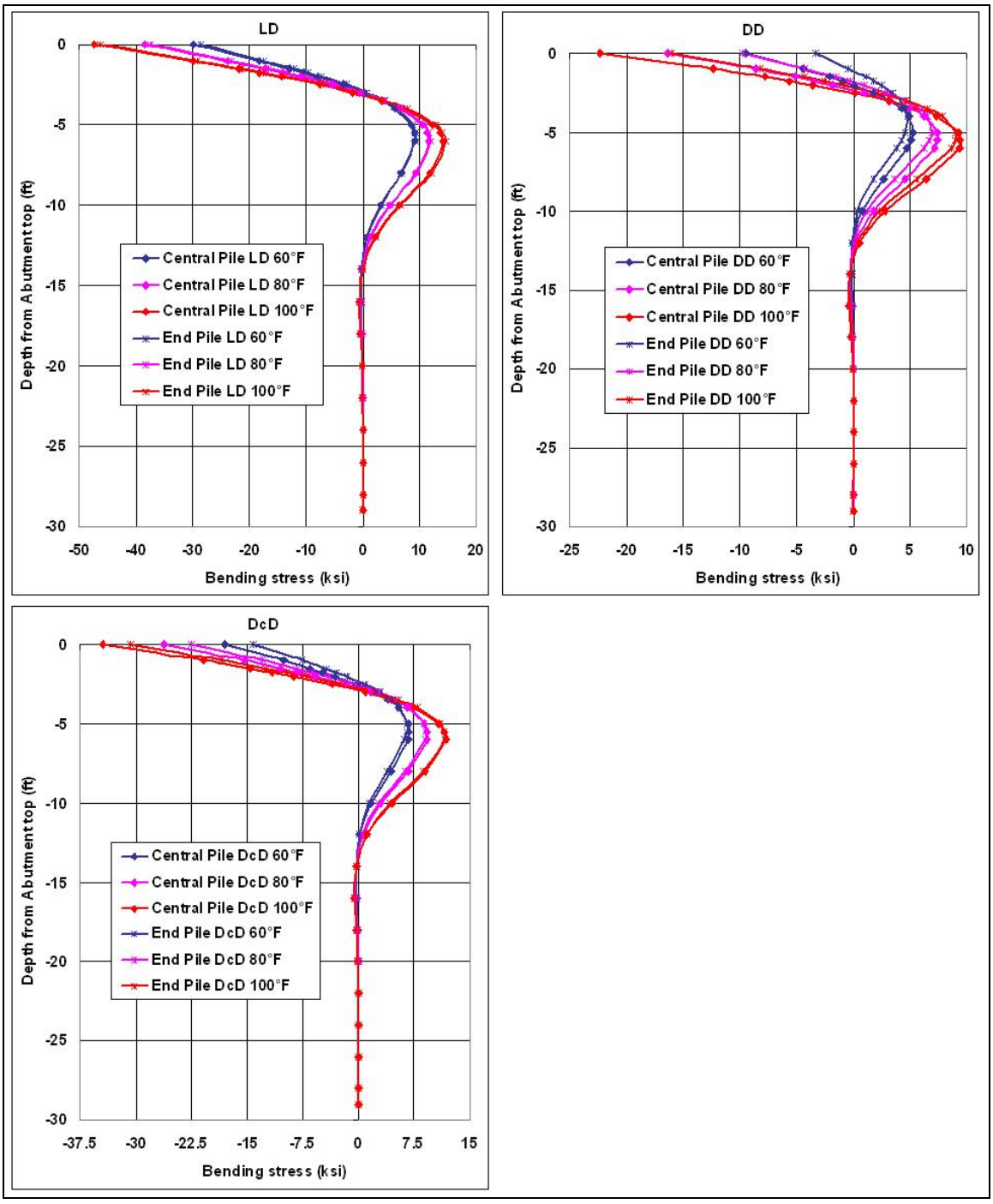

4.5.5.4 Discussion

The differences in the behavior of the central pile and end pile are shown in Figures 4-24, 4-25 and 4-26. 3D analysis enabled the comparison depicted in these figures. While the deflection curves, bending moment and bending stress diagrams show the same trends, it is interesting to observe that the end pile deflected slightly more than the central pile when loose soil was behind the abutment. Conversely, when the soil behind the abutment got denser, the central pile deflected relatively more than the end pile. The trends in the bending moments and bending stresses are traceable to the deflections observed.

4.5.6 Axial Compressive Stress in Girders

One of the interesting observations of the IAB behavior is the generation of compressive axial stresses in the girders (Figure 4-5). Though it is premature to say that this behavior can help in higher load carrying capacity of the bridge structure, this observation definitely needs more attention. Figure 4-27 shows the maximum bending stresses observed in the central girder near the joint of girder and abutment wall.

Figure 4-27 Maximum Axial Stress in the Central Girder Vs. ΔT

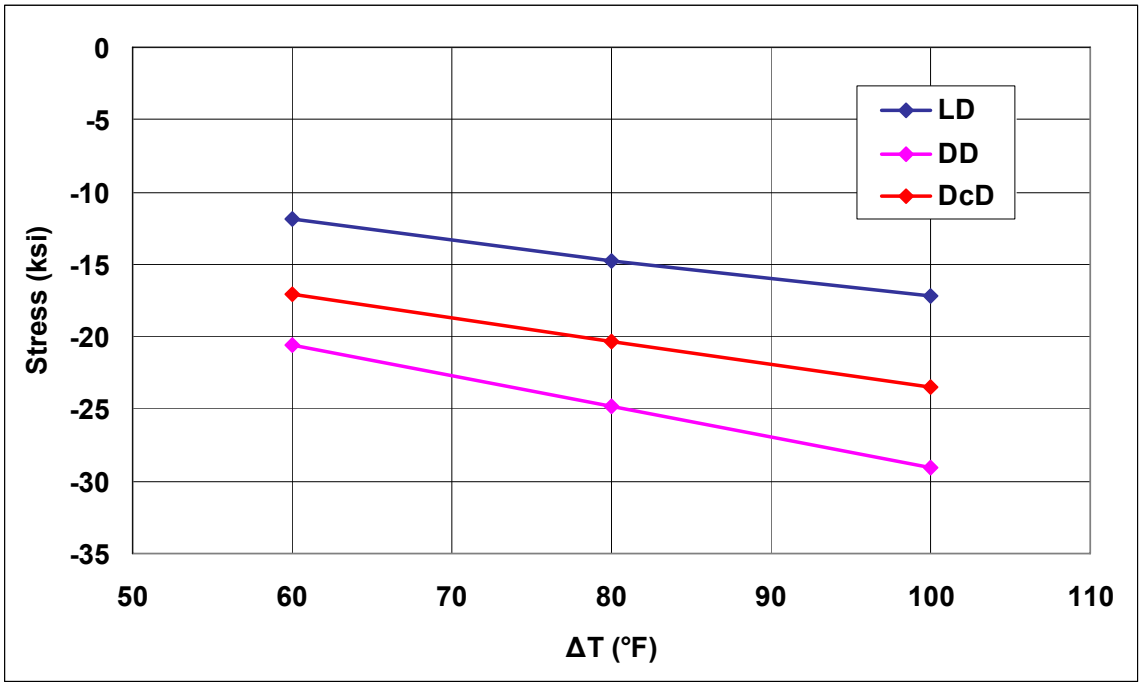

For increase in relative compaction of soil behind abutment from 90% to 96 %, maximum axial compressive stress in girders increases by 67% or more. It is noted that the increase in maximum axial compressive stress in girders is linear with temperature change range.

4.5.7 Convergence of Iterations

As defined in section 3.4.3, when the error falls below 1% or 0.01 the iterations are considered to have converged. The convergence plots for δ_T and δ_R for all the three cases of 80˚F, along with mathematical representation of the curve, are presented (Figure 4-28, and 4-29).

The equation of the form

$$y = ae^{bx} + c \tag{4.3}$$

where,

$y =$ y co-ordinate of the plot,

$x =$ x co-ordinate of the plot,

$a, b, c =$ constants

is used for the mathematical representation of the convergence of each of the displacements.

Table 4.4 lists the values of a_r, b_r, c_r, a_t, b_t and c_t for the cases LD, DD and DcD for 80°F respectively. The subscript 'r' stand for rotational displacement and the subscript 't' stand for translational displacement

Table 4.4 Values of the coefficient of exponential equation

	80°F		
	LD	**DD**	**DcD**
$\mathbf{a_r}$	-1.48601	-1.02017	-1.05633
$\mathbf{b_r}$	-2.08768	-1.20335	-1.42882
$\mathbf{c_r}$	0.0919705	0.213985	0.16083
$\mathbf{a_t}$	1.57927	1.1226	1.23635
$\mathbf{b_t}$	2.07749	-1.19902	1.49593
$\mathbf{c_t}$	0.331372	0.190714	0.252176

Figure 4-28 80˚F - Convergence of Translational Displacement

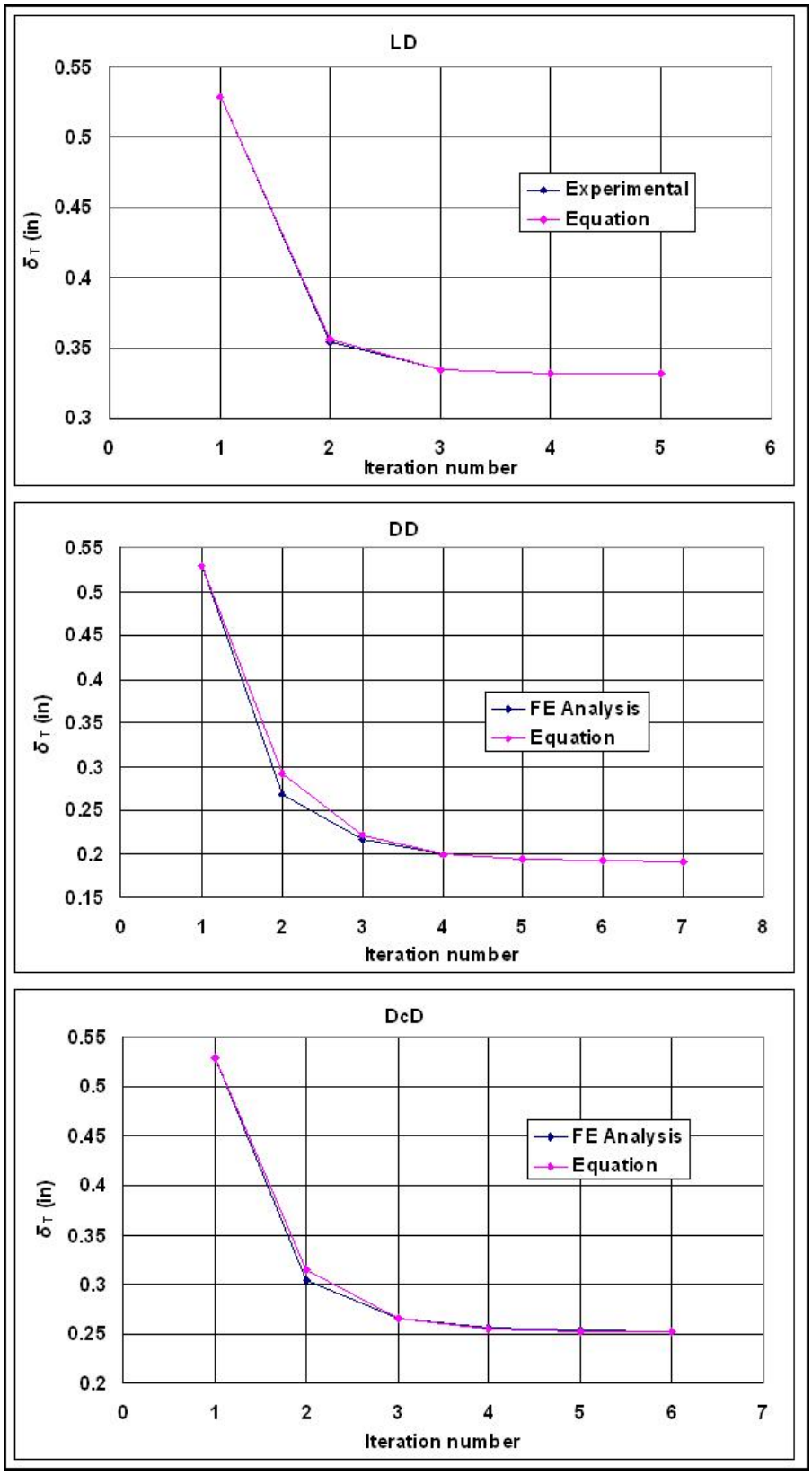

Figure 4-29 80˚F - Convergence of Rotational Displacement

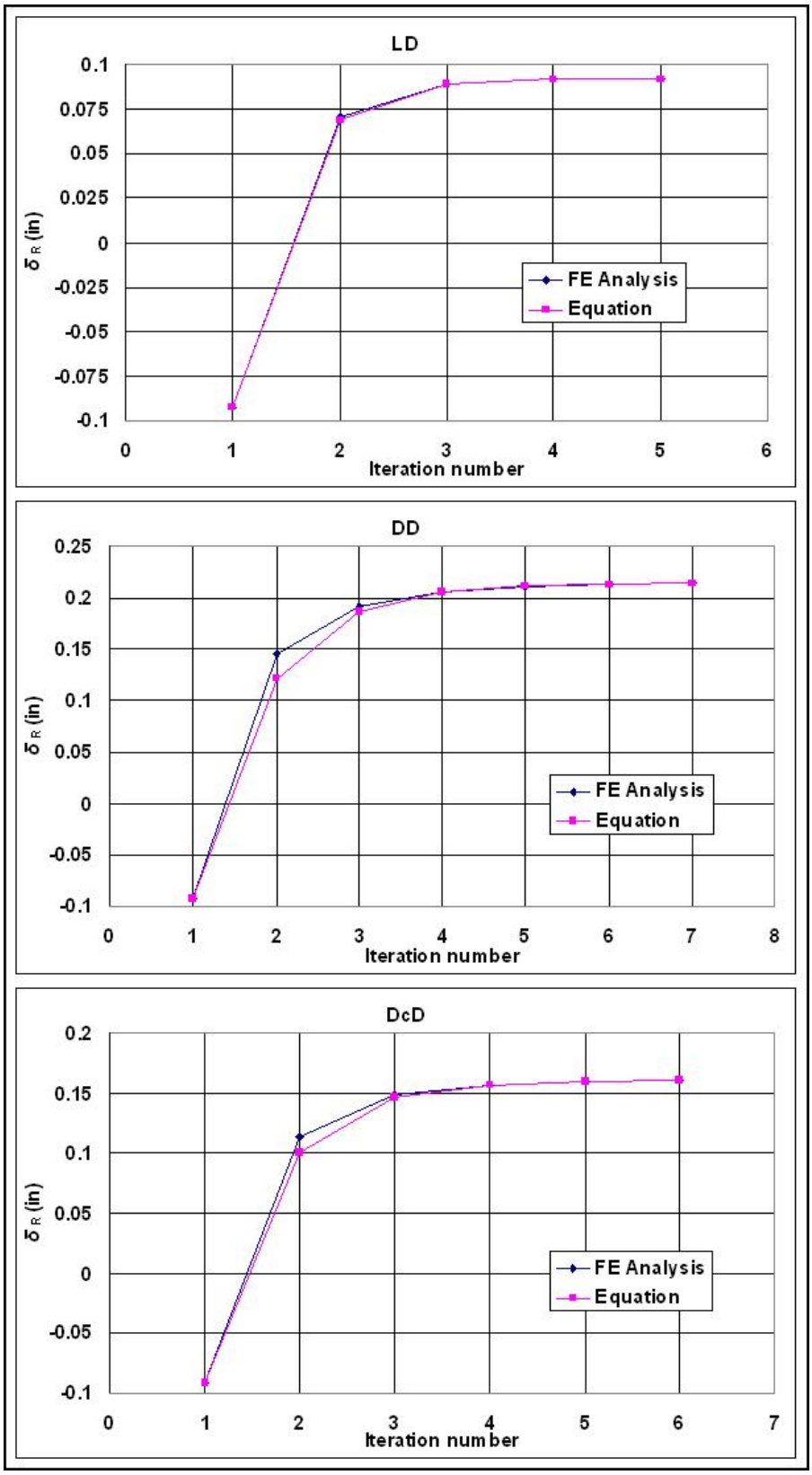

CHAPTER 5 Conclusions and Recommendations

A full 3D finite element analysis of a typical 3-span IAB, incorporating nonlinear soil response, has been performed to study the complexities of the soil-structure interaction generated due to the ambient temperature change. The sample bridge, Bemis Road Bridge: F-4-20, Fitchburg, Massachusetts, was model using 191894 eight-node coupled temperature-displacement elements (C3D8T), 277530 nodes, 12 connector elements (CONN3D2) modeling hinges, and 546 linear spring elements. Only half of the bridge was modeled due to symmetry in geometry and loading.

The nonlinear force-displacement relationship of the soil is modeled using linear springs and an iterative equivalent linear approach. The stiffnesses of the springs attached to abutment wall are determined based on the design recommendations by NCHRP (1991) and CGS (1992). The stiffnesses of the springs attached to piles are calculated based on the recommendations by Prakash & Kumar (1996).

Although the use of springs as a substitution for soil in numerical modeling is rather an outdated approach for standard geotechnical applications, a further refinement of the bridge-soil model needs justification in improved accuracy of the results against incurring high computational costs. Due to a lack of deeper understanding of the soil-structure interaction in IABs, improved accuracy is not possible at this stage. It is this unavailability of information about the backfill that justifies the absence of greater modeling sophistication and the use of springs for soils.

Earth pressure generation is sensitive to the angle of internal friction of the backfill. However NCHRP (1991) guidelines offer the coefficients of lateral pressure for only three synthetic cohesionless soils with internal friction angles of 30°, 37°, and 45° respectively, which are based on the results of a 2D FE analysis conducted by Clough and Duncan (1971). CGS (1992) offers similar design curves for coefficients of lateral pressure with the exception of dense sand whose design curve significantly differs from and is a better alternative to the one proposed by NCHRP (1991) as observed by Ting & Faraji (1998).

Thus, for this research, the extreme cases offered by NHCRP (1991) corresponding to internal friction angles of 30°, and 45° have been adopted. This approach covered a full potential range of actual lateral earth pressures. Along with that, the design curve recommended by CGS (1992) for dense soil has been included under the DcD case since it differs from the one recommended by NCHRP (1991) as mentioned earlier.

5.1 Conclusions

The results of the 3D analyses, presented in chapter 4, clearly show that the overall behavior of IABs is significantly affected by the type of soil adjacent to the abutment. The following are the conclusion derived from this research:

1. Analysis shows linear response due to selected temperature change ranges.
2. The properties of soil adjacent to abutment are major factors governing the response of IABs to thermal loads:
    a. Increase in relative compaction (R) of the soil behind abutment from 90% to 96% decreases the pile top displacement and maximum bending moment by more than 39% and 53% respectively, increases the maximum compressive stresses in the girders by 67%, and increases the soil pressure on abutment by 4 to 4.5 times
    b. While translation of abutment is about 3.46 times larger than rotation for R=90%, the rotation is larger than translation by 1.44 times for R=96% when $\Delta T = 60^{\circ}F$. The difference entirely diminishes for $\Delta T = 100^{\circ}F$ and R=96%.
    c. 3D analyses show the largest difference in maximum bending moments between central and end piles occurs for R=96% and $\Delta T = 60^{\circ}F$
3. The effect of thermal gradient within the abutment has led to bending of the abutment though the behavior of the abutment has been assumed to be that of a rigid body

4. Although the most critical loading scenario for soil failure was R=96% and $\Delta T = 100^{\circ}F$, none of the loading scenarios considered herein have resulted in passive failure of the soil behind the abutment

The study is a stepping stone to a better theoretical understanding and numerical modeling of the behavior of non-skew and skew IABs

It serves as a basis for more complete analysis accounting for different loading conditions including thermal, gravity, live and seismic loads and thus helping streamline design process for IABs

5.2 Recommendations

Future work recommended in the field of IAB research includes the following:

1. The results of the research need to be supported by actual field data. Instrumentation and continuous monitoring of IABs is essential for a better understanding of the soil-structure interaction followed by a more refined and sophisticated soil model.
2. Nonlinear material models of concrete and steel need to be implemented to study the long term effects of cyclic loading during the lifespan of the IAB. This will help in resolving issues related to cracking of concrete decks and yielding of steel girders and piles.
3. The effect of different load properties including earthquake loads should be investigated.
4. The behavior of skewed IABs needs to be explored.

CHAPTER 6 References

1. ABAQUS Inc. (2004). "ABAQUS Analysis User's Manual 6.5-1"
2. ABAQUS Inc. (2004). "ABAQUS/CAE User's Manual 6.5-1"
3. Alampalli, S and Yannotti, A.P., (1998). "In-Service Performance of Integral Bridges and Jointless Decks", Transportation Research Record 1624, Paper No. 98-0540.
4. American Petroleum Institute (API), (1993). "Recommended practice for planning, designing, and constructing fixed offshore platforms – Working stress design." 20th Ed., API RP2A-WSD, Washington, D.C.
5. Arockiasamy, M., Butrieng, N. and Sivakumar M., (2004). "State-of-the-Art of Integral Abutment Bridges: Design and Practice", Journal of Bridge Engineering, Vol. 9, No. 5
6. Arsoy, S., Barker, R.M., Duncan, J.M., (1999). "The Behavior of Integral Abutment Bridges", Final Contract Report VTRC 00-CR3, Virginia Transportation Research Council, Charlottesville, Virginia
7. Arsoy, S., (2000). "Experimental and Analytical Investigations of Piles and Abutments of Integral Bridges", PhD Thesis, Virginia Polytechnic and State University, Blacksburg, Virginia.
8. Bakeer, R.M., Mattei, N.J., Almalik, B.K., Carr, S.P., Homes, D., (2005). "Evaluation of DOTD Semi-Integral Bridge and Abutment System", Final report FHWA/LA.05/397, Louisiana Transportation Research Center, Baton Rouge, LA.
9. Canadian Geotechnical Society (CGS), (1992). Canadian foundation engineering manual, 3rd Ed., Toronto
10. Ng, C.W.W., Springman, S.M., Norrish, A.R.M., (1998). "Soil-structure interaction of spread-base integral bridge abutments", Japanese Geotechnical Society, SOIL AND FOUNDATION, Vol. 38, No. 1, pp.145-162

11. Clough, G.W., Duncan, J.M., (1971). “Finite element analyses of retaining wall behavior”, Journal of the Soil Mechanics and Foundations Division, American Society of Civil Engineers, Vol. 97, No. SM12, pp. 1657-1673
12. Das, B.M., (1999). “Principles of Foundation Engineering”, 4th ed., PWS Publishing, Brooks/Cole Publishing Company
13. Emerson, M., (1976). “Bridge temperatures estimated from the shade temperature”, Transport and Road Research Laboratory Report 696, Transport Research Laboratory, UK
14. Faraji, S., (1997). “Behavior of integral abutment bridges in Massachusetts – Year II.” Report UMTC 96-5, University of Massachusetts Transportation Center, Amherst, MA
15. Faraji, S., Ting, J.M., Crovo, D.S., Ernst, H., (2001). “Non-linear Analysis of Integral Bridges: Finite Element Model”, Journal of Geotechnical and Geoenvironmental Engineering, Vol. 127, No. 5
16. Greimann, L. F., Abendroth, R. E., Johnson, D. E., and Ebner, P.B., (1987). “Pile design and tests for integral abutment bridges”, Iowa State University, December 1987.
17. Hoppe E.J. and Gomez, J.P., (1996). “Field study of an integral backwall bridge”, Virginia Transportation Research Council, VTRC 97-R7, October 1996.
18. Jayaram, R., Merz, P.B. and McLellan Pte Ltd, Singapore, (2001). “Integral Bridge Concept Applied to Rehabilitate an Existing Bridge and Construct a Dual-Use Bridge”, Proceedings of 26th Conference on Our World in Concrete and Structures
19. KDOT Bridge Design Manual, (2007). Kansas Department of Transportation
20. Khodair, Y.A., Hassiotis, S., (2005), “Analysis of soil-pile interaction in integral abutment”, Computers and Geotechnics 32, pp 201-209.
21. Lee, K.L. and Singh, A., (1971). “Relative Density and Relative Compaction”, Journal of the Soil Mechanics and Foundations Division, American Society of Civil Engineers, Vol. 96, No. SM1, pp. 73-110

22. Lock, R.J., (2002). “Integral bridge abutments”, M.Eng. Project Report CUED/D-SOILS/TR320, London, UK
23. Loveall, C. (1996). “Integral abutment bridges”, Workshop on Integral abutment bridges, November 13-15, 1996, Pittsburg, PA.
24. Mourad, S. and Tabsh, S.W., (1999). “Deck Slab Stresses in Integral Abutment Bridges”, Journal of Bridge Engineering, Vol. 4, No. 2
25. Mwindo, J.M., (1992). “Strain dependent soil modulus of horizontal subgrade reaction”, MS Thesis, University of Missouri-Rolla, Rolla, MO
26. National Cooperative Highway Research Program (NCHRP), (1991). “Manuals for design of bridge foundations”, Barker, R.M., Duncan, J.M., Rojiani, K.B., Ooi, P.S.K., Tan, C.K., and Kim, S.G., eds. Rep 343, Transportation Research Board, Washington, D.C.
27. Prakash, S., Kumar, S., (1996). “Nonlinear Lateral Pile Deflection Prediction in Sands”, Journal of Geotechnical Engineering., Vol. 122, No. 2, pp. 130-138
28. Roman, E., Khodair, Y.A., Hassiotis, S., (2002). “Design Details on Integral Bridges”, Proceedings of the Engineering Mechanics Conference, May, New York.
29. Shoukry, S.N., William, G.W., Riad, M.Y., McBride, K.C., (2006). “Field Monitoring and 3D FE Modeling of an Integral Abutment Bridge in West Virginia”, TRB 2006 Annual Meeting CD-ROM
30. Soltani, A. A. and Kukreti, A. R., (1996). “Performance evaluation of integral abutment bridges” Workshop on Integral abutment bridges, November 13-15, 1996, Pittsburg, PA, 29 p.
31. Soltani, A. A. and Kukreti, A. R., (1992). “Performance evaluation of integral abutment bridges”, Transportation Research Record 1371, Transportation Research Board, No. 1371, pp 17-25.
32. Ting, J.M., Faraji, S., (1998). “Streamlines analysis and design of Integral Abutment Bridges”, Report UMTC 97-13, University of Massachusetts Transportation Center, Amherst, MA
33. Wasserman, E.P., (2001). “Design of Integral Abutments for Jointless Bridges”, Structure, pp. 24-33

34. Wood, D.M., (2004). “Integral bridge abutment”, Chapter 8, section 8.10, Geotechnical Modelling, Spon Press, Taylor and Francis Group, London, UK and New York, USA.
35. Yang, Pe-Shen, Wolde-Tinsae, A.M., and Greimann, L.F., (1985). Effects of predrilling and layered soils on piles, Journal of Geotechnical Engineering, ASCE, Vol. 111, No. 1.

Appendix A - ABAQUS/CAE 6.5-1 User's Guide

This chapter provides the basic information about creating and analyzing a numerical model using ABAQUS/CAE 6.5-1. In order to maintain the consistency of the matter presented here with the user's manual, which is provided with the purchase of the software ABAQUS 6.5-1, majority of the text in this appendix has been taken directly from the "ABAQUS/CAE 6.5-1 User's Manual" and the "ABAQUS Analysis 6.5-1 User's Manual".

An introduction to ABAQUS/CAE is followed by a presentation of different modules. Next, the modeling strategy and the step-by-step procedure adopted for modeling the bridge for this research is presented.

Introduction to ABAQUS/CAE

ABAQUS/CAE is a complete ABAQUS environment that provides a simple and consistent interface for creating, submitting, monitoring, and evaluating results from ABAQUS/Standard and ABAQUS/Explicit simulations. ABAQUS/CAE is divided into modules, where each module defines a logical aspect of the modeling process; for example, defining the geometry, defining material properties, and generating a mesh. Proceeding from one module to another, the model is built from which ABAQUS/CAE generates an input file that is submitted to the ABAQUS/Standard or ABAQUS/Explicit analysis product. The analysis product performs the analysis, sends information to ABAQUS/CAE in order to monitor the progress of the job, and generates an output database. Finally, the Visualization module of ABAQUS/CAE is used to read the output database and view the results of the analysis.

Modules

ABAQUS/CAE is divided into functional units called modules. Each module contains only those tools that are relevant to a specific portion of the modeling task. The

following list of the modules which are available within ABAQUS/CAE briefly describes the modeling tasks one can perform in each module.

Part Module

Parts are the building blocks of the ABAQUS/CAE model. The part module is activated to create individual parts by sketching or importing their geometry. There are several ways to create a part in ABAQUS/CAE:

1. Create the part using the tools available in the Part module.
2. Import the part from a file containing geometry stored in a third-party format.
3. Import the part mesh from an output database.
4. Import a meshed part from an ABAQUS/Standard or ABAQUS/Explicit input file.
5. Merge or cut part instances in the Assembly module.
6. Create a meshed part in the Mesh module.

A part created using the Part module tools is called a native part and has a feature-based representation. A feature captures the design intent and contains geometry information as well as a set of rules that govern the behavior of the geometry.

Property Module

The purpose of the property module is to create section and material definitions and assign them to regions of parts. The property module is used to specify the properties of a part or part region by creating a section and assigning it to the part. In most cases, sections refer to materials that have been defined.

A material definition specifies all the property data relevant to a material. A material definition is specified by including a set of material behaviors, and supplying the property data with each material behavior included. The material editor is used to specify all the information that defines each material. Each material that is created is assigned its own name and is independent of any particular section.

A section contains information about the properties of a part or a region of a part. The information required in the definition of a section depends on the type of region in question. When a section is assigned to a part, ABAQUS/CAE automatically assigns that section to each instance of the part. As a result, the elements that are created due to

meshing of those part instances will have the properties specified in that section. A single material can be referred to in as many sections as necessary. Sections are named and created independently of any particular region, part, or assembly. Property module can be used to create solid sections, shell sections, beam sections, and other sections.

Assembly Module

The assembly module is used to create and modify the assembly. A model contains only one assembly, which is composed of instances of parts from the model. When a part is created, it exists in its own coordinate system, independent of other parts in the model. In contrast, the Assembly module is used to create instances of the parts and to position the instances relative to each other in a global coordinate system, thus creating the assembly. Part instances are positioned by sequentially applying position constraints that align selected faces, edges, or vertices or by applying simple translations and rotations.

A part instance can be thought of as a representation of the original part. A part is created in the Part module and its properties are defined in the Property module. However, when the model is assembled using the Assembly module, only part instances of the part are worked with, not the part itself. The Interaction and Load modules also operate on the assembly and, therefore, on part instances. In contrast, the Mesh module enables operation on either the assembly or one or more of its component parts.

A model can contain many parts, and a part can be instanced as many times in the assembly as required; however, a model contains only one assembly. Loads, boundary conditions, fields, and meshes are all applied to the assembly. Even if the model consists of only a single part, an assembly still must be created that consists of just a single instance of that part.

Merging and Cutting Native Part Instances

Instances of native parts created can be selected and merged into a single instance. In addition, an instance of a native part can be cut away using selected part instances to make the cut. When a part instance is merged or cut, the original part instances can be suppressed or retained.

Merging and Cutting Meshed Part Instances

Merging meshed part instances is similar to merging unmeshed part instances in that the operation creates a new part instance and a new part. Similarly, the original part instances can be suppressed or retained. The merging can be done in two ways:

1. Merging the geometry
2. Merging the meshes

If merging the geometry, ABAQUS/CAE creates a new part instance and a new part and the original meshes are deleted in the process. If merging the meshes, ABAQUS/CAE creates a new orphan mesh part instance and a new orphan mesh part and the original meshes are merged into a single mesh.

Step Module

Two major tasks are performed in the Step module.

1. Create analysis steps: Analysis steps are created using the Step module. Within a model a sequence of one or more analysis steps is defined. The step sequence provides a convenient way to capture changes in the loading and boundary conditions of the model, changes in the way parts of the model interact with each other, the removal or addition of parts, and any other changes that may occur in the model during the course of the analysis.
2. Specify output requests: ABAQUS writes output from the analysis to the output database. The output is specified by creating output requests that are propagated to subsequent analysis steps. An output request defines which variables will be output during an analysis step, from which region of the model they will be output, and at what rate they will be output.

An ABAQUS/CAE model uses the following two types of steps:

1. The initial step: ABAQUS/CAE creates a special initial step at the beginning of the model's step sequence and names it “Initial”. ABAQUS/CAE creates only one initial step for the model, and it cannot be renamed, edited, replaced, copied, or deleted.
2. Analysis steps: The initial step is followed by one or more analysis steps. Each analysis step is associated with a specific analysis procedure. There is no

limit to the number of analysis steps that can be defined, but there are restrictions on the step sequence.

Interaction Module

The Interaction module is used to define and manage the following objects:

1. Mechanical and thermal interactions between regions of a model or between a region of a model and its surroundings.
2. Analysis constraints between regions of a model.
3. Connectors between two points of a model or between a point of a model and ground.
4. Inertia (point mass, rotary inertia, and heat capacitance) on regions of the model.
5. Cracks on regions of the model.
6. Springs and dashpots between two points of a model or between a point of a model and ground.

Mesh Tie Constraints

A surface based tie constraint allows fusing together two surfaces even though the meshes created on them may be dissimilar. Thus there is no relative motion between the two surfaces for the duration of the simulation. The translational and rotational motions as well as all other active degrees of freedom become equal for the pair of surfaces tied together. One surface in the constraint is designated to be the slave surface; the other surface is the master surface. Nodes are tied only where the surfaces are close to one another. Default position tolerance is usually used. However, position tolerance can be specified to either include or exclude a set of nodes from the slave surface, as per the requirements of the model.

Connectors and Connector Properties

Connectors allow modeling mechanical relationships between two points in an assembly or between a point in an assembly and ground. A connector property and local orientations associated with the connector points are specified in order to define the function of a connector.

A connector property defines the connection type and may include connector behavior data. Multiple connectors can refer to the same connector property. ABAQUS provides two connection types—basic types and assembled types.

1. Basic types: Basic connection types include translational types, which affect translational degrees of freedom at both connector points and may affect rotational degrees of freedom at the first point, and rotational types, which affect only rotational degrees of freedom at both connector points.
2. Assembled types: Assembled connection types are predefined combinations of basic connection types.

Springs

Spring elements are used to model actual physical springs as well as idealizations of axial or torsional components. They can also model restraints to prevent rigid body motion. SPRING1 and SPRING2 elements are the two spring elements available in ABAQUS. SPRING1 is between a node and ground, acting in a fixed direction. SPRING2 is between two nodes, acting in a fixed direction.

Load Module

Load module is used to define and manage the following prescribed conditions:

1. Loads
2. Boundary conditions
3. Fields
4. Load cases

Prescribed conditions in ABAQUS/CAE are step-dependent objects, thus it is required to specify the analysis steps in which they are active. Amplitude toolset in the Load module can be used to specify complicated time or frequency dependencies that can be applied to prescribed conditions.

The following types of external conditions can be prescribed in an ABAQUS model:

1. Initial conditions: Nonzero initial conditions can be defined for many variables. They are specified for particular nodes or elements, as appropriate. The data can be provided directly; in an external input file; or, in some cases,

by a user subroutine or by the results or output database file from a previous ABAQUS analysis. If initial conditions are not specified, all initial conditions are zero except relative density in the porous metal plasticity model, which will have the value 1.0.

2. Boundary conditions: Boundary conditions are used to prescribe values of basic solution variables: displacements and rotations in stress/displacement analysis, temperature in heat transfer or coupled thermal-stress analysis, electrical potential in coupled thermal-electrical analysis, pore pressure in soils analysis, acoustic pressure in acoustic analysis, etc.
3. Loads: Many types of external loading are available, depending on the analysis procedure. They can be applied in the following forms: concentrated or distributed tractions, concentrated or distributed fluxes and incident wave loads.
4. Prescribed assembly loads: Pre-tension sections can be defined in ABAQUS/Standard to prescribe assembly loads in bolts or any other type of fasteners.
5. Connector loads and motions: Connector elements can be used to define complex mechanical connections between parts, including actuation with prescribed loads or motions.
6. Predefined fields: Predefined fields are time-dependent, non-solution-dependent fields that exist over the spatial domain of the model. Temperature is the most commonly defined field.

Amplitude Curves

Complex time- or frequency-dependent boundary conditions, loads, and predefined fields can be specified by referring to an amplitude curve in the prescribed condition definition. An amplitude curve:

1. allows arbitrary time (or frequency) variations of load, displacement, and other prescribed variables to be given throughout a step (using step time) or throughout the analysis (using total time);
2. can be defined as a mathematical function (such as a sinusoidal variation), as a series of values at points in time (such as a digitized acceleration-time record

from an earthquake), or as values calculated based on a solution-dependent variable (such as the maximum creep strain rate in a super-plastic forming problem);

3. can be referred to by name by any number of boundary conditions, loads, and predefined fields.

Mesh Module

The Mesh module contains tools that allow generating meshes on parts and assemblies created within ABAQUS/CAE. In addition, the Mesh module contains functions that verify an existing mesh. The Mesh module provides the following features:

1. Tools for prescribing mesh density at local and global levels.
2. Model coloring that indicates the meshing technique assigned to each region in the model.
3. A variety of mesh controls, such as: Element shape, Meshing technique, Meshing algorithm
4. A tool for assigning ABAQUS/Standard and ABAQUS/Explicit element types to mesh elements. The elements can belong either to a model that you created or to an orphan mesh.
5. A tool for verifying mesh quality.
6. Tools for refining the mesh and for improving the mesh quality.
7. A tool for saving the meshed assembly or a selected part instances as an orphan mesh part.

Job Module

Once all of the tasks involved in defining a model (such as defining the geometry of the model, assigning section properties, and defining contact) have been completed, the Job module is used to analyze the model. The Job module allows creating a job, submitting it to ABAQUS/Standard or ABAQUS/Explicit for analysis, and monitoring its progress. If desired, multiple models and jobs can be created, run and monitored simultaneously. Job module can be to perform the following tasks:

1. Create an analysis job.
2. Associate the analysis job with a particular model or input file.

3. Submit the analysis job for processing.
4. Monitor its progress during processing.
5. Kill a job before processing is complete.
6. Start the Visualization module and view a basic plot of the analysis results.

Sketch Module

Sketches are two-dimensional profiles that are used to help with defininf form the geometry of an ABAQUS/CAE native part. Sketch module is used to create a sketch that defines a planar part, a beam, or a partition or to create a sketch that might be extruded, swept, or revolved to form a three-dimensional part.

Visualization Module

The Visualization module provides the graphical display of finite element models and results. It obtains model and result information from the output database.

The model and results can be viewed by producing any of the following plots:

1. Fast plot: A fast plot is a quickly drawn representation of the model.
2. Undeformed shape: An undeformed shape plot displays the initial shape or the base state of the model.
3. Deformed shape: A deformed shape plot displays the shape of the model according to the values of a nodal variable such as displacement.
4. Contours: A contour plot displays the values of an analysis variable such as stress or strain at a specified step and frame of the analysis. The Visualization module represents the values as customized colored lines, colored bands, or colored faces on the model.
5. Symbols: A symbol plot displays the magnitude and direction of a particular vector or tensor variable at a specified step and frame of the analysis. The Visualization module represents the values as symbols (for example, arrows) at locations on the model.
6. Material orientations: A material orientation plot displays the material directions of elements in the model at a specified step and frame of the analysis. The Visualization module represents the material directions as material orientation triads at the element integration points.

7. X-Y data: An X–Y plot is a two-dimensional graph of one variable versus another.
8. Time history animation: Time history animation displays a series of plots in rapid succession, giving a movie-like effect. The individual plots vary according to actual result values over time.
9. Scale factor animation: Scale factor animation displays a series of plots in rapid succession, giving a movie-like effect. The individual plots vary in the scale factor applied to a particular deformation.
10. Harmonic animation: Harmonic animation displays a series of plots in rapid succession, giving a movie-like effect. The individual plots vary according to the angle applied to the complex number results being displayed.

Additional capabilities include:

1. Visualizing diagnostic information: Diagnostic information helps to determine the causes of non-convergence in a model. Information for each stage of the analysis can be viewed and ABAQUS/CAE can be used to highlight problematic areas of the model in the viewport.
2. Probing model and X–Y plots: Probing displays model data and analysis results as the cursor is moved around a model plot; probing an X–Y plot displays the coordinates of graph points. This information can be written to a file.
3. Results plotting along a path: A path is a line defined by specifying a series of points through the model. The results along the path can be viewed in the form of an X–Y plot.
4. Stress linearization: Stress linearization is the separation of stresses through a section into constant membrane and linear bending stresses. The section is specified as a path through the model, and the Visualization module displays the linearized stresses in the form of an X–Y plot.
5. Cutting through the model: View cuts allow slicing through a model so that the interior or selected sections of the model can be visualized. Planar, cylindrical, or spherical view cuts can be defined. In addition, a view cut along a constant contour variable value can also be defined.

6. X–Y and field output reporting: An X–Y report is a tabular listing of X- and Y-data values; a field output report is a tabular listing of field output values.
7. Plot customization: The Visualization module provides numerous options that can be used to customize the plots.

Modeling Strategy used for this Research

In this section, the modeling strategy employed to model the bridge for this research is being presented. The step-by-step explanation is presented as follows:

1. Part module: The deck slab, abutment, pile, girder, transverse beam, pier and pier cap are each modeled as individual parts in the part module.
2. Property module: In the property module, two materials named concrete and steel are created. All the properties are defined for each material. Two sections for the two materials namely “concrete elements” and “steel elements” are then created.
3. Assembly module: The instances of parts are created in the assembly. They are oriented and positioned as per the requirements of the model. Using the Merge/Cut option, the overlapping regions of the transverse beam with the girder are cut from the transverse beam thereby creating a new part and a new instance for the transverse beam named as “part-2”. Then, similarly, the overlapping regions of the abutment with the girder and part-2 are cut from the abutment thereby creating a new part and a new instance for the abutment named as “abut-cut”. Next, using the Merge/Cut option all the instances of the superstructure – slab, girder, part-2, pier cap and abut-cut – are merged thus creating a new part and a new instance named as “superstructure”. The existing surfaces of the original parts are retained in order to retain the concept of separate part instance whereby individual material sections can be assigned. The original instances in each of the above steps are suppressed from the assembly whereby they do not take part in analysis.
4. Mesh module: All the parts are individually seeded and meshed. The seeding is done such that the locations of nodes on the adjacent parts in the assembly results in mesh-compatibility. For the purpose of mesh compatibility, tools are

used for partitioning the individual parts at the desired locations using partition planes. This process requires strategy and engineering judgment in order to have the most efficient mesh. The analysis type selected is ABAQUS/STANDARD and element type selected is C3D8T – coupled temperature displacement elements.

5. Assembly module: In order to attach springs to the abutment and piles at discrete locations, and to attach connector elements at discrete locations that model the hinge between the piers and the superstructure, it is required to have orphan meshes of the parts. For this purpose, the Merge/Cut option is used and the meshes of all the instances of the two parts - superstructure and piles - are merged thus creating a new part and its new instance named "part-1". Similarly, the meshes of the instance of the piers are merged creating a new part and its new instance "pier-set".
6. Property module: Next, the material sections are assigned to the respective elements. Each set of elements is selected and the sections are assigned as per the requirements of the model – taking care that no element remained unassigned. "Concrete elements" section is assigned to the elements that represent the parts - slab, abutment, pier and pier cap. "Steel elements" section is applied to the elements that represent the parts – girder, transverse beam and pile.
7. Interaction module: CONN3D2 connector elements are attached between the pier and the pier-cap. The property of the connector element is defined such that the available CORM (components of relative motion) are the rotational displacements at either ends of the elements and the constrained CORM are the translational displacements, thus creating the hinge action. Spring elements SPRING1 are attached at the desired nodes on the abutment wall and piles by selecting each node individually.
8. Step module: By default an "initial" step is created in ABAQUS that cannot be deleted or altered. Second step named "gravity" is created, the analysis procedure for which is "static, general" as explained in the ABAQUS Analysis User's Manual. Third step named "temperature" is created, the

analysis procedure for which is “coupled temperature displacement”. The corresponding field output variable and history output variable are also selected as per results required from each analysis step.

9. Load module: In the initial step displacement boundary conditions are applied at the supports and at the middle of the bridge, thereby modeling the symmetry of the structure. In order to have the initial temperature of 50°F on the regions below the ground level, all the nodes are selected and a temperature field is assigned to them in the initial step. The gravity load is activated in the “gravity” step by applying the gravitational acceleration of 32.2 ft/sec^2 to the whole model. Temperature boundary conditions are applied in the “temperature” step, on each node of the regions of the model above the ground level. Amplitude curves are used to increase the temperature gradually over the “temperature” step.
10. Visualization module: Results can be viewed and imported to other files using the tools in this module. “Field Output” option is used to view the results of the particular output variable selected in the “Step” module. “Query” toolset is to probe the values of the output variables at different nodes and elements. They also provide the original and deformed co-ordinates of each point giving a better understanding of the behavior. “Contour options” toolset is useful for various purposes like selecting the deformation scale, adjusting the maximum and minimum limits of the contours, selecting the colors styles. “Viewport Annotations” toolset is used to create labels and annotations on the model. “Animate” option is used to create movies. “Report” option is used to extract output to a text file in a tabular format. “View Cut” option is used to slice through the model to see the details of the behavior within the structure. “Graphics Options” is used to change the background colors and other properties of the display.

Appendix B - Tabular data of results

Table B.1 Comparison of Longitudinal Displacements – Shah vs. Ting & Faraji (1998) (Refer Figure 4-7)

Depth from abutment top (ft)	Ting & Faraji - DD 80˚F		Depth from abutment top (ft)	Shah - DD 80˚F
(ft)	(in)		(ft)	(in)
0.76486	4.3230E-01		0.70833	0.435198
2.81790	3.8502E-01		1.83573	0.399427
4.79043	3.2615E-01		4.00667	0.32813
6.84347	2.6440E-01		5.35000	0.281844
8.81600	2.2773E-01		7.70083	0.195477
10.86904	1.4088E-01		8.70833	0.156673
12.84157	6.5617E-02		10.70833	0.085432
14.89461	1.9299E-02		12.70833	0.032563
16.86714	-1.9299E-03		14.70833	0.004911
18.92018	9.6495E-04		16.70833	-4.01E-03
20.89271	1.9299E-03		18.70833	-0.00403
22.94575	9.6495E-04		20.70833	-0.00193
24.91828	9.6495E-04		22.70833	-4.60E-04
26.97132	9.6495E-04		24.70833	8.18E-05
28.94385	0.0000E+00		26.70833	1.34E-04
30.99689	0.0000E+00		28.70833	6.32E-05
32.96942	0.0000E+00		30.70833	1.24E-05
35.02246	0.0000E+00		32.70833	-3.46E-06
			34.70833	-2.36E-06
			36.70833	2.37E-06
			37.70833	1.61E-33

Table B.2 LD - Trends in Longitudinal Displacement Due to Changes in Thermal Load (Refer Figure 4-10)

Depth from abutment top	LD 60˚F	LD 80˚F	LD 100˚F
(ft)	(in)	(in)	(in)
-0.70833	3.1655E-01	4.2337E-01	5.3066E-01
-1.83573	2.9604E-01	3.9624E-01	4.9741E-01
-4.00667	2.6627E-01	3.5712E-01	4.4994E-01
-5.35000	2.5470E-01	3.4221E-01	4.3236E-01
-7.70083	2.4670E-01	3.3259E-01	4.2226E-01
-8.70833	2.4628E-01	3.3257E-01	4.2313E-01
-10.70833	1.8922E-01	2.5993E-01	3.3528E-01
-12.70833	1.0432E-01	1.4849E-01	1.9675E-01
-14.70833	3.9023E-02	5.9509E-02	8.2907E-02
-16.70833	5.1872E-03	1.0709E-02	1.7783E-02
-18.70833	-5.4224E-03	-6.4816E-03	-7.0671E-03
-20.70833	-5.2000E-03	-7.6019E-03	-1.0124E-02
-22.70833	-2.4916E-03	-4.1386E-03	-6.0721E-03
-24.70833	-6.0380E-04	-1.2698E-03	-2.1558E-03
-26.70833	1.0532E-04	5.9945E-06	-1.9289E-04
-28.70833	1.8275E-04	2.6361E-04	3.2752E-04
-30.70833	9.1621E-05	1.6828E-04	2.5910E-04
-32.70833	2.1502E-05	5.4979E-05	1.0314E-04
-34.70833	-2.4095E-06	3.5307E-06	1.5924E-05
-36.70833	-3.1319E-06	-5.6855E-06	-7.5571E-06
-37.70833	-1.9283E-33	-3.1971E-33	-4.4874E-33

Table B.3 DD - Trends in Longitudinal Displacement Due to Changes in Thermal Load (Refer Figure 4-10)

Depth from abutment top	DD 60˚F	DD 80˚F	DD 100˚F
(ft)	(in)	(in)	(in)
-0.70833	2.9997E-01	4.0473E-01	5.0904E-01
-1.83573	2.6495E-01	3.6095E-01	4.5618E-01
-4.00667	2.0644E-01	2.8886E-01	3.6989E-01
-5.35000	1.7661E-01	2.5298E-01	3.2757E-01
-7.70083	1.3694E-01	2.0692E-01	2.7447E-01
-8.70833	1.2372E-01	1.9211E-01	2.5784E-01
-10.70833	7.9745E-02	1.3200E-01	1.8282E-01
-12.70833	3.6035E-02	6.5417E-02	9.5122E-02
-14.70833	9.1381E-03	2.0432E-02	3.2832E-02
-16.70833	-1.4610E-03	4.7672E-05	2.4488E-03
-18.70833	-2.9945E-03	-4.7133E-03	-6.1024E-03
-20.70833	-1.6928E-03	-3.3682E-03	-5.1117E-03
-22.70833	-4.9272E-04	-1.3046E-03	-2.2964E-03
-24.70833	1.3494E-05	-1.7728E-04	-4.9267E-04
-26.70833	9.4300E-05	1.3863E-04	1.4025E-04
-28.70833	5.0044E-05	1.1612E-04	1.8497E-04
-30.70833	1.1426E-05	4.2985E-05	8.7275E-05
-32.70833	-1.9191E-06	4.3776E-06	1.8450E-05
-34.70833	-2.6292E-06	-4.7551E-06	-4.6867E-06
-36.70833	-1.1270E-06	-3.9478E-06	-6.6869E-06
-37.70833	-1.4303E-33	-2.6206E-33	-3.7865E-33

Table B.4 DcD - Trends in Longitudinal Displacement Due to Changes in Thermal Load (Refer Figure 4-10)

Depth from abutment top (ft)	DcD 60˚F (in)	DcD 80˚F (in)	DcD 100˚F (in)
-0.70833	3.0681E-01	4.1296E-01	5.1939E-01
-1.83573	2.7768E-01	3.7644E-01	4.7586E-01
-4.00667	2.3083E-01	3.1870E-01	4.0804E-01
-5.35000	2.0840E-01	2.9196E-01	3.7748E-01
-7.70083	1.8155E-01	2.6174E-01	3.4482E-01
-8.70833	1.7350E-01	2.5335E-01	3.3649E-01
-10.70833	1.2361E-01	1.8721E-01	2.5487E-01
-12.70833	6.2621E-02	1.0052E-01	1.4244E-01
-14.70833	2.0144E-02	3.6319E-02	5.5526E-02
-16.70833	5.4807E-04	3.9372E-03	8.9375E-03
-18.70833	-4.1957E-03	-5.7702E-03	-6.9178E-03
-20.70833	-3.0603E-03	-5.1942E-03	-7.5237E-03
-22.70833	-1.1854E-03	-2.4220E-03	-3.9864E-03
-24.70833	-1.5939E-04	-5.5986E-04	-1.1803E-03
-26.70833	1.2441E-04	1.2091E-04	3.5437E-05
-28.70833	1.0228E-04	1.8513E-04	2.6543E-04
-30.70833	3.6728E-05	9.0680E-05	1.6398E-04
-32.70833	3.2395E-06	2.0508E-05	5.1911E-05
-34.70833	-3.7726E-06	-3.4473E-06	1.8266E-06
-36.70833	-1.9887E-06	-4.9252E-06	-7.5294E-06
-37.70833	-1.6291E-33	-2.8661E-33	-4.1215E-33

Table B.5 60˚F - Trends in Longitudinal Displacement Due to Changes in Soil Properties (Refer Figure 4-11)

Depth from abutment top	LD 60˚F	DD 60˚F	DcD 60˚F
(ft)	(in)	(in)	(in)
-0.70833	3.1655E-01	2.9997E-01	3.0681E-01
-1.83573	2.9604E-01	2.6495E-01	2.7768E-01
-4.00667	2.6627E-01	2.0644E-01	2.3083E-01
-5.35000	2.5470E-01	1.7661E-01	2.0840E-01
-7.70083	2.4670E-01	1.3694E-01	1.8155E-01
-8.70833	2.4628E-01	1.2372E-01	1.7350E-01
-10.70833	1.8922E-01	7.9745E-02	1.2361E-01
-12.70833	1.0432E-01	3.6035E-02	6.2621E-02
-14.70833	3.9023E-02	9.1381E-03	2.0144E-02
-16.70833	5.1872E-03	-1.4610E-03	5.4807E-04
-18.70833	-5.4224E-03	-2.9945E-03	-4.1957E-03
-20.70833	-5.2000E-03	-1.6928E-03	-3.0603E-03
-22.70833	-2.4916E-03	-4.9272E-04	-1.1854E-03
-24.70833	-6.0380E-04	1.3494E-05	-1.5939E-04
-26.70833	1.0532E-04	9.4300E-05	1.2441E-04
-28.70833	1.8275E-04	5.0044E-05	1.0228E-04
-30.70833	9.1621E-05	1.1426E-05	3.6728E-05
-32.70833	2.1502E-05	-1.9191E-06	3.2395E-06
-34.70833	-2.4095E-06	-2.6292E-06	-3.7726E-06
-36.70833	-3.1319E-06	-1.1270E-06	-1.9887E-06
-37.70833	-1.9283E-33	-1.4303E-33	-1.6291E-33

Table B.6 80˚F - Trends in Longitudinal Displacement Due to Changes in Soil Properties (Refer Figure 4-11)

Depth from abutment top (ft)	LD 80˚F (in)	DD 80˚F (in)	DcD 80˚F (in)
-0.70833	4.2337E-01	4.0473E-01	4.1296E-01
-1.83573	3.9624E-01	3.6095E-01	3.7644E-01
-4.00667	3.5712E-01	2.8886E-01	3.1870E-01
-5.35000	3.4221E-01	2.5298E-01	2.9196E-01
-7.70083	3.3259E-01	2.0692E-01	2.6174E-01
-8.70833	3.3257E-01	1.9211E-01	2.5335E-01
-10.70833	2.5993E-01	1.3200E-01	1.8721E-01
-12.70833	1.4849E-01	6.5417E-02	1.0052E-01
-14.70833	5.9509E-02	2.0432E-02	3.6319E-02
-16.70833	1.0709E-02	4.7672E-05	3.9372E-03
-18.70833	-6.4816E-03	-4.7133E-03	-5.7702E-03
-20.70833	-7.6019E-03	-3.3682E-03	-5.1942E-03
-22.70833	-4.1386E-03	-1.3046E-03	-2.4220E-03
-24.70833	-1.2698E-03	-1.7728E-04	-5.5986E-04
-26.70833	5.9945E-06	1.3863E-04	1.2091E-04
-28.70833	2.6361E-04	1.1612E-04	1.8513E-04
-30.70833	1.6828E-04	4.2985E-05	9.0680E-05
-32.70833	5.4979E-05	4.3776E-06	2.0508E-05
-34.70833	3.5307E-06	-4.7551E-06	-3.4473E-06
-36.70833	-5.6855E-06	-3.9478E-06	-4.9252E-06
-37.70833	-3.1971E-33	-2.6206E-33	-2.8661E-33

Table B.7 100˚F - Longitudinal Displacement Due to Changes in Soil Properties (Refer Figure 4-11)

Depth from abutment top (ft)	LD 100˚F (in)	DD 100˚F (in)	DcD 100˚F (in)
-0.70833	5.3066E-01	5.0904E-01	5.1939E-01
-1.83573	4.9741E-01	4.5618E-01	4.7586E-01
-4.00667	4.4994E-01	3.6989E-01	4.0804E-01
-5.35000	4.3236E-01	3.2757E-01	3.7748E-01
-7.70083	4.2226E-01	2.7447E-01	3.4482E-01
-8.70833	4.2313E-01	2.5784E-01	3.3649E-01
-10.70833	3.3528E-01	1.8282E-01	2.5487E-01
-12.70833	1.9675E-01	9.5122E-02	1.4244E-01
-14.70833	8.2907E-02	3.2832E-02	5.5526E-02
-16.70833	1.7783E-02	2.4488E-03	8.9375E-03
-18.70833	-7.0671E-03	-6.1024E-03	-6.9178E-03
-20.70833	-1.0124E-02	-5.1117E-03	-7.5237E-03
-22.70833	-6.0721E-03	-2.2964E-03	-3.9864E-03
-24.70833	-2.1558E-03	-4.9267E-04	-1.1803E-03
-26.70833	-1.9289E-04	1.4025E-04	3.5437E-05
-28.70833	3.2752E-04	1.8497E-04	2.6543E-04
-30.70833	2.5910E-04	8.7275E-05	1.6398E-04
-32.70833	1.0314E-04	1.8450E-05	5.1911E-05
-34.70833	1.5924E-05	-4.6867E-06	1.8266E-06
-36.70833	-7.5571E-06	-6.6869E-06	-7.5294E-06
-37.70833	-4.4874E-33	-3.7865E-33	-4.1215E-33

Table B.8 Displacement at Abutment Top vs. ΔT (Refer Figure 4-12)

Temperature (˚F)	LD (in)	DD (in)	DcD (in)
60	0.31655	0.29997	0.30681
80	0.42337	0.40473	0.41296
100	0.53066	0.50904	0.51939

Table B.9 δ_T and δ_R Vs. ΔT (Refer Figure 4-13)

	Translational displacement			Rotational displacement		
Temperature	**LD**	**DD**	**DcD**	**LD**	**DD**	**DcD**
(˚F)	**(in)**	**(in)**	**(in)**	**(in)**	**(in)**	**(in)**
60	0.24566	0.12283	0.17272	0.07089	0.17714	0.13409
80	0.33171	0.19097	0.25233	0.09166	0.21376	0.16063
100	0.42203	0.25642	0.33523	0.10863	0.25263	0.18416

Table B.10 LD - Comparison of Deck Displacement (Refer Figure 4-14)

Temperature	Deck top	Pile Head	Abutment top	Analytical
(˚F)	**(in)**	**(in)**	**(in)**	**(in)**
60	0.32797	0.24628	0.31655	0.32473
80	0.43847	0.33257	0.42337	0.43297
100	0.54912	0.42313	0.53066	0.54121

Table B.11 DD - Comparison of Deck Displacement (Refer Figure 4-14)

Temperature	Deck top	Pile Head	Abutment top	Analytical
(˚F)	**(in)**	**(in)**	**(in)**	**(in)**
60	0.32051	0.12371	0.29997	0.32473
80	0.43029	0.19210	0.40473	0.43297
100	0.53982	0.25782	0.50904	0.54121

Table B.12 DcD - Comparison of Deck Displacement (Refer Figure 4-14)

Temperature	Deck top	Pile Head	Analytical	Abutment top
(˚F)	**(in)**	**(in)**	**(in)**	**(in)**
60	0.32365	0.17349	0.32473	0.30681
80	0.43397	0.25334	0.43297	0.41296
100	0.54431	0.33649	0.54121	0.51939

Table B.13 LD - Trends in Central Pile Bending Moment Due to Changes in Thermal Load (Refer Figure 4-15)

Depth from pile top (ft)	LD 60˚F (kip-ft)	LD 80˚F (kip-ft)	LD 100˚F (kip-ft)
0.00	-7.5924E+01	-9.7793E+01	-1.2037E+02
-1.00	-4.6215E+01	-6.0680E+01	-7.5799E+01
-1.50	-3.2702E+01	-4.3827E+01	-5.5589E+01
-1.75	-2.6463E+01	-3.6003E+01	-4.6168E+01
-2.00	-2.0097E+01	-2.7979E+01	-3.6469E+01
-2.50	-8.8782E+00	-1.3757E+01	-1.9205E+01
-3.00	6.3522E-01	-1.5552E+00	-4.2700E+00
-3.50	8.4161E+00	8.5700E+00	8.2537E+00
-4.00	1.4415E+01	1.6542E+01	1.8262E+01
-5.00	2.1562E+01	2.6532E+01	3.1238E+01
-5.50	2.3014E+01	2.8876E+01	3.4552E+01
-6.00	2.3313E+01	2.9742E+01	3.6065E+01
-8.00	1.7264E+01	2.3457E+01	2.9829E+01
-10.00	8.0489E+00	1.1922E+01	1.6111E+01
-12.00	1.8171E+00	3.3652E+00	5.1975E+00
-14.00	-6.5062E-01	-4.9145E-01	-1.7313E-01
-16.00	-9.0529E-01	-1.2211E+00	-1.4978E+00
-18.00	-4.8171E-01	-7.7424E-01	-1.0912E+00
-20.00	-1.2639E-01	-2.6551E-01	-4.3987E-01
-22.00	1.8121E-02	-1.0786E-02	-6.1174E-02
-24.00	3.6463E-02	4.8838E-02	5.4860E-02
-26.00	1.8094E-02	3.2791E-02	4.9105E-02
-28.00	8.0422E-04	7.5467E-03	1.8409E-02
-29.00	-4.8609E-03	-1.6135E-03	5.8189E-03

Table B.14 DD - Trends in Central Pile Bending Moment Due to Changes in Thermal Load (Refer Figure 4-15)

Depth from pile top	DD 60˚F	DD 80˚F	DD 100˚F
(ft)	(kip-ft)	(kip-ft)	(kip-ft)
0.00	-2.4100E+01	-4.1578E+01	-5.6674E+01
-1.00	-1.1113E+01	-2.1890E+01	-3.1353E+01
-1.50	-5.1254E+00	-1.2856E+01	-1.9759E+01
-1.75	-2.4594E+00	-8.7635E+00	-1.4462E+01
-2.00	1.7418E-01	-4.6594E+00	-9.1105E+00
-2.50	4.6348E+00	2.4275E+00	2.1727E-01
-3.00	8.1279E+00	8.2014E+00	7.9596E+00
-3.50	1.0691E+01	1.2680E+01	1.4117E+01
-4.00	1.2342E+01	1.5861E+01	1.8666E+01
-5.00	1.3348E+01	1.8824E+01	2.3466E+01
-5.50	1.2937E+01	1.8886E+01	2.4026E+01
-6.00	1.2096E+01	1.8225E+01	2.3615E+01
-8.00	6.7604E+00	1.1618E+01	1.6208E+01
-10.00	2.1056E+00	4.5332E+00	7.0767E+00
-12.00	-9.9694E-02	5.0447E-01	1.3201E+00
-14.00	-5.4005E-01	-7.2900E-01	-7.9223E-01
-16.00	-3.2872E-01	-6.2361E-01	-8.9725E-01
-18.00	-9.5552E-02	-2.5820E-01	-4.4771E-01
-20.00	5.5571E-03	-3.6971E-02	-1.0633E-01
-22.00	2.0287E-02	2.7849E-02	2.4012E-02
-24.00	1.0034E-02	2.3237E-02	3.5917E-02
-26.00	1.7126E-03	7.7119E-03	1.6351E-02
-28.00	-1.2171E-03	-6.7336E-04	1.6135E-03
-29.00	-1.3391E-03	-1.6389E-03	-1.3086E-03

Table B.15 DcD - Trends in Central Pile Bending Moment Due to Changes in Thermal Load (Refer Figure 4-15)

Depth from pile top (ft)	DcD 60˚F (kip-ft)	DcD 80˚F (kip-ft)	DcD 100˚F (kip-ft)
0.00	-4.5908E+01	-6.6796E+01	-8.7499E+01
-1.00	-2.5710E+01	-3.9131E+01	-5.2718E+01
-1.50	-1.6470E+01	-2.6511E+01	-3.6882E+01
-1.75	-1.2265E+01	-2.0711E+01	-2.9558E+01
-2.00	-8.0284E+00	-1.4818E+01	-2.2074E+01
-2.50	-6.7515E-01	-4.4837E+00	-8.8604E+00
-3.00	5.3770E+00	4.2002E+00	2.3911E+00
-3.50	1.0138E+01	1.1219E+01	1.1640E+01
-4.00	1.3600E+01	1.6536E+01	1.8824E+01
-5.00	1.7095E+01	2.2573E+01	2.7520E+01
-5.50	1.7402E+01	2.3602E+01	2.9364E+01
-6.00	1.6966E+01	2.3561E+01	2.9827E+01
-8.00	1.1058E+01	1.6844E+01	2.2747E+01
-10.00	4.3720E+00	7.6343E+00	1.1255E+01
-12.00	5.2354E-01	1.5988E+00	3.0045E+00
-14.00	-6.6270E-01	-7.1712E-01	-6.0278E-01
-16.00	-5.7156E-01	-9.0631E-01	-1.2161E+00
-18.00	-2.3384E-01	-4.6973E-01	-7.4451E-01
-20.00	-3.1633E-02	-1.1877E-01	-2.4597E-01
-22.00	2.5914E-02	2.0569E-02	-4.1799E-03
-24.00	2.0935E-02	3.6412E-02	4.8825E-02
-26.00	6.8746E-03	1.7457E-02	3.1254E-02
-28.00	-1.3505E-03	1.3086E-03	7.3689E-03
-29.00	-3.2461E-03	-3.0619E-03	-3.4303E-04

Table B.16 60˚F - Trends in Central Pile Bending Moment Due to Changes in Soil Properties (Refer Figure 4-16)

Depth from pile top (ft)	LD 60˚F (kip-ft)	DD 60˚F (kip-ft)	DcD 60˚F (kip-ft)
0.00	-7.5924E+01	-2.4100E+01	-4.5908E+01
-1.00	-4.6215E+01	-1.1113E+01	-2.5710E+01
-1.50	-3.2702E+01	-5.1254E+00	-1.6470E+01
-1.75	-2.6463E+01	-2.4594E+00	-1.2265E+01
-2.00	-2.0097E+01	1.7418E-01	-8.0284E+00
-2.50	-8.8782E+00	4.6348E+00	-6.7515E-01
-3.00	6.3522E-01	8.1279E+00	5.3770E+00
-3.50	8.4161E+00	1.0691E+01	1.0138E+01
-4.00	1.4415E+01	1.2342E+01	1.3600E+01
-5.00	2.1562E+01	1.3348E+01	1.7095E+01
-5.50	2.3014E+01	1.2937E+01	1.7402E+01
-6.00	2.3313E+01	1.2096E+01	1.6966E+01
-8.00	1.7264E+01	6.7604E+00	1.1058E+01
-10.00	8.0489E+00	2.1056E+00	4.3720E+00
-12.00	1.8171E+00	-9.9694E-02	5.2354E-01
-14.00	-6.5062E-01	-5.4005E-01	-6.6270E-01
-16.00	-9.0529E-01	-3.2872E-01	-5.7156E-01
-18.00	-4.8171E-01	-9.5552E-02	-2.3384E-01
-20.00	-1.2639E-01	5.5571E-03	-3.1633E-02
-22.00	1.8121E-02	2.0287E-02	2.5914E-02
-24.00	3.6463E-02	1.0034E-02	2.0935E-02
-26.00	1.8094E-02	1.7126E-03	6.8746E-03
-28.00	8.0422E-04	-1.2171E-03	-1.3505E-03
-29.00	-4.8609E-03	-1.3391E-03	-3.2461E-03

Table B.17 80˚F - Trends in Central Pile Bending Moment Due to Changes in Soil Properties (Refer Figure 4-16)

Depth from pile top (ft)	LD 80˚F (kip-ft)	DD 80˚F (kip-ft)	DcD 80˚F (kip-ft)
0.00	-9.7793E+01	-4.1578E+01	-6.6796E+01
-1.00	-6.0680E+01	-2.1890E+01	-3.9131E+01
-1.50	-4.3827E+01	-1.2856E+01	-2.6511E+01
-1.75	-3.6003E+01	-8.7635E+00	-2.0711E+01
-2.00	-2.7979E+01	-4.6594E+00	-1.4818E+01
-2.50	-1.3757E+01	2.4275E+00	-4.4837E+00
-3.00	-1.5552E+00	8.2014E+00	4.2002E+00
-3.50	8.5700E+00	1.2680E+01	1.1219E+01
-4.00	1.6542E+01	1.5861E+01	1.6536E+01
-5.00	2.6532E+01	1.8824E+01	2.2573E+01
-5.50	2.8876E+01	1.8886E+01	2.3602E+01
-6.00	2.9742E+01	1.8225E+01	2.3561E+01
-8.00	2.3457E+01	1.1618E+01	1.6844E+01
-10.00	1.1922E+01	4.5332E+00	7.6343E+00
-12.00	3.3652E+00	5.0447E-01	1.5988E+00
-14.00	-4.9145E-01	-7.2900E-01	-7.1712E-01
-16.00	-1.2211E+00	-6.2361E-01	-9.0631E-01
-18.00	-7.7424E-01	-2.5820E-01	-4.6973E-01
-20.00	-2.6551E-01	-3.6971E-02	-1.1877E-01
-22.00	-1.0786E-02	2.7849E-02	2.0569E-02
-24.00	4.8838E-02	2.3237E-02	3.6412E-02
-26.00	3.2791E-02	7.7119E-03	1.7457E-02
-28.00	7.5467E-03	-6.7336E-04	1.3086E-03
-29.00	-1.6135E-03	-1.6389E-03	-3.0619E-03

Table B.18 100˚F - Trends in Central Pile Bending Moment Due to Changes in Soil Properties (Refer Figure 4-16)

Depth from pile top (ft)	LD 100˚F (kip-ft)	DD 100˚F (kip-ft)	DcD 100˚F (kip-ft)
0.00	-1.2037E+02	-5.6674E+01	-8.7638E+01
-1.00	-7.5799E+01	-3.1353E+01	-5.2844E+01
-1.50	-5.5589E+01	-1.9759E+01	-3.7003E+01
-1.75	-4.6168E+01	-1.4462E+01	-2.9675E+01
-2.00	-3.6469E+01	-9.1105E+00	-2.2186E+01
-2.50	-1.9205E+01	2.1727E-01	-8.9606E+00
-3.00	-4.2700E+00	7.9596E+00	2.3047E+00
-3.50	8.2537E+00	1.4117E+01	1.1569E+01
-4.00	1.8262E+01	1.8666E+01	1.8770E+01
-5.00	3.1238E+01	2.3466E+01	2.7501E+01
-5.50	3.4552E+01	2.4026E+01	2.9361E+01
-6.00	3.6065E+01	2.3615E+01	2.9839E+01
-8.00	2.9829E+01	1.6208E+01	2.2798E+01
-10.00	1.6111E+01	7.0767E+00	1.1307E+01
-12.00	5.1975E+00	1.3201E+00	3.0358E+00
-14.00	-1.7313E-01	-7.9223E-01	-5.9280E-01
-16.00	-1.4978E+00	-8.9725E-01	-1.2180E+00
-18.00	-1.0912E+00	-4.4771E-01	-7.4916E-01
-20.00	-4.3987E-01	-1.0633E-01	-2.4909E-01
-22.00	-6.1174E-02	2.4012E-02	-5.2725E-03
-24.00	5.4860E-02	3.5917E-02	4.8850E-02
-26.00	4.9105E-02	1.6351E-02	3.1546E-02
-28.00	1.8409E-02	1.6135E-03	7.5721E-03
-29.00	5.8189E-03	-1.3086E-03	-2.2869E-04

Table B.19 Displacement at the Pile Top in Central Pile Vs. ΔT (Refer Figure 4-17)

Temperature (˚F)	LD (in)	DD (in)	DcD (in)
60	0.24628	0.12372	0.1735
80	0.33257	0.19211	0.25335
100	0.42313	0.25784	0.33649

Table B.20 Maximum Bending Moment in Central Pile Vs. ΔT (Refer Figure 4-18)

Temperature (˚F)	LD (kip-ft)	DD (kip-ft)	DcD (kip-ft)
60	-75.9242	-24.0998	-45.9080
80	-97.7928	-41.5776	-66.7959
100	-120.3846	-56.6738	-87.6380

Table B.21 LD - Trends in Central Pile Bending Stress Due to Changes in Thermal Load (Refer Figure 4-19)

Depth from pile top	LD 60˚F	LD 80˚F	LD 100˚F
(ft)	(ksi)	(ksi)	(ksi)
0.00	-2.9880E+01	-3.8486E+01	-4.7377E+01
-1.00	-1.8188E+01	-2.3881E+01	-2.9848E+01
-1.50	-1.2870E+01	-1.7248E+01	-2.1899E+01
-1.75	-1.0414E+01	-1.4169E+01	-1.8193E+01
-2.00	-7.9091E+00	-1.1011E+01	-1.4378E+01
-2.50	-3.4940E+00	-5.4139E+00	-7.5858E+00
-3.00	2.4999E-01	-6.1203E-01	-1.7086E+00
-3.50	3.3121E+00	3.3727E+00	3.2211E+00
-4.00	5.6731E+00	6.5103E+00	7.1620E+00
-5.00	8.4856E+00	1.0442E+01	1.2277E+01
-5.50	9.0572E+00	1.1364E+01	1.3586E+01
-6.00	9.1749E+00	1.1705E+01	1.4186E+01
-8.00	6.7942E+00	9.2315E+00	1.1749E+01
-10.00	3.1676E+00	4.6918E+00	6.3560E+00
-12.00	7.1510E-01	1.3244E+00	2.0573E+00
-14.00	-2.5605E-01	-1.9341E-01	-6.2955E-02
-16.00	-3.5628E-01	-4.8057E-01	-5.8908E-01
-18.00	-1.8957E-01	-3.0470E-01	-4.3085E-01
-20.00	-4.9742E-02	-1.0449E-01	-1.7439E-01
-22.00	7.1315E-03	-4.2450E-03	-2.4665E-02
-24.00	1.4350E-02	1.9220E-02	2.1490E-02
-26.00	7.1210E-03	1.2905E-02	1.9415E-02
-28.00	3.1650E-04	2.9700E-03	7.3500E-03
-29.00	-1.9130E-03	-6.3500E-04	2.3800E-03

Table B.22 DD - Trends in Central Pile Bending Stress Due to Changes in Thermal Load (Refer Figure 4-19)

Depth from pile top	DD 60˚F	DD 80˚F	DD 100˚F
(ft)	(ksi)	(ksi)	(ksi)
0.00	-9.4845E+00	-1.6363E+01	-2.2304E+01
-1.00	-4.3734E+00	-8.6148E+00	-1.2339E+01
-1.50	-2.0171E+00	-5.0594E+00	-7.7761E+00
-1.75	-9.6789E-01	-3.4489E+00	-5.6916E+00
-2.00	6.8547E-02	-1.8337E+00	-3.5854E+00
-2.50	1.8240E+00	9.5535E-01	8.5505E-02
-3.00	3.1987E+00	3.2276E+00	3.1325E+00
-3.50	4.2073E+00	4.9903E+00	5.5556E+00
-4.00	4.8572E+00	6.2422E+00	7.3459E+00
-5.00	5.2532E+00	7.4081E+00	9.2349E+00
-5.50	5.0915E+00	7.4325E+00	9.4554E+00
-6.00	4.7603E+00	7.1726E+00	9.2937E+00
-8.00	2.6605E+00	4.5723E+00	6.3788E+00
-10.00	8.2867E-01	1.7840E+00	2.7850E+00
-12.00	-3.9235E-02	1.9854E-01	5.1954E-01
-14.00	-2.1253E-01	-2.8690E-01	-3.1178E-01
-16.00	-1.2937E-01	-2.4542E-01	-3.5311E-01
-18.00	-3.7605E-02	-1.0162E-01	-1.7620E-01
-20.00	2.1870E-03	-1.4550E-02	-4.1845E-02
-22.00	7.9840E-03	1.0960E-02	9.4500E-03
-24.00	3.9490E-03	9.1450E-03	1.4135E-02
-26.00	6.7400E-04	3.0350E-03	6.4350E-03
-28.00	-4.7900E-04	-2.6500E-04	6.3500E-04
-29.00	-5.2700E-04	-6.4500E-04	-5.1500E-04

Table B.23 DcD - Trends in Central Pile Bending Stress Due to Changes in Thermal Load (Refer Figure 4-19)

Depth from pile top (ft)	DcD 60˚F (ksi)	DcD 80˚F (ksi)	DcD 100˚F (ksi)
0.00	-1.8067E+01	-2.6287E+01	-3.4490E+01
-1.00	-1.0118E+01	-1.5400E+01	-2.0797E+01
-1.50	-6.4818E+00	-1.0433E+01	-1.4562E+01
-1.75	-4.8268E+00	-8.1508E+00	-1.1679E+01
-2.00	-3.1596E+00	-5.8318E+00	-8.7313E+00
-2.50	-2.6570E-01	-1.7645E+00	-3.5264E+00
-3.00	2.1161E+00	1.6530E+00	9.0703E-01
-3.50	3.9900E+00	4.4151E+00	4.5531E+00
-4.00	5.3522E+00	6.5076E+00	7.3869E+00
-5.00	6.7278E+00	8.8838E+00	1.0823E+01
-5.50	6.8484E+00	9.2885E+00	1.1555E+01
-6.00	6.6771E+00	9.2726E+00	1.1743E+01
-8.00	4.3518E+00	6.6288E+00	8.9720E+00
-10.00	1.7206E+00	3.0045E+00	4.4497E+00
-12.00	2.0604E-01	6.2922E-01	1.1947E+00
-14.00	-2.6081E-01	-2.8222E-01	-2.3330E-01
-16.00	-2.2494E-01	-3.5668E-01	-4.7934E-01
-18.00	-9.2029E-02	-1.8486E-01	-2.9483E-01
-20.00	-1.2449E-02	-4.6740E-02	-9.8030E-02
-22.00	1.0199E-02	8.0950E-03	-2.0750E-03
-24.00	8.2390E-03	1.4330E-02	1.9225E-02
-26.00	2.7055E-03	6.8700E-03	1.2415E-02
-28.00	-5.3150E-04	5.1500E-04	2.9800E-03
-29.00	-1.2775E-03	-1.2050E-03	-9.0000E-05

Table B.24 60˚F – Trends in Central Pile Bending Stress Due to Changes in Soil Properties (Refer Figure 4-20)

Depth from pile top	LD 60˚F	DD 60˚F	DcD 60˚F
(ft)	(ksi)	(ksi)	(ksi)
0.00	-2.9880E+01	-9.4845E+00	-1.8067E+01
-1.00	-1.8188E+01	-4.3734E+00	-1.0118E+01
-1.50	-1.2870E+01	-2.0171E+00	-6.4818E+00
-1.75	-1.0414E+01	-9.6789E-01	-4.8268E+00
-2.00	-7.9091E+00	6.8547E-02	-3.1596E+00
-2.50	-3.4940E+00	1.8240E+00	-2.6570E-01
-3.00	2.4999E-01	3.1987E+00	2.1161E+00
-3.50	3.3121E+00	4.2073E+00	3.9900E+00
-4.00	5.6731E+00	4.8572E+00	5.3522E+00
-5.00	8.4856E+00	5.2532E+00	6.7278E+00
-5.50	9.0572E+00	5.0915E+00	6.8484E+00
-6.00	9.1749E+00	4.7603E+00	6.6771E+00
-8.00	6.7942E+00	2.6605E+00	4.3518E+00
-10.00	3.1676E+00	8.2867E-01	1.7206E+00
-12.00	7.1510E-01	-3.9235E-02	2.0604E-01
-14.00	-2.5605E-01	-2.1253E-01	-2.6081E-01
-16.00	-3.5628E-01	-1.2937E-01	-2.2494E-01
-18.00	-1.8957E-01	-3.7605E-02	-9.2029E-02
-20.00	-4.9742E-02	2.1870E-03	-1.2449E-02
-22.00	7.1315E-03	7.9840E-03	1.0199E-02
-24.00	1.4350E-02	3.9490E-03	8.2390E-03
-26.00	7.1210E-03	6.7400E-04	2.7055E-03
-28.00	3.1650E-04	-4.7900E-04	-5.3150E-04
-29.00	-1.9130E-03	-5.2700E-04	-1.2775E-03

Table B.25 80˚F – Trends in Central Pile Bending Stress Due to Changes in Soil Properties (Refer Figure 4-20)

Depth from pile top	LD 80˚F	DD 80˚F	DcD 80˚F
(ft)	(ksi)	(ksi)	(ksi)
0.00	-3.8486E+01	-1.6363E+01	-2.6287E+01
-1.00	-2.3881E+01	-8.6148E+00	-1.5400E+01
-1.50	-1.7248E+01	-5.0594E+00	-1.0433E+01
-1.75	-1.4169E+01	-3.4489E+00	-8.1508E+00
-2.00	-1.1011E+01	-1.8337E+00	-5.8318E+00
-2.50	-5.4139E+00	9.5535E-01	-1.7645E+00
-3.00	-6.1203E-01	3.2276E+00	1.6530E+00
-3.50	3.3727E+00	4.9903E+00	4.4151E+00
-4.00	6.5103E+00	6.2422E+00	6.5076E+00
-5.00	1.0442E+01	7.4081E+00	8.8838E+00
-5.50	1.1364E+01	7.4325E+00	9.2885E+00
-6.00	1.1705E+01	7.1726E+00	9.2726E+00
-8.00	9.2315E+00	4.5723E+00	6.6288E+00
-10.00	4.6918E+00	1.7840E+00	3.0045E+00
-12.00	1.3244E+00	1.9854E-01	6.2922E-01
-14.00	-1.9341E-01	-2.8690E-01	-2.8222E-01
-16.00	-4.8057E-01	-2.4542E-01	-3.5668E-01
-18.00	-3.0470E-01	-1.0162E-01	-1.8486E-01
-20.00	-1.0449E-01	-1.4550E-02	-4.6740E-02
-22.00	-4.2450E-03	1.0960E-02	8.0950E-03
-24.00	1.9220E-02	9.1450E-03	1.4330E-02
-26.00	1.2905E-02	3.0350E-03	6.8700E-03
-28.00	2.9700E-03	-2.6500E-04	5.1500E-04
-29.00	-6.3500E-04	-6.4500E-04	-1.2050E-03

Table B.26 100˚F – Trends in Central Pile Bending Stress Due to Changes in Soil Properties (Refer Figure 4-20)

Depth from pile top	LD 100˚F	DD 100˚F	DcD 100˚F
(ft)	(ksi)	(ksi)	(ksi)
0.00	-4.7377E+01	-2.2304E+01	-3.4490E+01
-1.00	-2.9848E+01	-1.2339E+01	-2.0797E+01
-1.50	-2.1899E+01	-7.7761E+00	-1.4562E+01
-1.75	-1.8193E+01	-5.6916E+00	-1.1679E+01
-2.00	-1.4378E+01	-3.5854E+00	-8.7313E+00
-2.50	-7.5858E+00	8.5505E-02	-3.5264E+00
-3.00	-1.7086E+00	3.1325E+00	9.0703E-01
-3.50	3.2211E+00	5.5556E+00	4.5531E+00
-4.00	7.1620E+00	7.3459E+00	7.3869E+00
-5.00	1.2277E+01	9.2349E+00	1.0823E+01
-5.50	1.3586E+01	9.4554E+00	1.1555E+01
-6.00	1.4186E+01	9.2937E+00	1.1743E+01
-8.00	1.1749E+01	6.3788E+00	8.9720E+00
-10.00	6.3560E+00	2.7850E+00	4.4497E+00
-12.00	2.0573E+00	5.1954E-01	1.1947E+00
-14.00	-6.2955E-02	-3.1178E-01	-2.3330E-01
-16.00	-5.8908E-01	-3.5311E-01	-4.7934E-01
-18.00	-4.3085E-01	-1.7620E-01	-2.9483E-01
-20.00	-1.7439E-01	-4.1845E-02	-9.8030E-02
-22.00	-2.4665E-02	9.4500E-03	-2.0750E-03
-24.00	2.1490E-02	1.4135E-02	1.9225E-02
-26.00	1.9415E-02	6.4350E-03	1.2415E-02
-28.00	7.3500E-03	6.3500E-04	2.9800E-03
-29.00	2.3800E-03	-5.1500E-04	-9.0000E-05

Table B.27 Maximum Bending Stress in Central Pile vs. ΔT (Refer Figure 4-21)

Temperature	LD	DD	DcD
˚F	(ksi)	(ksi)	(ksi)
60	-29.8799	-9.4845	-18.0670
80	-38.4862	-16.3628	-26.2874
100	-47.3772	-22.3039	-34.4898

Table B.28 LD – Trends in Soil Pressure on Abutment Due to Changes in Thermal Load (Refer Figure 4-22)

Depth from Abutment Top (in)	60˚F lb/in^2	80˚F lb/in^2	100˚F lb/in^2
0.00	0.0000	0.0000	0.0000
13.53	0.9064	1.0728	1.1398
39.58	2.6516	3.1383	3.3344
55.70	3.7315	4.4165	4.6924
83.91	5.6213	6.6533	7.0690
96.00	6.4313	7.6119	8.0875

Table B.29 DD – Trends in Soil Pressure on Abutment Due to Changes in Thermal Load (Refer Figure 4-22)

Depth from Abutment Top (in)	60˚F lb/in^2	80˚F lb/in^2	100˚F lb/in^2
0.00	0.0000	0.0000	0.0000
13.53	3.9791	4.4142	5.0380
39.58	11.6404	12.9130	14.7381
55.70	16.3812	18.1721	20.7405
83.91	24.6777	27.3756	31.2448
96.00	28.2333	31.3200	35.7467

Table B.30 DcD – Trends in Soil Pressure on Abutment Due to Changes in Thermal Load (Refer Figure 4-22)

Depth from Abutment Top (in)	60˚F lb/in^2	80˚F lb/in^2	100˚F lb/in^2
0.00	0.0000	0.0000	0.0000
13.53	2.6806	2.9381	3.1672
39.58	7.8418	8.5949	9.2653
55.70	11.0356	12.0954	13.0388
83.91	16.6247	18.2213	19.6425
96.00	19.0200	20.8467	22.4727

Table B.31 60˚F – Trends in Soil Pressure on Abutment Due to Changes in Soil Properties (Refer Figure 4-23)

Depth from Abutment Top	LD	DD	DcD
(in)	lb/in^2	lb/in^2	lb/in^2
0.00	0.0000	0.0000	0.0000
13.53	0.9064	3.9791	2.6806
39.58	2.6516	11.6404	7.8418
55.70	3.7315	16.3812	11.0356
83.91	5.6213	24.6777	16.6247
96.00	6.4313	28.2333	19.0200

Table B.32 80˚F – Trends in Soil Pressure on Abutment Due to Changes in Soil Properties (Refer Figure 4-23)

Depth from Abutment Top	LD	DD	DcD
(in)	lb/in^2	lb/in^2	lb/in^2
0.00	0.0000	0.0000	0.0000
13.53	1.0728	4.4142	2.9381
39.58	3.1383	12.9130	8.5949
55.70	4.4165	18.1721	12.0954
83.91	6.6533	27.3756	18.2213
96.00	7.6119	31.3200	20.8467

Table B.33 100˚F – Trends in Soil Pressure on Abutment Due to Changes in Soil Properties (Refer Figure 4-23)

Depth from Abutment Top	LD	DD	DcD
(in)	lb/in^2	lb/in^2	lb/in^2
0.00	0.0000	0.0000	0.0000
13.53	1.1398	5.0380	3.1672
39.58	3.3344	14.7381	9.2653
55.70	4.6924	20.7405	13.0388
83.91	7.0690	31.2448	19.6425
96.00	8.0875	35.7467	22.4727

Table B.34 LD - Longitudinal Displacement Comparison of Central Pile Vs. End Pile (Refer Figure 4-24)

	Central pile			End pile		
Depth from pile top	**LD 60˚F**	**LD 80˚F**	**LD 100˚F**	**LD 60˚F**	**LD 80˚F**	**LD 100˚F**
(ft)	**(in)**	**(in)**	**(in)**	**(in)**	**(in)**	**(in)**
0	2.463E-01	3.326E-01	4.231E-01	2.528E-01	3.450E-01	4.414E-01
-2	1.892E-01	2.599E-01	3.353E-01	1.916E-01	2.665E-01	3.461E-01
-4	1.043E-01	1.485E-01	1.968E-01	1.050E-01	1.516E-01	2.024E-01
-6	3.902E-02	5.951E-02	8.291E-02	3.915E-02	6.077E-02	8.544E-02
-8	5.187E-03	1.071E-02	1.778E-02	5.231E-03	1.110E-02	1.864E-02
-10	-5.422E-03	-6.482E-03	-7.067E-03	-5.382E-03	-6.436E-03	-6.964E-03
-12	-5.200E-03	-7.602E-03	-1.012E-02	-5.170E-03	-7.656E-03	-1.025E-02
-14	-2.492E-03	-4.139E-03	-6.072E-03	-2.478E-03	-4.192E-03	-6.202E-03
-16	-6.038E-04	-1.270E-03	-2.156E-03	-6.042E-04	-1.300E-03	-2.228E-03
-18	1.053E-04	5.994E-06	-1.929E-04	9.732E-05	-8.921E-06	-2.213E-04
-20	1.827E-04	2.636E-04	3.275E-04	1.723E-04	2.536E-04	3.167E-04
-22	9.162E-05	1.683E-04	2.591E-04	8.243E-05	1.595E-04	2.520E-04
-24	2.150E-05	5.498E-05	1.031E-04	1.697E-05	5.053E-05	1.002E-04
-26	-2.410E-06	3.531E-06	1.592E-05	2.588E-06	1.100E-05	2.668E-05
-28	-3.132E-06	-5.686E-06	-7.557E-06	1.511E-05	1.902E-05	2.378E-05
-29	-1.928E-33	-3.197E-33	-4.487E-33	8.504E-33	1.056E-32	1.260E-32

Table B.35 DD - Longitudinal Displacement Comparison of Central Pile Vs. End Pile (Refer Figure 4-24)

	Central pile			End pile		
Depth from pile top	**DD 60˚F**	**DD 80˚F**	**DD 100˚F**	**DD 60˚F**	**DD 80˚F**	**DD 100˚F**
(ft)	**(in)**	**(in)**	**(in)**	**(in)**	**(in)**	**(in)**
0	1.237E-01	1.921E-01	2.578E-01	1.023E-01	1.704E-01	2.418E-01
-2	7.975E-02	1.320E-01	1.828E-01	5.835E-02	1.085E-01	1.628E-01
-4	3.603E-02	6.542E-02	9.512E-02	2.283E-02	4.974E-02	8.072E-02
-6	9.138E-03	2.043E-02	3.283E-02	3.867E-03	1.336E-02	2.575E-02
-8	-1.461E-03	4.767E-05	2.449E-03	-2.250E-03	-1.576E-03	4.614E-04
-10	-2.994E-03	-4.713E-03	-6.102E-03	-2.329E-03	-4.175E-03	-5.813E-03
-12	-1.693E-03	-3.368E-03	-5.112E-03	-1.056E-03	-2.569E-03	-4.371E-03
-14	-4.927E-04	-1.305E-03	-2.296E-03	-2.149E-04	-8.588E-04	-1.810E-03
-16	1.349E-05	-1.773E-04	-4.927E-04	5.849E-05	-5.030E-05	-3.178E-04
-18	9.430E-05	1.386E-04	1.402E-04	6.618E-05	1.249E-04	1.483E-04
-20	5.004E-05	1.161E-04	1.850E-04	2.373E-05	7.838E-05	1.476E-04
-22	1.143E-05	4.298E-05	8.727E-05	2.470E-07	1.986E-05	5.726E-05
-24	-1.919E-06	4.378E-06	1.845E-05	-3.478E-06	-2.196E-06	7.124E-06
-26	-2.629E-06	-4.755E-06	-4.687E-06	3.547E-06	3.224E-06	4.318E-06
-28	-1.127E-06	-3.948E-06	-6.687E-06	1.662E-05	2.054E-05	2.424E-05
-29	-1.430E-33	-2.621E-33	-3.786E-33	9.258E-33	1.144E-32	1.359E-32

Table B.36 DcD - Longitudinal Displacement Comparison of Central Pile Vs. End Pile (Refer Figure 4-24)

	Central pile			End pile		
Depth from pile top	**DcD 60˚F**	**DcD 80˚F**	**DcD 100˚F**	**DcD 60˚F**	**DcD 80˚F**	**DcD 100˚F**
(ft)	**(in)**	**(in)**	**(in)**	**(in)**	**(in)**	**(in)**
0	1.735E-01	2.533E-01	3.365E-01	1.637E-01	2.482E-01	3.359E-01
-2	1.236E-01	1.872E-01	2.549E-01	1.117E-01	1.781E-01	2.485E-01
-4	6.262E-02	1.005E-01	1.424E-01	5.442E-02	9.337E-02	1.365E-01
-6	2.014E-02	3.632E-02	5.553E-02	1.641E-02	3.267E-02	5.220E-02
-8	5.481E-04	3.937E-03	8.938E-03	-3.017E-04	2.885E-03	7.828E-03
-10	-4.196E-03	-5.770E-03	-6.918E-03	-3.898E-03	-5.625E-03	-6.884E-03
-12	-3.060E-03	-5.194E-03	-7.524E-03	-2.631E-03	-4.802E-03	-7.184E-03
-14	-1.185E-03	-2.422E-03	-3.986E-03	-9.496E-04	-2.161E-03	-3.726E-03
-16	-1.594E-04	-5.599E-04	-1.180E-03	-9.534E-05	-4.655E-04	-1.069E-03
-18	1.244E-04	1.209E-04	3.544E-05	1.136E-04	1.235E-04	4.980E-05
-20	1.023E-04	1.851E-04	2.654E-04	7.924E-05	1.614E-04	2.440E-04
-22	3.673E-05	9.068E-05	1.640E-04	2.222E-05	7.065E-05	1.410E-04
-24	3.240E-06	2.051E-05	5.191E-05	-1.306E-06	1.229E-05	4.108E-05
-26	-3.773E-06	-3.447E-06	1.827E-06	1.817E-06	3.480E-06	1.034E-05
-28	-1.989E-06	-4.925E-06	-7.529E-06	1.616E-05	1.967E-05	2.356E-05
-29	-1.629E-33	-2.866E-33	-4.121E-33	8.947E-33	1.104E-32	1.313E-32

Table B.37 LD – Bending Moment Comparison of Central Pile Vs. End Pile (Refer Figure 4-25)

	Central pile			End pile		
Depth from pile top	**LD 60˚F**	**LD 80˚F**	**LD 100˚F**	**LD 60˚F**	**LD 80˚F**	**LD 100˚F**
(ft)	**(kip-ft)**	**(kip-ft)**	**(kip-ft)**	**(kip-ft)**	**(kip-ft)**	**(kip-ft)**
0	-7.59E+01	-9.78E+01	-1.20E+02	-7.28E+01	-9.50E+01	-1.18E+02
-1	-4.62E+01	-6.07E+01	-7.58E+01	-4.43E+01	-5.91E+01	-7.45E+01
-1.5	-3.27E+01	-4.38E+01	-5.56E+01	-3.09E+01	-4.22E+01	-5.41E+01
-1.75	-2.65E+01	-3.60E+01	-4.62E+01	-2.47E+01	-3.43E+01	-4.46E+01
-2	-2.01E+01	-2.80E+01	-3.65E+01	-1.85E+01	-2.64E+01	-3.50E+01
-2.5	-8.88E+00	-1.38E+01	-1.93E+01	-7.45E+00	-1.23E+01	-1.77E+01
-3	6.35E-01	-1.56E+00	-4.34E+00	1.86E+00	-1.74E-01	-2.83E+00
-3.5	8.42E+00	8.57E+00	8.18E+00	9.44E+00	9.83E+00	9.64E+00
-4	1.44E+01	1.65E+01	1.82E+01	1.53E+01	1.77E+01	1.96E+01
-5	2.16E+01	2.65E+01	3.12E+01	2.21E+01	2.74E+01	3.24E+01
-5.5	2.30E+01	2.89E+01	3.45E+01	2.34E+01	2.97E+01	3.57E+01
-6	2.33E+01	2.97E+01	3.60E+01	2.37E+01	3.05E+01	3.71E+01
-8	1.73E+01	2.35E+01	2.99E+01	1.74E+01	2.39E+01	3.06E+01
-10	8.05E+00	1.19E+01	1.62E+01	8.12E+00	1.22E+01	1.66E+01
-12	1.82E+00	3.37E+00	5.23E+00	1.88E+00	3.53E+00	5.51E+00
-14	-6.51E-01	-4.91E-01	-1.60E-01	-5.97E-01	-4.05E-01	-2.68E-02
-16	-9.05E-01	-1.22E+00	-1.50E+00	-8.68E-01	-1.18E+00	-1.44E+00
-18	-4.82E-01	-7.74E-01	-1.09E+00	-4.60E-01	-7.54E-01	-1.08E+00
-20	-1.26E-01	-2.66E-01	-4.43E-01	-1.16E-01	-2.55E-01	-4.33E-01
-22	1.81E-02	-1.08E-02	-6.27E-02	2.23E-02	-4.01E-03	-5.43E-02
-24	3.65E-02	4.88E-02	5.46E-02	3.91E-02	5.42E-02	6.26E-02
-26	1.81E-02	3.28E-02	4.93E-02	1.92E-02	3.46E-02	5.21E-02
-28	8.04E-04	7.55E-03	1.87E-02	-1.12E-02	-9.25E-03	-2.54E-03
-29	-4.86E-03	-1.61E-03	6.05E-03	-3.07E-02	-3.58E-02	-3.60E-02

Table B.38 DD – Bending Moment Comparison of Central Pile Vs. End Pile (Refer Figure 4-25)

	Central pile			End pile		
Depth from pile top	**DD 60˚F**	**DD 80˚F**	**DD 100˚F**	**DD 60˚F**	**DD 80˚F**	**DD 100˚F**
(ft)	**(kip-ft)**	**(kip-ft)**	**(kip-ft)**	**(kip-ft)**	**(kip-ft)**	**(kip-ft)**
0	-2.41E+01	-4.16E+01	-5.67E+01	-8.51E+00	-2.48E+01	-4.09E+01
-1	-1.11E+01	-2.19E+01	-3.14E+01	-1.10E+00	-1.09E+01	-2.09E+01
-1.5	-5.13E+00	-1.29E+01	-1.98E+01	2.87E+00	-3.85E+00	-1.10E+01
-1.75	-2.46E+00	-8.76E+00	-1.45E+01	4.58E+00	-6.98E-01	-6.51E+00
-2	1.74E-01	-4.66E+00	-9.11E+00	6.16E+00	2.34E+00	-2.09E+00
-2.5	4.63E+00	2.43E+00	2.17E-01	8.74E+00	7.53E+00	5.56E+00
-3	8.13E+00	8.20E+00	7.96E+00	1.06E+01	1.16E+01	1.18E+01
-3.5	1.07E+01	1.27E+01	1.41E+01	1.17E+01	1.45E+01	1.65E+01
-4	1.23E+01	1.59E+01	1.87E+01	1.22E+01	1.64E+01	1.99E+01
-5	1.33E+01	1.88E+01	2.35E+01	1.16E+01	1.75E+01	2.29E+01
-5.5	1.29E+01	1.89E+01	2.40E+01	1.07E+01	1.70E+01	2.29E+01
-6	1.21E+01	1.82E+01	2.36E+01	9.57E+00	1.59E+01	2.20E+01
-8	6.76E+00	1.16E+01	1.62E+01	4.54E+00	9.23E+00	1.42E+01
-10	2.11E+00	4.53E+00	7.08E+00	1.03E+00	3.17E+00	5.80E+00
-12	-9.97E-02	5.04E-01	1.32E+00	-3.21E-01	9.24E-02	8.62E-01
-14	-5.40E-01	-7.29E-01	-7.92E-01	-4.27E-01	-6.71E-01	-7.83E-01
-16	-3.29E-01	-6.24E-01	-8.97E-01	-1.99E-01	-4.71E-01	-7.57E-01
-18	-9.56E-02	-2.58E-01	-4.48E-01	-3.58E-02	-1.62E-01	-3.40E-01
-20	5.56E-03	-3.70E-02	-1.06E-01	1.54E-02	-5.84E-03	-6.09E-02
-22	2.03E-02	2.78E-02	2.40E-02	1.48E-02	2.84E-02	3.29E-02
-24	1.00E-02	2.32E-02	3.59E-02	7.66E-03	2.03E-02	3.56E-02
-26	1.71E-03	7.71E-03	1.64E-02	4.68E-03	8.59E-03	1.61E-02
-28	-1.22E-03	-6.73E-04	1.61E-03	-8.84E-03	-1.29E-02	-1.61E-02
-29	-1.34E-03	-1.64E-03	-1.31E-03	-2.63E-02	-3.30E-02	-4.07E-02

Table B.39 DcD – Bending Moment Comparison of Central Pile Vs. End Pile (Refer Figure 4-25)

	Central pile			End pile		
Depth from pile top	**DcD 60˚F**	**DcD 80˚F**	**DcD 100˚F**	**DcD 60˚F**	**DcD 80˚F**	**DcD 100˚F**
(ft)	**(kip-ft)**	**(kip-ft)**	**(kip-ft)**	**(kip-ft)**	**(kip-ft)**	**(kip-ft)**
0	-4.59E+01	-6.68E+01	-8.76E+01	-3.60E+01	-5.72E+01	-7.81E+01
-1	-2.57E+01	-3.91E+01	-5.28E+01	-1.93E+01	-3.29E+01	-4.67E+01
-1.5	-1.65E+01	-2.65E+01	-3.70E+01	-1.11E+01	-2.12E+01	-3.16E+01
-1.75	-1.23E+01	-2.07E+01	-2.97E+01	-7.44E+00	-1.58E+01	-2.46E+01
-2	-8.03E+00	-1.48E+01	-2.22E+01	-3.81E+00	-1.04E+01	-1.76E+01
-2.5	-6.75E-01	-4.48E+00	-8.96E+00	2.46E+00	-1.06E+00	-5.27E+00
-3	5.38E+00	4.20E+00	2.30E+00	7.52E+00	6.74E+00	5.18E+00
-3.5	1.01E+01	1.12E+01	1.16E+01	1.14E+01	1.30E+01	1.37E+01
-4	1.36E+01	1.65E+01	1.88E+01	1.41E+01	1.76E+01	2.02E+01
-5	1.71E+01	2.26E+01	2.75E+01	1.65E+01	2.26E+01	2.79E+01
-5.5	1.74E+01	2.36E+01	2.94E+01	1.65E+01	2.32E+01	2.94E+01
-6	1.70E+01	2.36E+01	2.98E+01	1.58E+01	2.29E+01	2.96E+01
-8	1.11E+01	1.68E+01	2.28E+01	9.81E+00	1.59E+01	2.21E+01
-10	4.37E+00	7.63E+00	1.13E+01	3.67E+00	7.00E+00	1.08E+01
-12	5.24E-01	1.60E+00	3.04E+00	3.26E-01	1.38E+00	2.84E+00
-14	-6.63E-01	-7.17E-01	-5.93E-01	-6.15E-01	-6.93E-01	-5.76E-01
-16	-5.72E-01	-9.06E-01	-1.22E+00	-4.80E-01	-8.18E-01	-1.13E+00
-18	-2.34E-01	-4.70E-01	-7.49E-01	-1.78E-01	-4.04E-01	-6.77E-01
-20	-3.16E-02	-1.19E-01	-2.49E-01	-1.37E-02	-8.96E-02	-2.11E-01
-22	2.59E-02	2.06E-02	-5.27E-03	2.64E-02	2.77E-02	8.51E-03
-24	2.09E-02	3.64E-02	4.89E-02	1.97E-02	3.76E-02	5.35E-02
-26	6.87E-03	1.75E-02	3.15E-02	7.94E-03	1.79E-02	3.19E-02
-28	-1.35E-03	1.31E-03	7.57E-03	-1.09E-02	-1.36E-02	-1.27E-02
-29	-3.25E-03	-3.06E-03	-2.29E-04	-2.77E-02	-3.57E-02	-4.13E-02

Table B.40 LD – Bending Stress Comparison of Central Pile Vs. End Pile (Refer Figure 4-26)

	Central pile			End pile		
Depth from pile top	**LD 60˚F**	**LD 80˚F**	**LD 100˚F**	**LD 60˚F**	**LD 80˚F**	**LD 100˚F**
(ft)	**(ksi)**	**(ksi)**	**(ksi)**	**(ksi)**	**(ksi)**	**(ksi)**
0	-2.99E+01	-3.85E+01	-4.74E+01	-2.86E+01	-3.74E+01	-4.64E+01
-1	-1.82E+01	-2.39E+01	-2.98E+01	-1.74E+01	-2.32E+01	-2.93E+01
-1.5	-1.29E+01	-1.72E+01	-2.19E+01	-1.22E+01	-1.66E+01	-2.13E+01
-1.75	-1.04E+01	-1.42E+01	-1.82E+01	-9.72E+00	-1.35E+01	-1.76E+01
-2	-7.91E+00	-1.10E+01	-1.44E+01	-7.27E+00	-1.04E+01	-1.38E+01
-2.5	-3.49E+00	-5.41E+00	-7.59E+00	-2.93E+00	-4.82E+00	-6.97E+00
-3	2.50E-01	-6.12E-01	-1.71E+00	7.31E-01	-6.85E-02	-1.11E+00
-3.5	3.31E+00	3.37E+00	3.22E+00	3.72E+00	3.87E+00	3.79E+00
-4	5.67E+00	6.51E+00	7.16E+00	6.01E+00	6.96E+00	7.71E+00
-5	8.49E+00	1.04E+01	1.23E+01	8.70E+00	1.08E+01	1.28E+01
-5.5	9.06E+00	1.14E+01	1.36E+01	9.23E+00	1.17E+01	1.40E+01
-6	9.17E+00	1.17E+01	1.42E+01	9.31E+00	1.20E+01	1.46E+01
-8	6.79E+00	9.23E+00	1.17E+01	6.84E+00	9.41E+00	1.21E+01
-10	3.17E+00	4.69E+00	6.36E+00	3.19E+00	4.80E+00	6.55E+00
-12	7.15E-01	1.32E+00	2.06E+00	7.39E-01	1.39E+00	2.17E+00
-14	-2.56E-01	-1.93E-01	-6.30E-02	-2.35E-01	-1.59E-01	-1.06E-02
-16	-3.56E-01	-4.81E-01	-5.89E-01	-3.42E-01	-4.64E-01	-5.68E-01
-18	-1.90E-01	-3.05E-01	-4.31E-01	-1.81E-01	-2.97E-01	-4.23E-01
-20	-4.97E-02	-1.04E-01	-1.74E-01	-4.57E-02	-1.00E-01	-1.71E-01
-22	7.13E-03	-4.24E-03	-2.47E-02	8.77E-03	-1.58E-03	-2.14E-02
-24	1.44E-02	1.92E-02	2.15E-02	1.54E-02	2.13E-02	2.46E-02
-26	7.12E-03	1.29E-02	1.94E-02	7.56E-03	1.36E-02	2.05E-02
-28	3.17E-04	2.97E-03	7.35E-03	-4.41E-03	-3.64E-03	-1.00E-03
-29	-1.91E-03	-6.35E-04	2.38E-03	-1.21E-02	-1.41E-02	-1.41E-02

Table B.41 DD – Bending Stress Comparison of Central Pile Vs. End Pile (Refer Figure 4-26)

	Central pile			End pile		
Depth from pile top	**DD 60˚F**	**DD 80˚F**	**DD 100˚F**	**DD 60˚F**	**DD 80˚F**	**DD 100˚F**
(ft)	**(ksi)**	**(ksi)**	**(ksi)**	**(ksi)**	**(ksi)**	**(ksi)**
0	-9.48E+00	-1.64E+01	-2.23E+01	-3.35E+00	-9.75E+00	-1.61E+01
-1	-4.37E+00	-8.61E+00	-1.23E+01	-4.32E-01	-4.29E+00	-8.24E+00
-1.5	-2.02E+00	-5.06E+00	-7.78E+00	1.13E+00	-1.51E+00	-4.33E+00
-1.75	-9.68E-01	-3.45E+00	-5.69E+00	1.80E+00	-2.75E-01	-2.56E+00
-2	6.85E-02	-1.83E+00	-3.59E+00	2.42E+00	9.23E-01	-8.24E-01
-2.5	1.82E+00	9.55E-01	8.55E-02	3.44E+00	2.96E+00	2.19E+00
-3	3.20E+00	3.23E+00	3.13E+00	4.16E+00	4.55E+00	4.63E+00
-3.5	4.21E+00	4.99E+00	5.56E+00	4.60E+00	5.72E+00	6.51E+00
-4	4.86E+00	6.24E+00	7.35E+00	4.79E+00	6.47E+00	7.83E+00
-5	5.25E+00	7.41E+00	9.23E+00	4.55E+00	6.90E+00	9.02E+00
-5.5	5.09E+00	7.43E+00	9.46E+00	4.20E+00	6.69E+00	9.00E+00
-6	4.76E+00	7.17E+00	9.29E+00	3.77E+00	6.27E+00	8.66E+00
-8	2.66E+00	4.57E+00	6.38E+00	1.79E+00	3.63E+00	5.59E+00
-10	8.29E-01	1.78E+00	2.79E+00	4.05E-01	1.25E+00	2.28E+00
-12	-3.92E-02	1.99E-01	5.20E-01	-1.26E-01	3.64E-02	3.39E-01
-14	-2.13E-01	-2.87E-01	-3.12E-01	-1.68E-01	-2.64E-01	-3.08E-01
-16	-1.29E-01	-2.45E-01	-3.53E-01	-7.82E-02	-1.85E-01	-2.98E-01
-18	-3.76E-02	-1.02E-01	-1.76E-01	-1.41E-02	-6.37E-02	-1.34E-01
-20	2.19E-03	-1.46E-02	-4.18E-02	6.05E-03	-2.30E-03	-2.39E-02
-22	7.98E-03	1.10E-02	9.45E-03	5.81E-03	1.12E-02	1.29E-02
-24	3.95E-03	9.14E-03	1.41E-02	3.02E-03	7.97E-03	1.40E-02
-26	6.74E-04	3.04E-03	6.43E-03	1.84E-03	3.38E-03	6.35E-03
-28	-4.79E-04	-2.65E-04	6.35E-04	-3.48E-03	-5.07E-03	-6.35E-03
-29	-5.27E-04	-6.45E-04	-5.15E-04	-1.04E-02	-1.30E-02	-1.60E-02

Table B.42 DcD – Bending Stress Comparison of Central Pile Vs. End Pile (Refer Figure 4-26)

	Central pile			End pile		
Depth from pile top	**DcD 60˚F**	**DcD 80˚F**	**DcD 100˚F**	**DcD 60˚F**	**DcD 80˚F**	**DcD 100˚F**
(ft)	**(ksi)**	**(ksi)**	**(ksi)**	**(ksi)**	**(ksi)**	**(ksi)**
0	-1.81E+01	-2.63E+01	-3.45E+01	-1.42E+01	-2.25E+01	-3.08E+01
-1	-1.01E+01	-1.54E+01	-2.08E+01	-7.58E+00	-1.30E+01	-1.84E+01
-1.5	-6.48E+00	-1.04E+01	-1.46E+01	-4.38E+00	-8.33E+00	-1.24E+01
-1.75	-4.83E+00	-8.15E+00	-1.17E+01	-2.93E+00	-6.22E+00	-9.70E+00
-2	-3.16E+00	-5.83E+00	-8.73E+00	-1.50E+00	-4.11E+00	-6.94E+00
-2.5	-2.66E-01	-1.76E+00	-3.53E+00	9.68E-01	-4.17E-01	-2.07E+00
-3	2.12E+00	1.65E+00	9.07E-01	2.96E+00	2.65E+00	2.04E+00
-3.5	3.99E+00	4.42E+00	4.55E+00	4.49E+00	5.10E+00	5.39E+00
-4	5.35E+00	6.51E+00	7.39E+00	5.56E+00	6.93E+00	7.97E+00
-5	6.73E+00	8.88E+00	1.08E+01	6.51E+00	8.88E+00	1.10E+01
-5.5	6.85E+00	9.29E+00	1.16E+01	6.49E+00	9.14E+00	1.16E+01
-6	6.68E+00	9.27E+00	1.17E+01	6.23E+00	9.02E+00	1.16E+01
-8	4.35E+00	6.63E+00	8.97E+00	3.86E+00	6.25E+00	8.69E+00
-10	1.72E+00	3.00E+00	4.45E+00	1.44E+00	2.76E+00	4.24E+00
-12	2.06E-01	6.29E-01	1.19E+00	1.28E-01	5.45E-01	1.12E+00
-14	-2.61E-01	-2.82E-01	-2.33E-01	-2.42E-01	-2.73E-01	-2.27E-01
-16	-2.25E-01	-3.57E-01	-4.79E-01	-1.89E-01	-3.22E-01	-4.46E-01
-18	-9.20E-02	-1.85E-01	-2.95E-01	-7.00E-02	-1.59E-01	-2.67E-01
-20	-1.24E-02	-4.67E-02	-9.80E-02	-5.38E-03	-3.53E-02	-8.31E-02
-22	1.02E-02	8.10E-03	-2.08E-03	1.04E-02	1.09E-02	3.35E-03
-24	8.24E-03	1.43E-02	1.92E-02	7.76E-03	1.48E-02	2.10E-02
-26	2.71E-03	6.87E-03	1.24E-02	3.13E-03	7.04E-03	1.25E-02
-28	-5.32E-04	5.15E-04	2.98E-03	-4.31E-03	-5.35E-03	-5.00E-03
-29	-1.28E-03	-1.20E-03	-9.00E-05	-1.09E-02	-1.40E-02	-1.63E-02

Table B.43 Maximum Axial Stress in the Central Girder Vs. ΔT (Refer Figure 4-27)

Temperature	**LD**	**DD**	**DcD**
˚F	**(ksi)**	**(ksi)**	**(ksi)**
60	-11.921	-20.635	-17.125
80	-14.729	-24.836	-20.382
100	-17.255	-29.031	-23.440

Table B.44 LD 80˚F - Convergence of Displacement (Refer Figure 4-28, 4-29)

Iteration number	δ_R (in)	δ_T (in)
1	-0.09226	0.529168
2	0.071107	0.354317
3	0.089139	0.334475
4	0.091659	0.33171
5	0.091927	0.331421

Table B.45 DD 80˚F - Convergence of Displacement (Refer Figure 4-28, 4-29)

Iteration number	δ_R (in)	δ_T (in)
1	-0.09226	0.529168
2	0.145376	0.267649
3	0.19152	0.215859
4	0.205701	0.199989
5	0.210976	0.19408
6	0.213025	0.191788
7	0.213761	0.190968

Table B.46 DcD 80˚F - Convergence of Displacement (Refer Figure 4-28, 4-29)

Iteration number	δ_R (in)	δ_T (in)
1	-0.09226	0.529168
2	0.113991	0.304394
3	0.148324	0.266079
4	0.157349	0.255992
5	0.159963	0.253071
6	0.16063	0.252332